A Comparison of Gas Exchange Models in the Estimation of CO_2 Fluxes in the South Atlantic South of Africa for the Summer Season of 2008/2009

Stephanie Megan Rainier

Thesis presented for the Degree of

MASTER OF SCIENCE

in the Department of Oceanography

UNIVERSITY OF CAPE TOWN

November 2011

ACKNOWLEDGEMENTS

Thank you to Dr Pedro Monteiro and Dr Howard Waldron for their patience and supervision. The scientists, officers, and crew on the RV SA Agulhas for their help in the data collection. Dr Nicolas Fauchereau for his help in extracting the wind speed product from QuikSCAT. Dr Isabelle Ansorge (UCT) for her advice and support. Marié Smith and Laura Barrett for their guidance. Nick McGee and Natasha Day for their moral support. And to my sister Philippa, my mother Gail, and my father John for their encouragement, patience and love.

For Funding: ACCESS and NRF through CSIR

TABLE OF CONTENTS

List of figures..... 5
List of tables..... 10
Abstract..... 12
1. Introduction..... 14
1.1. Global Ocean Carbon Fluxes..... 15
1.1.1. The Ocean as a CO_2 Reservoir..... 17
1.2. Ocean – Atmosphere CO_2 Fluxes..... 19
1.2.1. Experimental Direct Determination of the Gas Transfer Velocity 22
1.2.2. Gas Transfer Velocity derived from the proxies: sea surface microlayer thickness and wind..... 26
1.2.3. Uncertainties in Global Fluxes..... 28
1.3. Purpose of this study..... 29
2. Data and Methods..... 30
2.1. Data Collection..... 31
2.1.1. pCO_2/xCO_2..... 33
2.1.2. Physical Properties of Seawater..... 36
2.1.3. Gas Transfer Rates: Winds..... 37
2.1.4. Ship Track Interpolation..... 38
2.2. Data Analysis..... 40
2.2.1. Gas Transfer Velocity..... 40
2.2.2. Air-Sea Gas Flux..... 43
2.3. Limitations..... 44
3. Results..... 46
3.1. Frontal Zone Positions Used in the Spatial Averaging of the data... 47
3.2. Geographical Differences in Physical Properties and Wind Speed.. 50
3.2.1. Surface Oceanography of Southern Ocean: South East Atlantic..... 50

3.2.2. Wind Speed..... 56
3.3. Gas Transfer Velocity..... 60
3.3.1. Change in Gas Transfer Velocity Models with Wind Speed and the Uncertainty in the Wind Speed Product..... 61
3.3.2. The Gas Transfer Velocities Models plotted versus the Wind Speeds used in this study..... 65
3.4. Air-Sea CO_2 Flux..... 68
3.4.1. Geographical Differences of Air-Sea CO_2 Fluxes..... 69
3.4.2. Response of the difference Air-Sea CO_2 Fluxes to the uncertainty in Wind Speed of $2m.s^{-1}$..... 78
3.4.3. Response of the Air-Sea CO_2 flux to the uncertainty in Temperature and ΔfCO_2..... 81
4. Discussion..... 82
4.1. Introduction..... 83
4.2 Oceanography of the Southern Ocean..... 83
4.2.1. Fronts and Physical Properties..... 83
4.2.2. Wind Speed..... 88
4.3. Comparison of the Fluxes calculated using the Different Gas Transfer Velocity Models..... 90
4.3.1. Change in Gas Transfer Velocity Models with Wind Speed and the Uncertainty in the Wind Speed Product..... 92
4.3.2. Change in the Air-Sea CO_2 Fluxes with Wind Speed and the Uncertainty in the Wind Speed Product..... 96
4.4. Comparison of the Flux from this Study to the Flux used in Takahashi et al., (2009)..... 98
5. Synthesis..... 107
Appendix 1: Weightings using in averaging weekly winds..... 111
Appendix 2: Tables showing response of CO_2 flux to uncertainties in temperature, ΔfCO_2 and winds..... 112
References..... 114

LIST OF FIGURES

Figure 1: Schematic representation of the pre-industrial ocean carbon cycle. Fluxes (arrows) are in Pg C.year^{-1} (petagrams of carbon: 1Pg = 1x10^{15}g) and reservoir sizes (numbers in square brackets) are in Pg C. Abbreviations: PIC, particulate inorganic carbon; DOC, dissolved organic carbon; DIC, dissolved inorganic carbon. (Sabine and Feely, 2007) 16
Figure 2: Schematic representation of the ocean carbon cycle with pre-industrial fluxes and reservoir sizes (upright) and average values for the 1980s and 1990s (circled). Fluxes (arrows) are in Pg C/year and reservoir sizes (numbers in square brackets) are in Pg C. (Sabine and Feely, 2007) 18
Figure 3: Map with the three separate cruises tracks done during data collection on the SA Agulhas. 32
Figure 4: Schematic of the underway pCO_2 system used on the RV SA Agulhas (Pierrot et al., 2009) 35
Figure 5: Linear interpolation of the latitudes and longitudes used in filling in missing coordinates. The original coordinates are red, and the interpolated coordinates are blue. 39
Figure 6: Map showing regions used in averaging the data. The writing in bold print labels the different regions, and the writing in italics represents the three different cruises during which the data were obtained. All three cruises occur in the Subtropical Zone, the Sub-Antarctic Zone, and the northern Polar Frontal Zone, so there is data for spring, summer and autumn in those regions. Only the SANAE cruise data occur in the southern Polar Frontal Zone, the Eastern Weddell region, and at the Antarctic continent, so there is only data for summer in those regions. The data will be analysed in two parts; one section with seasonal data (33.5°S-50°S) and the other section with data for the summer season only (50°S -Shelf). It must be noted that this map represents a great simplification of the fronts. 48
Figure 7: The Southern Ocean circumpolar fronts as published by Orsi et al. (1995). This is a more detailed and accurate representation of the fronts. The area of frontal

positions in comparison with this study is outlined in red at the top of the figure, from 40°W to 40°E..... 49
Figure 8: Plots showing physical properties from the three separate cruises during which the data were collected. Plot (a) shows the temperature (in °C), plot (b) is the salinity, and plot (c) is showing ΔfCO_2 (which was calculated as fCO_{2ocean} – $fCO_{2atmosphere}$) (in µatm)..... 51
Figure 9: Graph showing the average seasonal variation of the physical properties in the Sub Tropics, Sub Antarctic Zone and Polar Frontal Zone (North). Temperature and salinity are on the primary axis, and ΔfCO_2 (which was calculated as fCO_{2ocean} – $fCO_{2atmosphere}$) is on the secondary axis. The standard deviation is shown by the error bars. 53
Figure 10: Graph showing the averages of temperature, salinity and ΔfCO_2 for each region from the Polar Frontal Zone (South) to the Shelf for the summer season. Temperature and salinity are on the primary axis, and ΔfCO_2 (which was calculated as fCO_{2ocean} – $fCO_{2atmosphere}$) is on the secondary axis. The standard deviation is shown by the error bars..... 55
Figure 11: Graph showing the average seasonal variation of the daily wind speed and weighted average of the wind speed for the week preceding the day of daily wind for Sub Tropic Region, Sub Antarctic Zone and Polar Frontal Zone (North)..... 57
Figure 12: Graph showing the averages for each region from the Polar Frontal Zone (South) to the Shelf of daily wind speed and weighted average of the wind speed for the week preceding the day of daily wind for the summer season. 59
Figure 13: Graph showing the sensitivity of the gas transfer velocities (*k*) of each model to uncertainties in the wind product in low wind ($3m.s^{-1}$), medium strength wind ($8m.s^{-1}$) and high wind ($14m.s^{-1}$). The uncertainty of the wind speed from Seawinds on QuikSCAT is $2m.s^{-1}$ (Perry, 2000). All gas transfer velocities are normalised to a Schmidt number of 660. The error bars represent gas transfer velocities at wind speeds of $=2m.s^{-1}$ (upper bar) or $-2m.s^{-1}$ (lower bar) relative to the low, medium and high wind speeds. B74 is the Broecker and Peng 'Stagnant Film Model; LM86 is the Liss and Merlivat Relationship; W92 is the quadratic Wanninkhof Relationship; WM99 is the

Wanninkhof and McGillis cubic relationship and N00 is the Nightingale et al. quadratic parameterisation..... 62
Figure 14: Plot of the wind speed from this study versus the gas transfer velocities. The wind speed used in this plot is the daily wind speed. The gas transfer velocities have been calculated using the different parameterisations. B74 is the Broecker and Peng 'Stagnant Film Model; LM86 is the Liss and Merlivat Relationship; W92 is the quadratic Wanninkhof Relationship; WM99 is the Wanninkhof and McGillis cubic relationship and N00 is the Nightingale et al. quadratic parameterisation. 65
Figure 15: Plot of the wind speed from this study versus the gas transfer velocities. Wind speed used in this plot is weighted average wind speed. The gas transfer velocities have been calculated using the different parameterisations. B74 is the Broecker and Peng 'Stagnant Film Model; LM86 is the Liss and Merlivat Relationship; W92 is the quadratic Wanninkhof Relationship; WM99 is the Wanninkhof and McGillis cubic relationship and N00 is the Nightingale et al. quadratic parameterisation. 67
Figure 16: Graph showing the average air-sea CO_2 flux for each model across each region from the Sub Tropics to the Polar Frontal Zone (North), separated into seasons (cruises). The gas transfer velocities were calculated using a daily wind speed. Errors are shown in Table 3 using standard deviations. B74 is the Broecker and Peng 'Stagnant Film Model; LM86 is the Liss and Merlivat Relationship; W92 is the quadratic Wanninkhof Relationship; WM99 is the Wanninkhof and McGillis cubic relationship and N00 is the Nightingale et al. quadratic parameterisation. Positive values indicate sea-to-air fluxes, and negative values indicate air-to-sea fluxes. 69
Figure 17: Graph showing the average air-sea CO_2 flux for each model for the summer season, for the regions from the Polar Frontal Zone (South) to the Antarctic Shelf. The gas transfer velocities were calculated using a daily wind speed. Errors are shown in Table 3 using standard deviations. B74 is the Broecker and Peng 'Stagnant Film Model; LM86 is the Liss and Merlivat Relationship; W92 is the quadratic Wanninkhof Relationship; WM99 is the Wanninkhof and McGillis cubic relationship and N00 is the Nightingale et al. quadratic parameterisation. Note the scale change from Figure 16. Positive values indicate sea-to-air fluxes, and negative values indicate air-to-sea fluxes. 71

Figure 18: Graph showing the average air-sea CO_2 flux for each model across each region, separated into seasons (cruises). The gas transfer velocities were calculated using a weighted weekly average of the wind speed. Errors are shown in Table 4 using standard deviation. B74 is the Broecker and Peng 'Stagnant Film Model; LM86 is the Liss and Merlivat Relationship; W92 is the quadratic Wanninkhof Relationship; WM99 is the Wanninkhof and McGillis cubic relationship and N00 is the Nightingale et al. quadratic parameterisation. Positive values indicate sea-to-air fluxes, and negative values indicate air-to-sea fluxes. 74
Figure 19: Graph showing the average air-sea CO_2 flux for each model for the summer season, for the regions from the Polar Frontal Zone (South) to the Antarctic Shelf. The gas transfer velocities were calculated using a weighted weekly average of the wind speed. Errors are shown in table Table 4 using standard deviation. B74 is the Broecker and Peng 'Stagnant Film Model; LM86 is the Liss and Merlivat Relationship; W92 is the quadratic Wanninkhof Relationship; WM99 is the Wanninkhof and McGillis cubic relationship and N00 is the Nightingale et al. quadratic parameterisation. Positive values indicate sea-to-air fluxes, and negative values indicate air-to-sea fluxes. Note the scale change from Figure 18. 76
Figure 20: Graph showing the sensitivity of the fluxes calculated with the gas transfer velocities of each model to uncertainties in the wind product in low wind ($3m.s^{-1}$), medium strength wind ($8m.s^{-1}$) and high wind ($14m.s^{-1}$). The uncertainty of the wind speed from Seawinds on QuikSCAT is $2m.s^{-1}$ (Perry, 2000). All gas transfer velocities are normalised to a Schmidt number of 660. The error bars represent gas transfer velocities at wind speeds of =2m.s-1 (upper bar) or -2m.s-1 (lower bar) relative to the low, medium and high wind speeds. The fluxes were calculated using ΔfCO_2=-20µatm, temperature=5°C, salinity=33.5, and pressure=0.5bar. B74 is the Broecker and Peng 'Stagnant Film Model; LM86 is the Liss and Merlivat Relationship; W92 is the quadratic Wanninkhof Relationship; WM99 is the Wanninkhof and McGillis cubic relationship and N00 is the Nightingale et al. quadratic parameterisation. Negative values indicate air-to-sea fluxes. 79
Figure 21:Block diagram showing the water circulation of the Southern Ocean from Sverdrup et al., (1942), with the addition of the frontal locations (STF: Subtropical Front,

SAF: Sub Antarctic Front, PF: Polar Front, CWB: Continental Water Boundary) (Tomczak and Godfrey (2003)) South of the Polar Front the Deep Water is the North Atlantic Deep Water (NADW) and the Circumpolar Deep Water (CDW), the Intermediate Water is the Antarctic Intermediate Water (AAIW), the Bottom Water is the Antarctic Bottom Water (AABW) and the Surface Water is the Antarctic Surface Water (AASW). 84

Figure 22: Graph showing the average air-sea CO_2 flux calculated using the gas transfer velocity model from Wanninkhof (1992) and the ΔfCO_2 recorded in this study. The gas transfer velocity was determined using daily wind speed. Note that positive values indicate sea-to-air fluxes, and negative values indicate air-to-sea values..... 99

Figure 23: Plot (a) shows the monthly mean sea-air CO_2 flux of the Atlantic Ocean and plot (b) shows the monthly mean sea-air CO_2 flux of the Southern and Global Oceans. The fluxes are in the unit of Tons-C.km^{-2}.month^{-1} (Ton=10^{6}g). Months 1 and 13 are January and Month 12 is December. For the region 'South of 62°S' the black solid curve with open diamonds indicates the flux per km^2 of geographic area including ice cover; and the black dashed curve with solid circles indicates the flux per km^2 of water exposed to the air in leads and polynyas in the ice fields. Positive values indicate sea-to-air fluxes, and negative values indicate air-to-sea fluxes. Figure 23 is taken from Takahashi et al., (2009)..... 101

Figure 24: Graph showing the CO_2 flux data extrapolated from Takahashi et al., (2009) in Figure 23 with the air-sea CO_2 flux data from this study. The flux from this study was calculated using daily winds. The gas transfer velocity model used in determining the CO_2 flux is Wanninkhof (1992). Note that positive values indicate sea-to-air fluxes, and negative values indicate air-to-sea values..... 103

LIST OF TABLES

Table 1: Cruise Information of the RV Agulhas. 31
Table 2: Physical properties from the pCO_2 system that are used 37
Table 3: Table showing the regional averages of the fluxes determined using *k* from the different relationships, included are the standard deviations from the mean for each region. It also includes the standard deviations. The different gas transfer velocities were calculated using the daily wind speed. The flux is in $mmol.m^{-2}.day^{-1}$. B74 is the Broecker and Peng 'Stagnant Film Model; LM86 is the Liss and Merlivat Relationship; W92 is the quadratic Wanninkhof Relationship; WM99 is the Wanninkhof and McGillis cubic relationship and N00 is the Nightingale et al. quadratic parameterisation. Positive values indicate sea-to-air fluxes, and negative values indicate air-to-sea fluxes..... 72
Table 4: Table showing the regional averages of the fluxes determined using *k* from the different relationships, included are the standard deviations from the mean for each region. It also includes the standard deviations. The different gas transfer velocities were calculated using the weighted weekly average of the wind speed. The flux is in $mmol.m^{-2}.day^{-1}$. B74 is the Broecker and Peng 'Stagnant Film Model; LM86 is the Liss and Merlivat Relationship; W92 is the quadratic Wanninkhof Relationship; WM99 is the Wanninkhof and McGillis cubic relationship and N00 is the Nightingale et al. quadratic parameterisation. Positive values indicate sea-to-air fluxes, and negative values indicate air-to-sea fluxes. 77
Table 5: The air-sea CO_2 flux values used in the comparison between the results from this study to the results from Takahashi et al., (2009). The values from Takahashi et al., (2009) were taken from Figure 23 and then converted from $tons\text{-}C.km^{-2}month^{-1}$ into the same units used in this study ($mmol.m^{-2}day^{-1}$). The Wanninkhof (1992) relationship between wind speed and gas transfer velocity was used to determine the air-sea CO_2 flux in the comparison. 102
Table 6: Table showing the mean difference between the air-sea CO_2 fluxes calculated in this study, with the Wanninkhof (1992) relationship between wind speed and gas

transfer velocity, using the daily wind speed, and the CO_2 fluxes extrapolated from Figure 23(a) and (b) from Takahashi et al., (2009) and shown in Table 5 and Figure 24 105
Table 7: Table showing change in the Flux because of uncertainty in the temperature of 0.05°C, which affects solubility. A change in temperature also affects the Schmidt number, and in turn, the gas transfer velocity. All columns except for Temperature and Solubility remain to 4 decimal points to show the small changes that occur. 112
Table 8: Table showing change in the Flux because of uncertainty in ΔfCO_2 of 1µatm. Temperature used to calculate Solubility is 5°C, Salinity is 33.50 113
Table 9: Table showing change in the Flux because of the uncertainty in the wind product of 2m.s^{-1}. Temperature used to calculate Solubility is 5°C, Salinity is 33.50. 113

ABSTRACT

There is a problem in the determination of air-sea CO_2 fluxes because of the number of different relationships used in calculating gas transfer velocities. There is also a problem with the CO_2 sink in the Southern Ocean being greatly underestimated. Data were collected underway using an autonomous pCO_2 system during three separate relief cruises over the course of austral spring 2008 to austral autumn 2009 onboard the RV SA Agulhas in the South Atlantic Ocean. The wind speed product was extracted from QuikSCAT. Using the data we investigated the sensitivity of the five gas transfer velocity parameterisations to the uncertainty in the wind speed product of $2m.s^{-1}$. We found that the Stagnant Film Model was unresponsive. Liss and Merlivat's (1986) linear model for three wind regimes showed a gradual increase in sensitivity with wind speed. The quadratic relationship developed by Nightingale et al., (2000) also showed a steady increase in sensitivity with an increase in wind speed. Wanninkhof's (1992) quadratic relationship showed the greatest response at low wind speeds and then a continuing increase in response through medium to high wind regimes. The cubic relationship from Wanninkhof and McGillis (1999) showed the smallest response at low wind speeds but had the greatest response to the uncertainty in the wind speed product in medium and high wind regimes. We also calculated regional and seasonal averages of the CO_2 flux with the five gas transfer velocities based on the different relationships between gas transfer velocity and wind speed. We found that there was a CO_2 flux into the ocean ranging from $4mmol.m^{-2}.day^{-1}$ to $12mmol.m^{-2}.day^{-1}$ between 33.5 and 68°S, except during autumn between 45-50°S where there is a flux out of the ocean of $2mmol.m^{-2}.day^{-1}$. Between 68-70°S the flux into the ocean strengthens to between $28mmol.m^{-2}.day^{-1}$ and $52mmol.m^{-2}.day^{-1}$. Gas transfer velocity is not dependant on wind speed alone, but currently it is the only variable that it measureable on a global scale. Further investigations are in place to measure gas transfer velocity *in situ*. The Southern Ocean is greatly undersampled spatially and temporally which leads to a lack of understanding

about possibly one of the most important CO_2 sinks. New methods are being taken on to increase the sampling resolution.

Chapter 1:

INTRODUCTION

1.1 Global Ocean Carbon Fluxes

Based on carbon and carbon isotopic records in ice cores and tree rings, we know that atmospheric CO_2 levels remained reasonably constant in the millennium preceding the industrial revolution in the 1800's (Post et al., 1990; Schimel et al., 1994; Levin and Hesshaimer, 2000). The notable consistency of atmospheric CO_2 suggests the carbon content in the reservoirs was in an inter-glacial 'steady state', so that there was a well-balanced global carbon cycle (Broecker and Peng, 1982; Wanninkhof and Feely, 2004). There are sizeable spatial and temporal variations in the partial pressure of carbon dioxide (pCO_2) in the surface oceans (between 150µatm and 550µatm) (Takahashi et al., 2002; Liss et al., 2004). In the subpolar Southern Ocean surface water undergoes seasonal changes of up at 60µatm due to deep mixing in winter and photosynthesis in summer (Takahashi et al., 2009). The atmosphere has a concentration that is more uniform (around 384.5µatm (from this study)) (Broecker and Peng, 1982), therefore 'steady state' is used rather than saying the reservoirs were in equilibrium. Variations in the ocean pCO_2 are a result of a complex relationship between seasonal temperature cycles, mixing dynamics of the upper ocean, and biological production and consumption (Broecker and Peng, 1982; Nightingale and Liss, 2006). There has been an increase in atmospheric CO_2 from approximately 280µatm before the industrial revolution to approximately 384.5µatm (from this study, 2009). Atmospheric CO_2 has increased mainly because of fossil fuel combustion, as well as land use practices such as deforestation. Of the approximate 8.7±0.5 Pg C produced anthropogenically each year, about 3 Pg C stays in the atmosphere, while the ocean and terrestrial systems store approximately 2.2±0.4 Pg C and 2.6±0.7 respectively (Le Quéré et al., 2009).

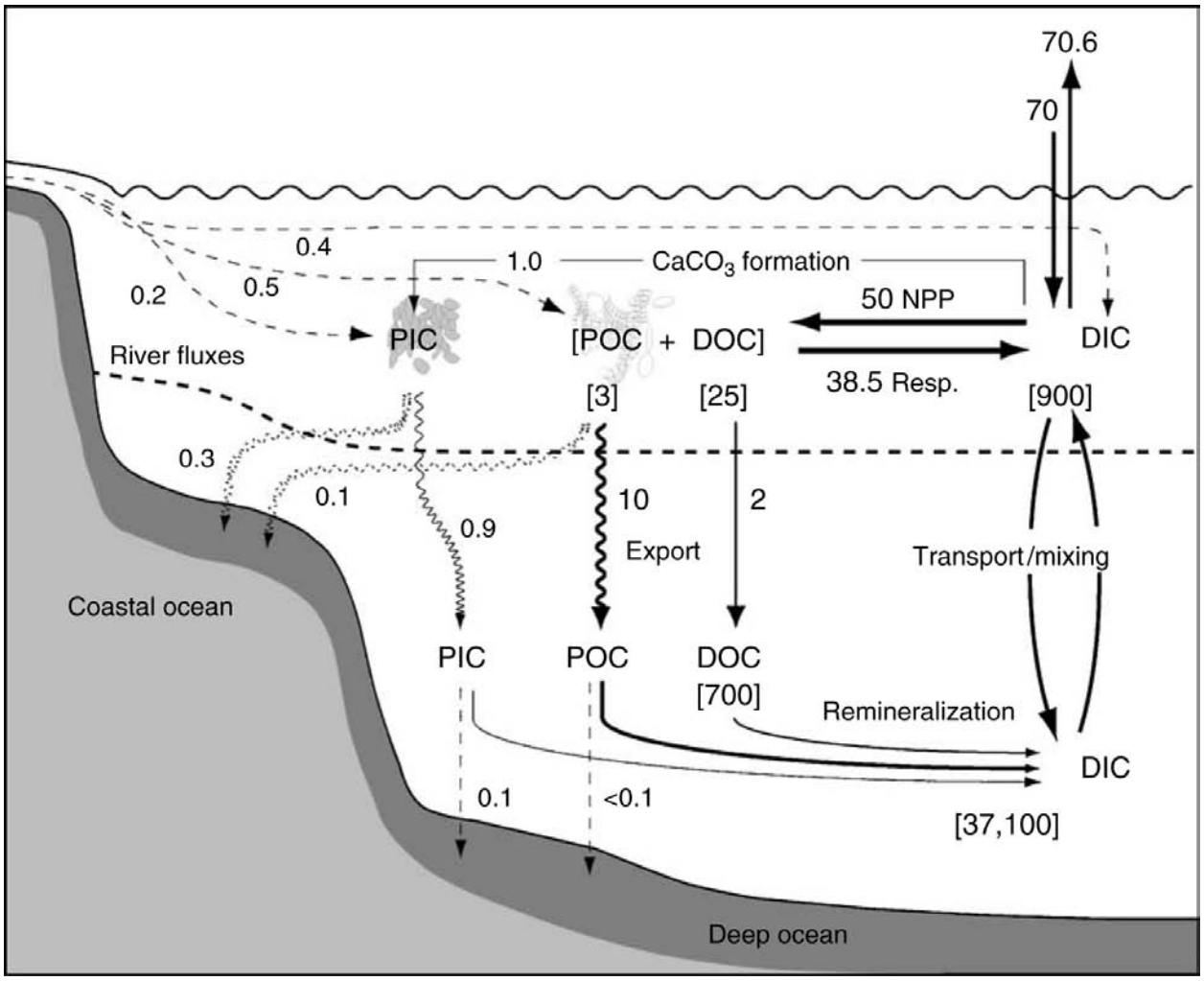

Figure 1: Schematic representation of the pre-industrial ocean carbon cycle. Fluxes (arrows) are in Pg C.year^{-1} (petagrams of carbon: 1Pg = 1x10^{15}g) and reservoir sizes (numbers in square brackets) are in Pg C. Abbreviations: PIC, particulate inorganic carbon; DOC, dissolved organic carbon; DIC, dissolved inorganic carbon. (Sabine and Feely, 2007)

The total exchanges across the air-sea interface are estimated to be approximately 70Pg C/year (Sabine and Feely, 2007). The pre-industrial ocean is estimated to have a small net flux (approximately 0.6Pg C/year) out of the ocean. Model studies suggest that prior to the 1800's, the Southern Ocean was a net source of CO_2 to the atmosphere (Sabine and Feely, 2007).

Human interference with the carbon cycle seems small compared to the natural fluxes of carbon between the atmospheric, ocean and terrestrial systems. Analysis of the air trapped in ice cores shows that over the past 160 000 years, atmospheric CO_2 has varied from under 200µatm at the height of the last glaciations to 260 and 300µatm during inter-glacial periods (Post et al., 1990). Sabine and Feely (2007) state that anthropogenically produced CO_2 accumulation in the ocean over the last 200 years is generally 3% of the natural carbon in the surface ocean. This makes it complicated to distinguish anthropogenic CO_2 from the observed natural variability. Models and observations suggest that the increasing CO_2 levels are causing an increase in the global temperature, although this has not yet been unequivocally established (Wanninkhof and Feely, 2004).

1.1.1 The Ocean as a CO_2 Reservoir

Oceans currently take up about 25-30% of the annual anthropogenic CO_2 emissions (2±1Pg C) (Feely et al., 2004; Sabine et al., 2004; Canadell et al., 2007; Arrigo et al., 2008; Doney et al., 2009; Monteiro et al., 2010). In the long-term, the oceans can hold more carbon than the other reservoirs because most of the CO_2 that diffuses into the oceans dissolves in seawater to form carbonic acid (~1%) and its dissociation products bicarbonate (~90%) and carbonate ions (~9%) (Feely et al., 2001). This process also decreases the pH of seawater, known as ocean acidification. Oceanic carbon uptake slows the growth rate of atmospheric CO_2 and as a result reduces the magnitude of human driven climate change (Wanninkhof et al., 2009), but in doing so also lowers the surface-water pH particularly in areas where DIC/Total Alkalinity ratio is high. The resulting ocean acidification can lead to significant disruption of marine ecosystems (Feely et al., 2004; Feely et al., Doney et al., 2009) by either changing calcification rates or marine organisms or affecting the metabolic physiology of the marine organisms (Fabry et al., 2008). Carbon dioxide is produced and consumed in large quantities by biogeochemical processes in the oceans. Biological production removes carbon from

surface waters to form organic material. As organisms die, they decompose and release carbon dioxide into the water (Sabine and Feely, 2007).

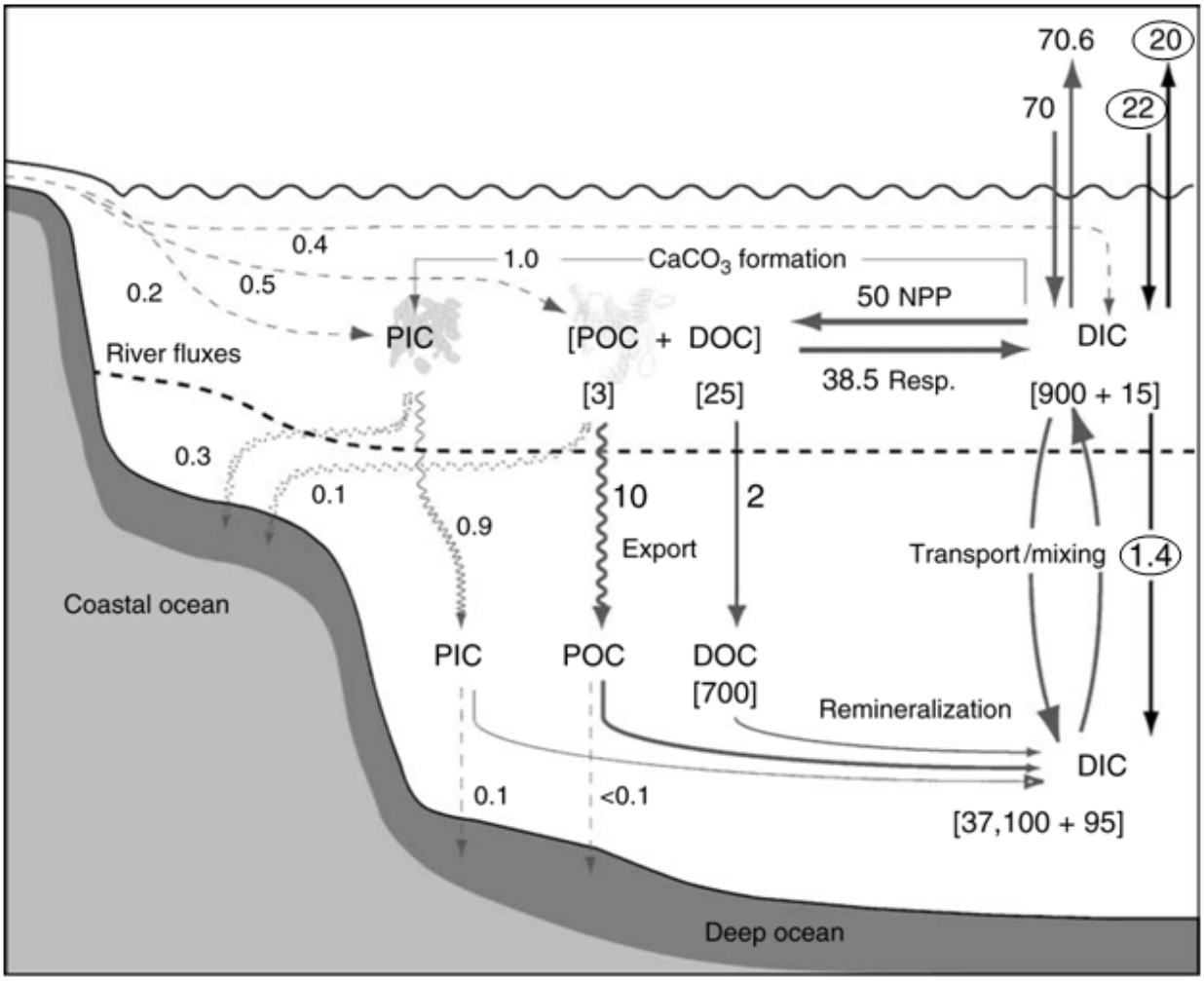

Figure 2: Schematic representation of the ocean carbon cycle with pre-industrial fluxes and reservoir sizes (upright) and average values for the 1980s and 1990s (circled). Fluxes (arrows) are in Pg C/year and reservoir sizes (numbers in square brackets) are in Pg C. (Sabine and Feely, 2007)

Figure 2 shows that the role of the ocean in the global carbon cycle has changed from being a net source of CO_2 to the atmosphere to a net sink of CO_2 of approximately 2PgC/year.

There is an understandable scientific interest in the changing ocean uptake of CO_2 and Le Quéré et al., (2007) has proposed that the Southern Ocean fluxes may be changing. There are three main reasons why it is important to measure ocean – atmosphere CO_2 fluxes accurately: 1) Ocean plays a key role in mitigating anthropogenic CO_2 emissions and emissions reductions targets need to be aware of any changes in that role. 2) The oceans regulate the nature variability in the atmospheric CO_2. 3) Terrestrial CO_2 fluxes are still derived from the difference between the more precisely determined emissions, the atmospheric reservoir and the ocean uptake (Monteiro et al., 2010). Fluxes can be derived using the gradient in pCO_2 between the ocean and the atmosphere, as well as the solubility of CO_2 in the ocean, and the rate at which the gas is exchanged. This approach makes it necessary to measure air-sea gas exchange accurately in order to be able to derive the flux of CO_2. Although there are experimental methods to measure gas exchange transfer these are impractical to use systematically and on a large scale therefore other proxies (wind) that are easier to observe are preferable.

There are different models used to calculate the gas transfer coefficients via proxies most of which try to establish a relationship between wind speed and gas transfer rates. Examining the extent to which they make this approximation and the inherent uncertainties is the key objective of this project.

1.2 Ocean – Atmosphere CO_2 Fluxes

Currently no direct or accurate measurement of a flux of a gas fCO_2 across the air-sea boundary has been made at sea, mostly because of technical limitations (Nightingale et al., 2000). Therefore air-sea CO_2 fluxes are derived as a function of the gas transfer velocity, *k* (which is a primary function of wind), solubility, α (which is dependent on

temperature), and the difference between the ocean and atmospheric CO_2 concentration, ΔpCO_2 (Sarmiento and Gruber, 2006).

$$F_{CO_2} = k \propto \Delta pCO_2 \quad (1)$$

PCO_2 in mixed-layer water that exchange CO_2 directly with the atmosphere is affected by temperature, total CO_2 concentration and alkalinity. Temperature is primarily regulated by physical processes, while total CO_2 concentration and alkalinity are controlled by biological processes and the upwelling of subsurface waters that are rich in CO_2 (Feely et al., 2001; Takahashi et al., 2002). Globally, the impact of biological drawdown on surface water pCO_2 is similar in magnitude to the effect of temperature, but the two effects can often balance each other out (Sarmiento and Gruber, 2006). The increasing effect of summer warming on seawater pCO_2 is commonly opposed by the lowering effect of photosynthesis during the summer months. The decreasing effect on pCO_2 of winter cooling of the water is counteracted by the increase in the total CO_2 concentration caused by the winter convective mixing of deep waters that are rich in CO_2 (Sweeney et al., 2002). As a result, the distribution of pCO_2 in surface waters in space and time, and therefore the air-sea CO_2 flux, is governed by compensation between the changes in the temperature of the seawater, net biological utilisation of CO_2 and the upwelling flux of subsurface waters that are rich in CO_2 (Feely et al., 2001).

Takahashi et al., (2009) constructed a climatological mean distribution of surface water ΔpCO_2 over the global open oceans for a reference year 2000 based upon 3 million measurements of surface water pCO_2 obtained from 1970 to 2007 by a large number of international investigators. The climatology excluded data from El Niño years, as well as data made in coastal waters within 200km from the shore. El Niño has an effect on the upwelling of CO_2 rich waters and advection of CO_2 depleted waters, which in turn have an effect on the interannual variability of air-sea CO_2 fluxes. Seasonal changes

expressed as monthly means in ΔpCO_2 were presented for the Atlantic, Pacific, Indian and Southern Oceans. This study will focus on the Takahashi et al., (2009) results for the temperate South Atlantic Ocean and the Southern Ocean during the summer season.

Ocean circulation also results in air-sea exchange of CO_2 because the solubility of CO_2 is temperature dependent. Cooling increases solubility so that CO_2 is under saturated with respect to the atmosphere and causes a net flux of CO_2 from the atmosphere into the ocean. There is a net flux of CO_2 from the ocean into the atmosphere if the water temperature increases (Nightingale and Liss, 2004).

The Southern Ocean covers 30% of the world's ocean (Wanninkhof et al., 2004), and it is within the Southern Ocean that most of the deep waters of the world are ventilated by exchanging carbon dioxide with the atmosphere (Anderson and Smith, 2001). It is, nevertheless, the most under-sampled basin, leading to a lack of knowledge about its magnitude and trends (Liss et al., 2004). There are large differences in the air-sea CO_2 fluxes derived from gas transfer velocities and ΔpCO_2 and those established from atmospheric observations and models. This is because of the lack of pCO_2 data and the parameterisation of gas exchange and wind speed (Wanninkhof et al., 2004). The discrepancies could be a due to the Southern Ocean being characterised by high winds, and also because the current parameterisation of gas exchange with wind speed does not account properly for bubble mediated gas transfer that dominates exchange fluxes at high wind stress (Wanninkhof et al., 2004).

The CO_2 flux is a function of gas transfer velocity (k), solubility (α) and the change in the partial pressure of CO_2 between the ocean and the atmosphere (ΔpCO_2). Solubility and ΔpCO_2 can be measured *in situ*, but there is an uncertainty in the measurement of gas transfer velocity.

1.2.1 Experimental Direct Determination of the Gas Transfer Velocity

Measurements of gas transfer coefficients *k* have been made either directly or indirectly in wind-wave tunnels, as well as with the use of *in situ* tracers in the field (Woolf, 2005; Sarmiento and Gruber, 2006). A comparable number of attempts have been made to place the measurements in a model framework (Sarmiento and Gruber, 2006). The measurements and theory implies that the gas transfer velocity is a proxy of the level of turbulence near the air-sea interface. The level of turbulence is mainly dominated by wind stress at the boundary, but wind by itself cannot completely control the turbulence. Other factors include bubble entrainment (Schudlich and Emerson, 1996), temperature and humidity gradients (Nightingale et al., 2000), surfactants (Sarmiento and Gruber, 2006), friction velocity, fetch, rain (Wanninkhof, 1992; Wanninkhof and McGillis, 1999; Wanninkhof et al., 2009) and chemical enhancement (Kuss and Schneider, 2004). Currently wind is the most useful variable available, because it is a remotely-sensed product that can be obtained on a global scale (Wanninkhof and McGillis, 1999; Nightingale et al., 2000), which is why it has been used in this study. Gas transfer velocity may vary with wind speed, but the relationship between gas transfer rates and wind speed changes from one model to another (Broecker and Peng, 1974; Liss and Merlivat, 1986; Wanninkhof, 1992; Wanninkhof and McGillis, 1999; Nightingale et al., 2000). Different models parameterise the complexity of gas transfer mechanisms in different ways using wind as a directly observable variable.

There have been many experiments measuring gas exchange in wind tunnels, lakes and in the ocean. Laboratory studies reveal that gas exchange is sensitive to a variety of conditions whose natural distribution is difficult to reproduce accurately in a laboratory environment. *Inter alia,* lack of boundary conditions and the fact that they are fetch limited environments. Methods have been developed to study gas exchange under more realistic conditions in the field (Sarmiento and Gruber, 2006). The most common are listed and will be introduced below.

1. Radiocarbon (^{14}C) (Broecker and Peng, 1974)
2. O_2/N_2 (Nightingale and Liss, 2004)
3. Radon (Broecker and Peng, 1974; Sarmiento and Gruber, 2006)
4. Deliberate tracer experiments (Nightingale et al., 2000)
5. Direct covariance (Wanninkhof and McGillis, 1999)

Radiocarbon is produced naturally in the atmosphere, and is then transferred across the air-sea interface into the oceans as $^{14}CO_2$ (Broecker and Peng, 1974). Assuming the system is in a steady state, the mass of ^{14}C from the atmosphere must be balanced by the decay of ^{14}C in the water column (Nightingale and Liss, 2004) and the magnitude of the mass can be calculated using a budgeting technique. The global mean gas transfer velocity measured using this method is approximately 20cm.h^{-1} (Sarmiento and Gruber, 2006). This allows a reasonable estimate of globally averaged CO_2 uptake by the oceans, but it yields little information on how *k* varies in time and space or how to calculate *k* for other gases (Nightingale et al., 2000).

The O_2/N_2 technique is used to derive regional estimates of *k*, and is dependent on the use of CO_2 data to correct for the effects of land/atmosphere fluxes on O_2/N_2 ratios, and on an atmospheric transport model to simulate oceanic fluxes. It is based on high precision measurements of atmosphere O_2/N_2 ratios from the baseline sites positioned around the world (Nightingale and Liss, 2004).

The radon isotopic method was first proposed by Broecker and Peng in 1971. It yields gas exchange rates for local areas of the ocean integrated over days, rather than the radiocarbon approach which is for large areas over many years. Radon gas is generated within the ocean by the decay of dissolved radium and results in a loss of

radon from the surface mixed layer to the atmosphere before it has undergone radioactive decay (Broecker and Peng, 1974). A mass budget can be made of the radon that has been lost by assuming steady state with the deeper waters, and then a value for *k* can be determined (Nightingale and Liss, 2004). The average global gas transfer velocity determined using this method is 18cm.h^{-1} (Sarmiento and Gruber, 2006). This technique also assumes that the effects of horizontal transport are negligible and that the sea state conditions remain constant for more than a mean lifetime of a radon atom (approximately 6 days) (Broecker and Peng, 1974). The time scale of the measurement of radon profiles is problematic when one considers the difficulty of keeping factors like wind and surface tension constant over the period of measurements (Broecker et al., 1978).

In the dual tracer experiments, inert volatile tracers are deliberately added to bodies of water in order to determine *k* via water-based mass budgeting techniques (Nightingale and Liss, 2004). Sulphur hexafluoride (SF_6) is most commonly used as the tracer in these experiments because it can be detected at low concentrations, there is a lack of production and removal processes in the water column and its relative ease of analysis (Nightingale and Liss, 2004). SF_6 is inert and present in water at very low concentrations, this results in an excellent signal-to-noise ratio (Wanninkhof et al., 2009). It was widely used to estimate gas transfer in contained systems such as wind tunnels and lakes, where the decrease of total mass of the tracer can be accurately determined and used to estimate *k*. When used in the open ocean, dilution of SF_6 will occur through gas exchange and by advection and dispersion, therefore the surface area and volume exposed to the atmosphere will change (Nightingale and Liss, 2004). This means that for correct determination of *k*, a second tracer needs to be used in addition to SF_6. Ideally a non-volatile tracer should be used because its decrease in concentration over time would be affected only by advection and dispersion. Helium-3 (^{3}He) meets the same standard of inertness, low background and low detection limits as SF_6 (Wanninkhof et al., 2009). It can be used as the additional tracer, and it diffuses quicker than SF_6. The two gases are released in a constant ratio, and the values can

be calculated from the change in the two tracers over time, and later correlated with environmental variables (Nightingale and Liss, 2004). The SAGE experiment (SOLAS Air-Sea Gas Exchange) was performed in the Southern Ocean and used the $^{3}He/SF_6$ dual tracer technique (Ho et al., 2006). In the opinion of Wanninkhof et al., (2004), the dual-tracer method is a powerful technique, as it a robust integrative method to estimate gas transfer over a period of days. A limitation of using a dual-tracer is that the time interval over which the measurements are made is usually 8-72 hours and that only a small number of data can be obtained per experiment (Nightingale and Liss, 2006). The experiments were performed in fetch limited environments, and this could introduce a bias in the resulting parameterisation, but Wanninkhof et al. (2009) state that is not clear. The global average gas transfer velocity determined using the dual-tracer method is 13.7cm.h^{-1} (Sarmiento and Gruber, 2006).

The direct covariance or eddy correlation technique is based on the very fast and accurate measurement of atmospheric gas concentrations and correlations with the simultaneously measured wind velocity (Nightingale and Liss, 2004). A covariance measurement takes approximately 30 minutes to be completed and means that episodic high wind events can be captured (Wanninkhof and McGillis, 1999). Only fluxes of CO_2 can be measured using this method, although it has been successful in measurements of gases where the gas transfer velocity in the air dominates. An experiment located on a stable platform, which minimised problems with flow distortion and motion contamination, in the North Sea showed the range in the CO_2 gas transfer velocities determined using more established techniques such as deliberate tracers and direct covariance was decreasing, mostly because of improvements in the sensitivity of CO_2 analysers (Nightingale and Liss, 2004).

1.2.2 Gas Transfer Velocity derived from the proxies: sea surface microlayer thickness and wind

Gas transfer velocity is a function of wind speed and a dimensionless parameter called the Schmidt number. Five models are used in this study to examine the sensitivity of the gas transfer velocity to the assumptions and limitations used to derive each model.

1. The Stagnant Film Model (Broecker and Peng, 1974)
2. Liss and Merlivat (1986)
3. Wanninkhof (1992)
4. Wanninkhof and McGillis (1999)
5. Nightingale et al. (2000)

The simple 'Stagnant Film Model' was first presented by Whitman (1923) and later explained in Broecker and Peng (1974). It investigated the relationship between the sea surface film thickness and wind velocity. It is the simplest of all the models used in this project because it takes only two types of wind into account by using the thickness film separating the two well mixed layers as a variable. The thinner the film, the greater the agitation of the sea state meaning high wind speeds, the alternative condition is calm or low wind speed which would mean a thicker film. The piston velocity (gas transfer velocity) is the molecular diffusivity of CO_2 (D) [$cm^2.s^{-1}$] divided by the thickness of the film (z) [μ]. The model assumes that there is a stagnant film separating two bodies of air and water that are well mixed. This means that the concentration of the gas is uniform throughout each of the respective bodies. It also assumes that mass transfer occurs only by molecular diffusion through the stagnant film, and the mass transfer through the film occurs at a steady state. A limitation of this model is that the film thickness cannot be measured, therefore it is not practical in the physical environment. The next four models use the Schmidt number as a variable for working

out the gas transfer velocity because they take the sea state into consideration. The kinematic viscosity of water changes with temperature, and when kinematic viscosity is divided by the molecular diffusivity of a gas it results in the dimensionless Schmidt Number

The second model is from Liss and Merlivat (1986). They use three regimes of wind strength where different physical processes appear to be controlling gas exchange: smooth surface regime, rough surface regime, and breaking wave regime. The relationship is linear for the three regimes, and is based on tracer experiments conducted during a lake study, using the tracer SF^6, and data obtained in laboratory experiments for the breaking wave regime (winds above 13.5m.s^{-1}) (Nightingale et al., 2000). This relationship was developed specifically for CO_2 exchange (Wanninkhof, 1992).

The quadratic (non-linear) relationship derived by Wanninkhof (1992) uses the trend of gas transfer with wind speed. This was conducted in wind-wave tanks to determine the general shape of the curve and has been chosen such that it goes through the origin and gives a global average transfer velocity equal to that derived from the bomb ^{14}C data. This method assumed a Rayleigh distribution of the wind speed with a mean of 7.4 ms^{-1} (Matthews, 2000; Sweeney et al., 2007). It is only used for steady winds.

The fourth model proposed by Wanninkhof and McGillis (1999) is a cubic relationship based on CO_2 covariance measurements collected during the Gas Ex-98 cruise in June 1998. It is suitable for steady, short-term winds. With respect to long term winds, a different equation must be used. For the purpose of research done in this project, only the equation for steady, short-term winds has been be used. This technique is based on very fast and accurate measurements of atmospheric gas concentrations and

correlation with the simultaneously measured vertical wind velocity (Jones and Smith, 1977, cited in Nightingale and Liss, 2006).

The final model, Nightingale et al. (2000) is a quadratic relationship based on the $^3He/SF_6$ tracer method and was used in two cruises in the coastal ocean of the North Sea during February 1992 and February 1993.

1.2.3 Uncertainties of Global Air-Sea CO_2 Fluxes

The uncertainty of CO_2 fluxes on the global scale is considerable, currently estimated at 40-50% (Monteiro et al., 2010). In order for the data to be useful for global budget calculations and the resolution of inter-annual trends it needs to be at 10-15%. Estimates of oceanic CO_2 uptake can fluctuate by 30-50% when using different parameterisations of gas exchange as a function of wind speed and assuming the same wind field (Griessbaum et al., 2009). This is because the parameterisations are subject to many uncertainties that can be caused by, for example measurement errors, or sea state. When using a quadratic dependence between gas transfer velocity and wind speed, the relative wind difference in the wind speeds in the Southern Ocean results in a difference in the global mean air-sea CO_2 flux of approximately 25% (Wanninkhof et al., 2009).

Uncertainties in calculating gas transfer velocities also occur as a result of high wind speeds (usually greater than $22 m.s^{-1}$), because at high wind speeds bubbles are believed to play an important role in gas transfer (Nightingale and Liss, 2004; Wanninkhof et al., 2004; Sarmiento and Gruber, 2006; Ho et al., 2006; Wanninkhof et al., 2009). Bubble clouds increase the effective ocean surface area available for gas transfer, and therefore increase air-sea gas fluxes (D'Asaro and McNeil, 2008).

1.3 Purpose of this Study

The problem in the determination of air-sea CO_2 fluxes is that there are many different parameterisations used in the calculation of gas transfer velocity each of which makes particular assumptions to approximate the non-linear relationship between wind and gas transfer rates. In this study we will look at the differences in the different gas transfer models and their response to different wind speeds, and the uncertainty of the wind speed product as a result of their assumptions and limitations. We will also compare the results of the regional observed in the CO_2 fluxes in the Southern Ocean, determined using the five different relationships between *k* and wind speed, with those from Takahashi et al., (2009).

Chapter 2:

DATA AND METHODS

This project utilises three main sources of data in the calculation of the gas transfer velocity and the flux of carbon dioxide through the air-sea interface. They are the fugacity of CO_2 (fCO_2), scatterometer data and physical properties of seawater. The air-sea gas transfer velocity is usually parameterised by wind speed, and scatterometers provide global observations of wind speed and direction on a daily basis. The physical properties of seawater include temperature and salinity. Various gas exchange models have then been used in the determination of the CO_2 air-sea gas flux.

2.1 Data Collection

The data was collected on the three annual RV SA Agulhas relief cruises to Gough Island in spring and to Antarctica in summer and Marion Island in autumn from 2008 to 2009. The Antarctic cruise included a buoy run to South Sandwich Islands and South Georgia.

Table 1: Cruise Information of the RV Agulhas.

Cruise	Destination	Months	Season
Gough Relief Cruise	Gough Island	Beginning of September- beginning of October 2008	Austral Spring
SANAE Relief Cruise	Antarctica, South Georgia, South Sandwich Islands	Mid-December 2008 – beginning of March 2009	Austral Summer
Marion Relief Cruise	Marion Island	Beginning of April – mid- May 2009	Austral Autumn

The first cruise that is used in this study left from Cape Town harbour at the beginning of September 2008 and went to Gough Island and returned to Cape Town in early October 2008, and represents data collected in the austral spring. The second cruise left from Cape Town on 23 December 2008 and sailed along the Greenwich Meridian to Antarctica. The SA Agulhas then went on a buoy-run to the South Sandwich Islands

and South Georgia before returning to the Antarctic Continent, and then travelling back to Cape Town harbour at the beginning of March 2009. The data therefore are representative of austral summer conditions. The last cruise was to Marion Island from Cape Town, departing at the start of April 2009 and arriving back in Cape Town in the middle of May 2009, with data for the austral autumn.

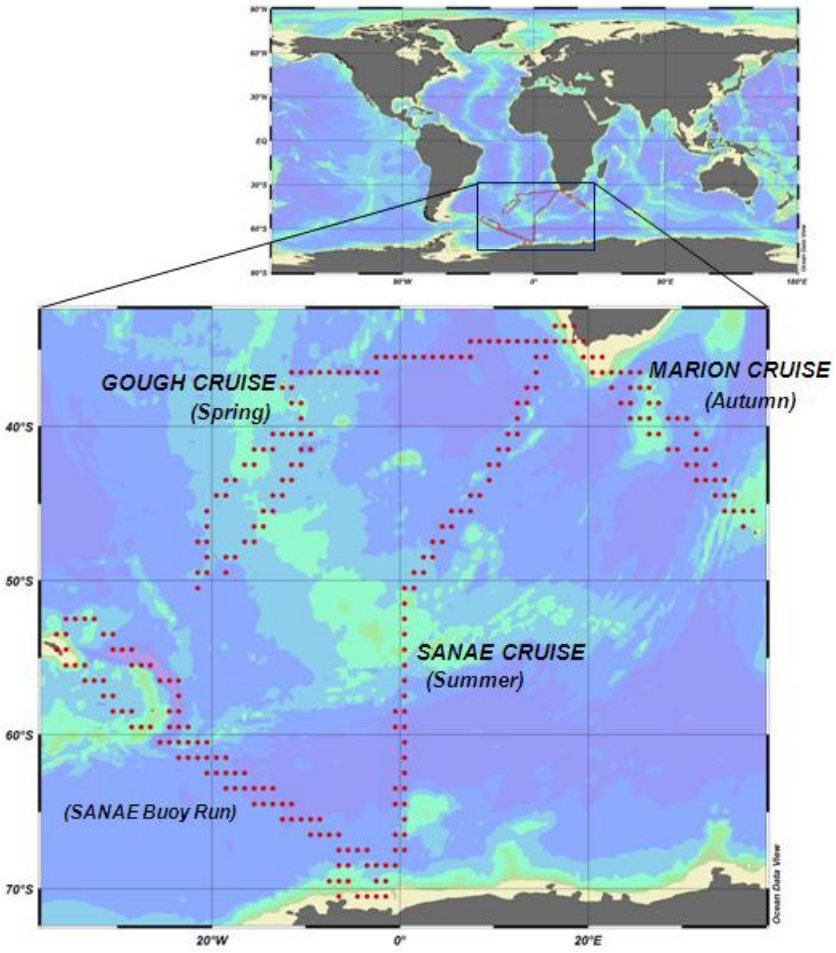

Figure 3: Map with the three separate cruises tracks done during data collection on the SA Agulhas.

2.1.1 pCO_2/xCO_2

The xCO_2 data was collected using a General Oceanic GO8050 autonomous underway pCO_2 measuring system positioned in a laboratory near the stern of the ship. The design and mode of operation of the system was formulated during a workshop at the NOAA Atlantic Oceanographic and Meteorological Laboratory (AOML) in Miami in 2002 (Pierrot et al., 2009). Its design overcomes the problem that pCO_2 measurement systems installed on stationary platforms (e.g. buoys) supply good temporal, but limited spatial information. The system is small with all the components closely packed, and is comprised of sampling hardware, an analysis system, and a data logging/transmission system. It analyses three types of gases: the standards, the atmospheric air, and the headspace gas from the equilibrator. It operates by directing sea water flow (at a rate of 1.5-2l.min^{-1}) through a chamber (the equilibrator) where the CO_2 contained in the water equilibrates with the gas present in the chamber (the headspace gas). To determine the CO_2 in the headspace gas, it is pumped through a non-dispersive infrared analyser, which measures its CO_2 mole fraction (xCO_2) instantaneously, and then returned to the equilibrator to form a closed loop.

The analyser was calibrated using four CO_2 standard gases at regular intervals (up to six standards can be used, but there were only four used in collecting the pCO_2 values in this project). Typical flow rates for standards are in the range of 50-60ml.min^{-1} for 4 minutes to allow adequate flushing of the lines while conserving the gases as much as possible. Periodically, atmospheric (dry) air is also pumped through the analyser and its CO_2 mole fraction is measured. The atmospheric air is pulled to the system at a high flow rate (0.5-2l.min^{-1}). Most of this flow is vented immediately after the pump in order to minimise the residence time of the atmospheric air in the [usually] very long gas line. The air that is not vented is dried in a condenser. This partially dried air flushes a chamber that is vented and remains at ambient temperature. The dried air inside the chamber is used as the counter flow in the Nafion® tubing. A vacuum pump pulls the

dried air from the chamber first through a fixed restrictor and then through the Nafion® tubes, thus creating an absolute pressure difference and corresponding partial pressure gradient for water vapor across the membrane. When atmospheric air is measured, some of the partially dried air (80–100 $ml.min^{-1}$) is pushed through a Nafion® tube, the analyzer and out of a vent instead of flushing the chamber.

The headspace gas, when being measured, is circulated in a closed loop through the analyzer at a rate similar to that of the atmospheric air (80–100 $ml.min^{-1}$). It is dried first in the condenser, then in a Nafion® tube prior to entering the analyzer and being returned to the equilibrator. Typically, the water mole fraction (xH_2O) in the dried gas is about two parts per thousand (ppt), which corresponds to a dew point temperature of about -20°C. At intervals determined by the user, the liquid water condensed out of the sample air streams is removed by peristaltic pumps (Pierrot et al, 2009).

The pCO_2 measuring system can run autonomously on ships because it shuts down before the data is unnecessarily modified, and then sends the data via satellite daily. All the cruises had technicians on board the SA Agulhas to repair any problems that occurred during the voyages, but the system would often shut down during times when the sea became rough, causing there to be gaps in the data. The atmospheric gas and standardised gases are run through the analyser approximately every four hours, and between that the equilibrator gas is read at irregular intervals of just over one minute.

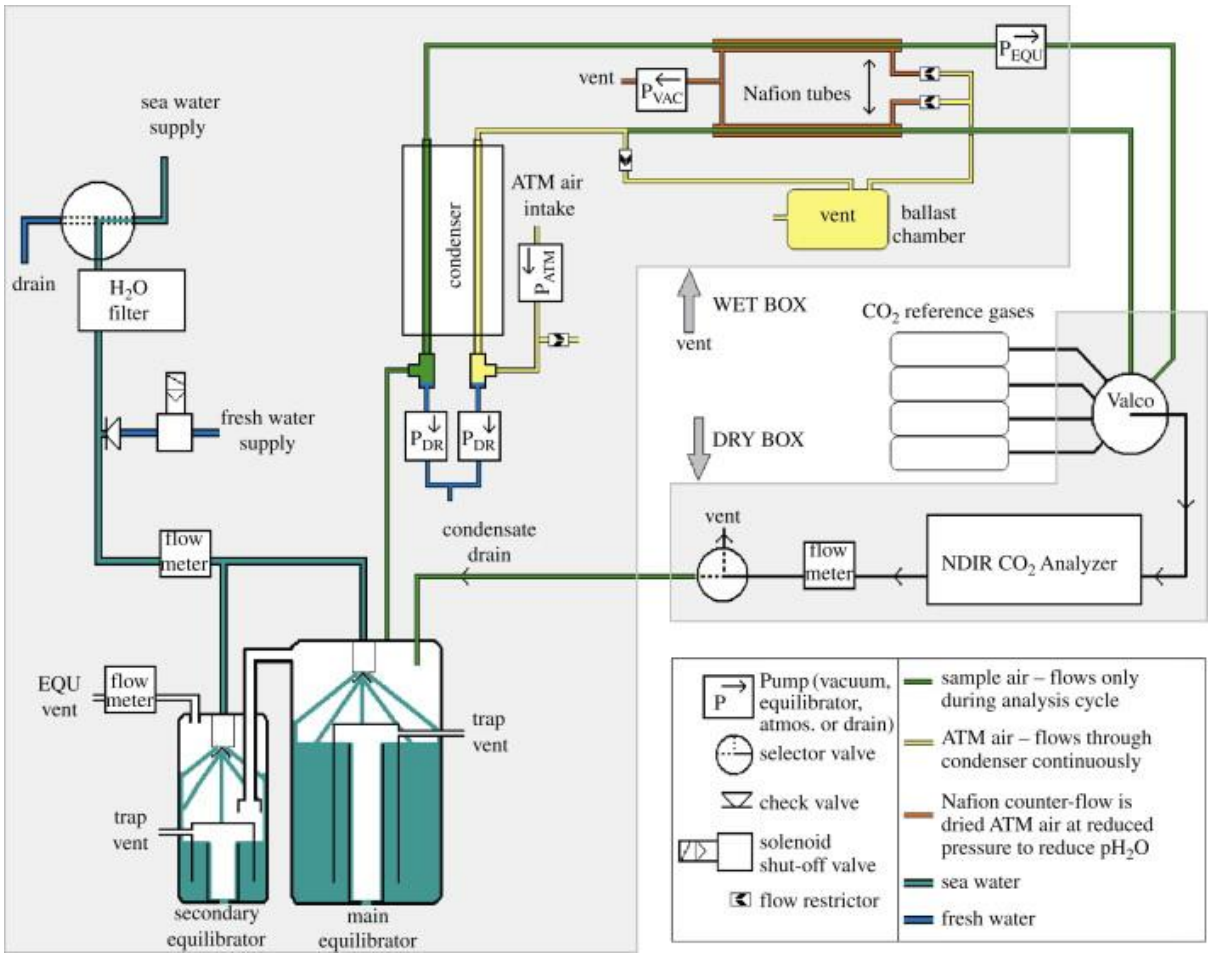

Figure 4: Schematic of the underway pCO_2 system used on the RV SA Agulhas (Pierrot et al., 2009)

There were corrections that needed to be applied to the pCO_2 system's original output for it to become comparable and usable. The output produced conductivity instead of salinity, so the conductivity data for all three cruises was converted into practical salinity (SAL78) using the conversion in the UNESCO Technical Papers in Marine Science (1983). Sampling done during the SANAE trip was used to calibrate some of the external sensors on the system; salinity was corrected by correlating the data from the pCO_2 system with the discrete salinity samples done during the cruise, and then using the correlation equation to correct the salinity data from the pCO_2 system.

The original partial pressure of CO_2 (pCO_2), which is the product of the mole fraction and total pressure, was corrected for non-ideality of the gas with respect to molecular interactions between CO_2 and other gases in air in order to get the fCO_2. The flux of CO_2 across the air-sea interface is directly proportional to the difference in fCO_2 between the ocean and the atmosphere. The temperature and pressure inside the equilibrator at the time of the equilibration are needed order to calculate fCO_2 correctly. The sea surface temperature and atmospheric pressure (needed for the atmospheric fCO_2 determinations) are also required. The pressure inside in the infrared analyser should also be measured as it is used by the analyser to correct the analogue signal for any pressure effects.

The measurement error of ΔfCO_2 is 1µatm, this is due to the uncertainty of the method, and would be just as important at a high ΔfCO_2 and at a low ΔfCO_2.

2.1.2 Physical Properties of Seawater

There are external sensors which measure the physical properties of seawater that is pumped through the system, as well as of the air around the system. The properties that are used in this project are listed in the table below. TEOS-10 (Thermodynamic Equation of Seawater 2010) was not used in this study as this study was started before it was practiced.

Table 2: Physical properties from the pCO_2 system that are used

Variable	Units	Reason for use
Temperature	°C	The solubility of carbon dioxide increases as the temperature decreases, cold water can hold more CO_2 than warm water. Temperature is also used in determining the Schmidt Number. The temperature has an error of 0.05°C.
Salinity	Dimensionless	As salinity increases solubility of carbon dioxide decreases.

The data was averaged to five minute intervals, making it easier to compare to, and use with other data sets. All of the sensors have been averaged from the combined data of the equilibrator, atmospheric and standardised gases and the oceanic pCO_2 that had been averaged only from the equilibrator file was merged into the full data set of sensors averaged from all three of the gas files. The fCO_2 values for seawater and atmosphere have been corrected from the original data and were also averaged separately and added to the complete data set, as they were received at a much later date.

2.1.3 Gas Transfer Rates: Winds

The daily zonal (u) and meridional (v) components of surface winds have been extracted from the SeaWinds dataset over the relevant periods. This product is a blended and gridded dataset merging different satellite estimates (up to six, including Scatterometers (QuikSCAT), SSMIs, TMI and AMSR-E) observations, on a global 0.25-degree grid and is described e.g. in (Zhang et al., 2006). It has been obtained from http://www.ncdc.noaa.gov/oa/rsad/blendedseawinds.html and re-gridded on a one

degree grid. Two different products were used: The realtime product (the wind direction is given by the ERA 40 reanalyses), and near-realtime (wind direction is given by NCEP/DOE II reanalyses). The realtime product is used for the SANAE cruise, but was not available for the time of the Gough and Marion cruise, so the near realtime product is used. Switching wind speed products between cruises will not add any error to final product. The wind speed measurements are in the range of 3-20m.s^{-1}, with an accuracy of 2m.s^{-1} (Perry, 2000).

2.1.4 Ship Track Interpolation

The missing coordinates in the ship tracks have been linearly interpolated (see image below). The original coordinates are in red, the interpolated coordinates in blue.

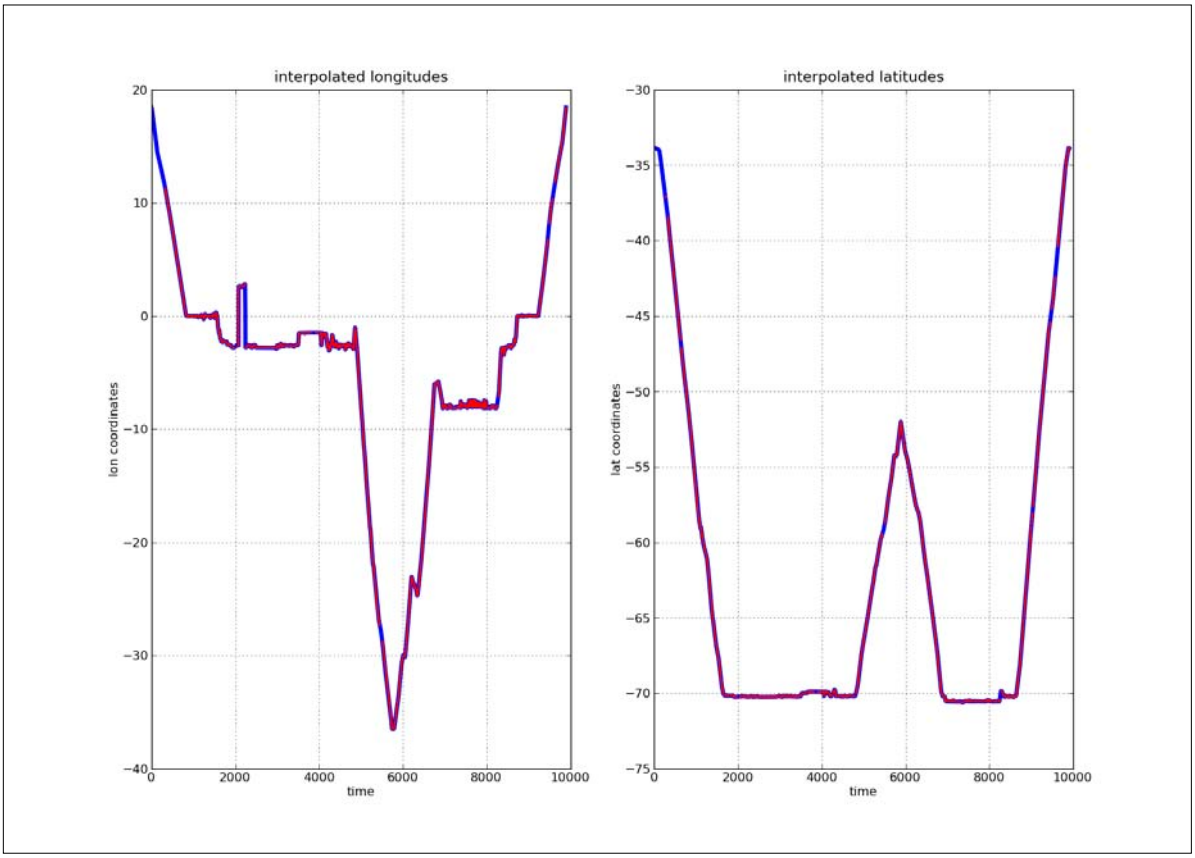

Figure 5: Linear interpolation of the latitudes and longitudes used in filling in missing coordinates. The original coordinates are red, and the interpolated coordinates are blue.

For each coordinate in the cruise data, the corresponding daily zonal (u) and meridional (v) components of surface winds (winds at 10m height) (i.e. the values corresponding to the grid-point including the cruise coordinates) have been extracted for the day of, as well as the nine previous days (only wind values for the day of observation, as well as the six days prior to that day were used in this project). This is so that the winds were weighted and then averaged, with the day of the observation having the highest weighting and the winds on the day six days before that with the lowest weighting (refer to Appendix 1 for the values of weightings used). This was done so that if there had been strong winds throughout the week before the day and then weak winds on the day (or *vice versa*) it would not shift the mean and produce a large error. The winds from the day of the data collection were also used separately.

The data was then averaged into the one degree blocks from the wind speed product. This is so that the results can be made to determine any geographical differences that might occur throughout cruises and not just differences in the gas exchange models. Regional averages were then made according to frontal zones for comparison.

2.2 Data Analysis

2.2.1 Gas Transfer Velocity

Once all the data was collected, quality controlled and calibrated, the calculations to work out the gas transfer velocity (*k*) (units in $cm.h^{-1}$) could commence. Five models were used in this project,

1. The Stagnant Film Model (Broecker and Peng, 1974)

$$k = \frac{D}{z} \quad (2)$$

D = molecular diffusivity [$cm^2.s^{-1}$]

z = thickness of film [μ]

z is affected by the agitation for CO_2 in seawater: high agitation = 129μ

low agitation = 311μ

2. Liss and Merlivat (1986)
   a) For a zonal component of surface wind speeds ($u \leq 3.6 m.s^{-1}$) (Smooth Surface or Boundary Layer Regime)

$$k_{600} = (0.17u)Sc^{-2/3} \quad (3.1)$$

b) For a zonal component of surface wind speeds ($3.6 m.s^{-1} < u \leq 13 m.s^{-1}$) (Rough Surface or Surface Renewal Regime)

$$k_{600} = (2.85u - 9.65)Sc^{-1/2} \quad (3.2)$$

c) For a zonal component of surface wind speeds ($u > 13 m.s^{-1}$) (Breaking Wave Regime)

$$k_{600} = (5.9u - 49.3)Sc^{-1/2} \quad (3.3)$$

3. Wanninkhof (1992)

$$k_{660} = 0.31u^2Sc^{-1/2} \quad (4)$$

4. Wanninkhof and McGillis (1999)

$$k_{660} = 0.0283u^3Sc^{-1/2} \quad (5)$$

5. Nightingale et al. (2000)

$$k_{600} = (0.222u^2 + 0.333u)Sc^{-1/2} \quad (6)$$

Models (2) to (5) use the Schmidt number as a variable in working out the gas transfer velocity. The Schmidt number (Sc) is determined from the ratio of the kinematic viscosity of water (v) and the molecular diffusivity (D) of the gas in seawater, and is used to scale the gas transfer velocity for different gases and under different physical processes (Sweeney et al., 2007). Gas transfer velocities are usually normalised to a common Schmidt number for CO_2 (either 600 for freshwater and 660 for seawater at 20°C) so that different physical conditions can be compared. The equation 7 used was taken from Wanninkhof '92. It is a non-dimensional number that is dependent on temperature.

$$Sc = A - Bt + Ct^2 - Dt^3 \quad (7)$$

(t in °C)

Where for CO_2: A = 2073.1

B = 125.62

C = 3.6276

D = 0.043219

It explains the differences in the rates at which individual gases pass through the air-sea interface at a given temperature and salinity (Jähne et al., 1984). The Schmidt number dependency of gas transfer velocity changes with the boundary conditions at the sea surface (Jähne et al., 2005). Direct measurements of the Schmidt number exponent *n* with dual tracer experiments (Jähne and Hauβecker, 1998) verified the change of *n* to ⅔ for a smooth surface, and to ½ for a rough, wave covered surface (Jähne et al., 2005). The Schmidt number exponent can be empirically related to the shape of turbulence decrease toward to interface (Jähne et al., 1987) This Schmidt dependency breaks down in situations with bubble entrainment (Wanninkhof et al., 2004).

It should be noted that it is assumed that for the smooth surface regime, *k* is proportional to $Sc^{-2/3}$ so that it is in agreement with the boundary layer models, and *k* is proportional to $Sc^{-1/2}$ for the regimes with higher wind speeds so that the surface renewal mechanisms dominate (Nightingale and Liss, 2006). In this model the Schmidt number has been normalised to 600. When it is not 600 there must be a discontinuity at u = 3.6m.s^{-1} (Matthews, 2000). The Liss and Merlivat model and the Nightingale et al. model have a Schmidt number that is normalised to 600, while the Wanninkhof and Wanninkhof and McGillis models have Schmidt numbers that are normalised to 660.

Wind is the second variable needed to calculate *k*. For each model, there is an equation using the wind on the day that the data was collected, as well as the average of the day and the six days previous to it, with each day given a weighting, with the day of data collection having the most weight. The weights are given in Appendix 1.

2.2.2 Air-Sea Gas Flux

Three variables are required to work out the CO_2 flux: solubility (α) in 'mol.kg^{-1}.at^{-1}', gas transfer velocity (*k*) in 'cm.h^{-1}' and ΔfCO_2 in 'µatm'.

$$F_{CO_2} = k \propto \Delta pCO_2 \qquad (1)$$

The gas transfer velocity has been described above, ΔfCO_2 was worked out by subtracting the atmospheric fCO_2 from the fCO_2 in the seawater, and solubility was worked out using the equation provided by Weiss (1974). Solubility is dependent on salinity and temperature.

$$\ln \alpha = A_1 + A_2\left(\frac{100}{T}\right) + A_3 \ln\left(\frac{T}{100}\right) + S\left[B_1 + B_2\left(\frac{T}{100}\right) + B_3\left(\frac{T}{100}\right)^2\right] \qquad (8)$$

(*T* in degrees Kelvin)

Where for CO_2: A_1 = -60.2409 B_1 = 0.023517

A_2 = 93.4517 B_2 = -0.023656

A_3 = 23.3585 B_3 = 0.0047036

To get the correct units, the variables used in the flux were altered so that they would lead to the correct units for the gas flux of 'mol.m^{-2}.day^{-1}'. *k* was changed from 'cm.h^{-1}' to 'm.day^{-1}' by multiplying the original result of *k* by 0.24, ΔfCO_2 was changed from

'µatm' to 'atm' by multiplying the answer by 10^{-6}, and the solubility, which was 'mol.kg^{-1}.at^{-1}' was multiplied by the density in order to convert to 'mol.m^{-3}.at^{-1}'.

The programmes used in manipulating the data and comparing the results include Matlab version 7.0.4, Microsoft Excel 2007, as well as Ocean Data View 4 (ODV). ODV has been the main programme used in plotting the results.

2.3 Limitations

There are limitations in the fCO_2 data as well as the scatterometer data because there are large gaps in both data sets. The pCO_2 system would stop logging for periods throughout the duration all three of the cruises, it would also disconnect from the GPS system, and would not log the position of the ship. During the cruise to Gough Island in September 2008, the pCO_2 system stopped recording data when the SA Agulhas was just off the coast of the island, so there is no data for the transect back to Cape Town. There are also large gaps with missing co-ordinates during the cruise, so interpolation was used where possible. During the SANAE cruise to Antarctica, South Georgia and the South Sandwich Islands the system had many problems on the first leg (from Cape Town to Antarctica). There were also times during this cruise when the system shut off completely resulting in an absence of data. There were too many errors and gaps for the first leg to be used in the data analysis. During the Marion relief voyage the system shut down on the way to the island and only started recording values again once the ship was at the island. The GPS stopped working before the other sensors cut out, and only started again after the other sensors. This happened twice, with the GPS not being recorded for 4 days the first time and 5 days the second time, and the sensors stopped for 2 days the first time and 4 days the second time. The data is no longer logged when the ship is approximately 2° away from Cape Town harbour in both latitude and longitude. For the SANAE data, some of the gaps in the coordinates were able to be

filled in using other sensors onboard the SA Agulhas, although not all the gaps could be filled. The sensors could also have been influenced by extra sources which would affect the readings that were made, for example the smoke from the funnel of the ship could have an effect on the fCO_2 readings, as well as when the SA Agulhas is near Cape Town harbour, the fCO_2 values increase rapidly, this could be due to other ships and factories in and around the harbour.

One of the limitations in respect of scatterometer data was the gap in the ship's positions provided by the pCO_2 system. Positioning was necessary for the scatterometer data to be acquired. Another problem with scatterometer data is that is cannot read through clouds, so when there was cloud cover during a day, winds values could not be given. There is also a problem with sea ice, so during the times when the ship was near or on the coast of the Antarctic continent, there are no wind values for those positions. Approximately 28 percent of the dataset cannot be used due to errors.

A limitation of using the Stagnant Film model is that it is a very simple model, and it only accounts for two types of sea state, calm or rough, and ignores the fact that the wind might only just have increased on the day of sampling, and the eventual flux result might not be as good as the other models that consider the actual wind speed in the calculation.

Chapter 3:

RESULTS

3.1 Frontal Zone Positions Used in the Spatial Averaging of the data

Six zones were used in order to get regional averages, the Subtropical Zone (33.5-41°S), the Sub Antarctic Zone (41-45°S), the Polar Frontal Zone (both the northerly and southerly zones of the Polar Front (45-50°S and 50-58°S respectively)), the Eastern Weddell (which has been separated into three parts (58-64°S; 64-68°S; 68-70°S), and the Antarctic Shelf (from 70°S towards the pole). All three cruises were in the Subtropical Zone, the Sub Antarctic Zone and the Northern Polar Frontal Zone, therefore a comparison of the seasons can also be made as well as a regional comparison. Only the summer cruise was south of the Polar Front, at 50°S, therefore there will only be a regional comparison of the data.

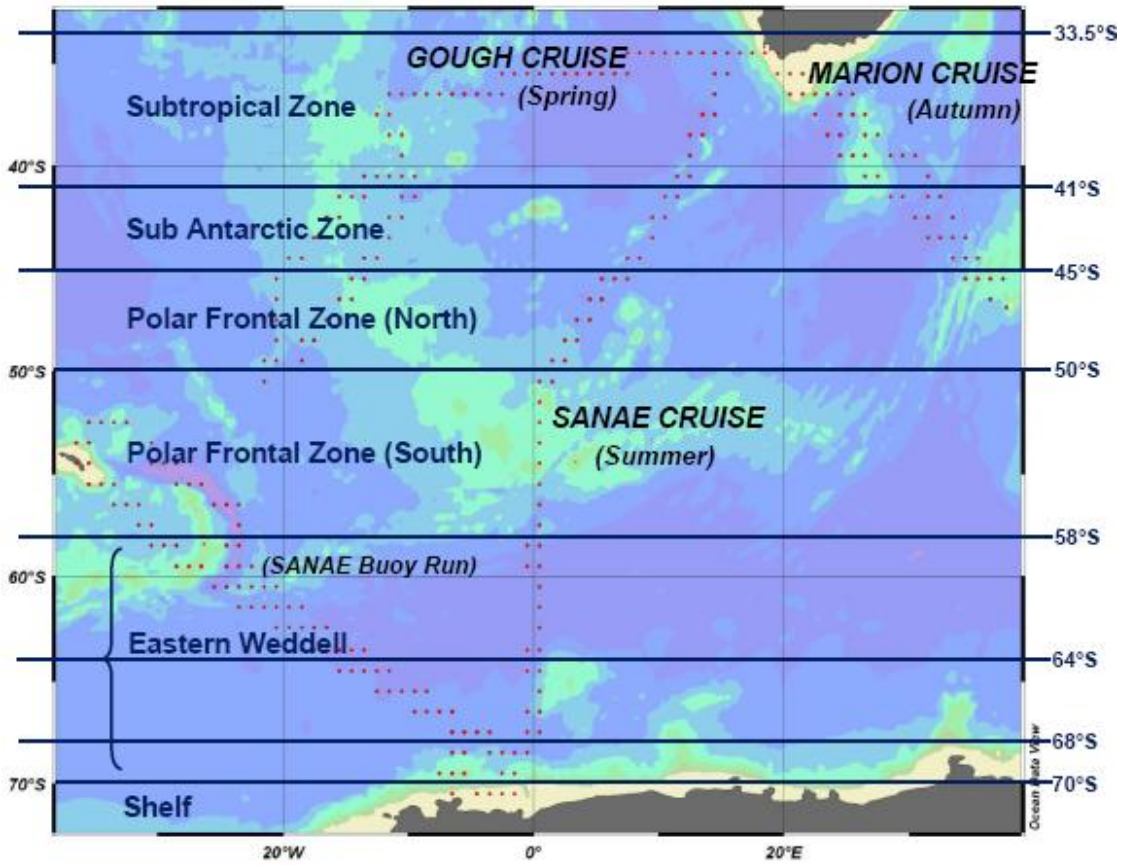

Figure 6: Map showing regions used in averaging the data. The writing in bold print labels the different regions, and the writing in italics represents the three different cruises during which the data were obtained. All three cruises occur in the Subtropical Zone, the Sub-Antarctic Zone, and the northern Polar Frontal Zone, so there is data for spring, summer and autumn in those regions. Only the SANAE cruise data occur in the southern Polar Frontal Zone, the Eastern Weddell region, and at the Antarctic continent, so there is only data for summer in those regions. The data will be analysed in two parts; one section with seasonal data (33.5°S-50°S) and the other section with data for the summer season only (50°S -Shelf). It must be noted that this map represents a great simplification of the fronts.

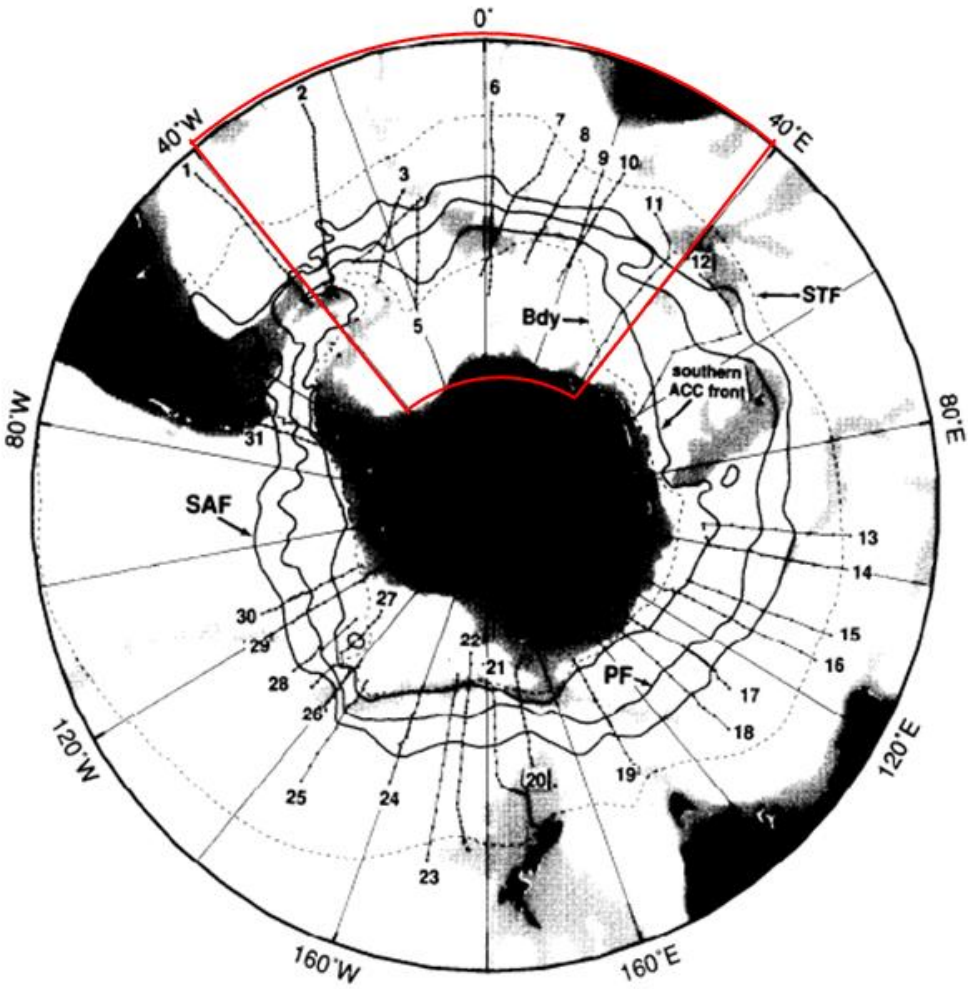

Figure 7: The Southern Ocean circumpolar fronts as published by Orsi et al. (1995). This is a more detailed and accurate representation of the fronts. The area of frontal positions in comparison with this study is outlined in red at the top of the figure, from 40°W to 40°E.

Figure 6 represents the simplified frontal zones used in this study to create regional averages of the data collected on the three cruises. Figure 7 by Orsi et al. (1995) is a more realistic representation of the fronts. The frontal positions were defined by Orsi et al., (1995) using physical properties such as temperature and salinity gradients. For the region where the data were collected, the simplified zonal boundaries are close to the mean frontal boundaries.

3.2 Geographical Differences in the Temperature, Salinity, ΔfCO_2 and Wind Speed

The temperature, salinity and ΔfCO_2 data were collected using a General Oceans GO8050 autonomous underway pCO_2 measuring system onboard the ship at a depth of 5m. ΔfCO_2 has been calculated as fCO_2 of the atmosphere subtracted from the fCO_2 of the ocean ($fCO_{2ocean} - fCO_{2atmosphere}$), therefore when ΔfCO_2 is negative, the CO_2 flux is from the atmosphere to the ocean, and the ocean is considered an fCO_2 sink.

3.2.1 Surface Oceanography of the Southern Ocean: South East Atlantic

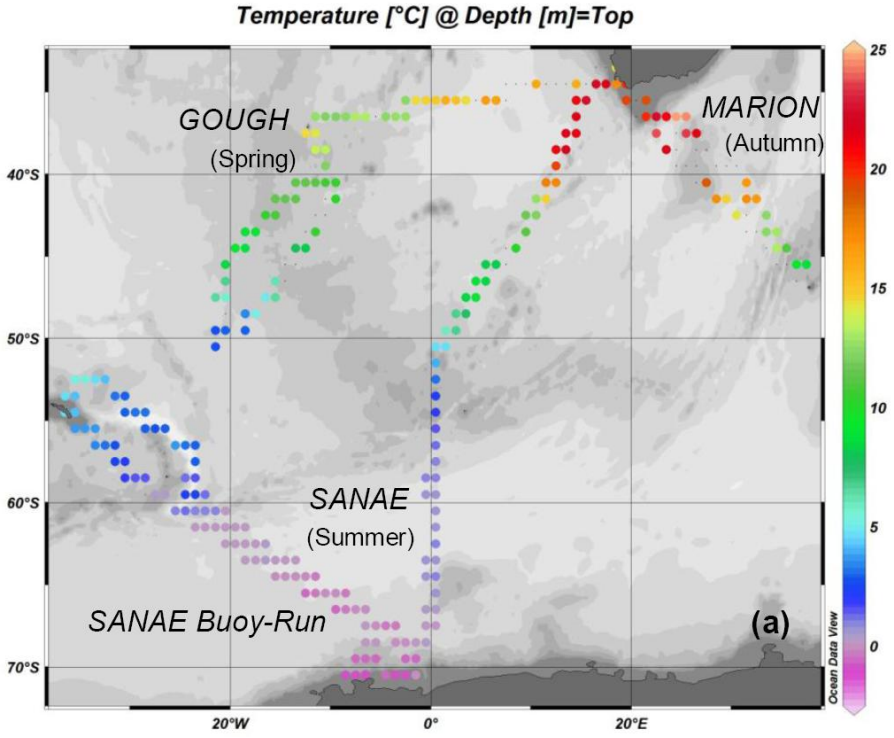

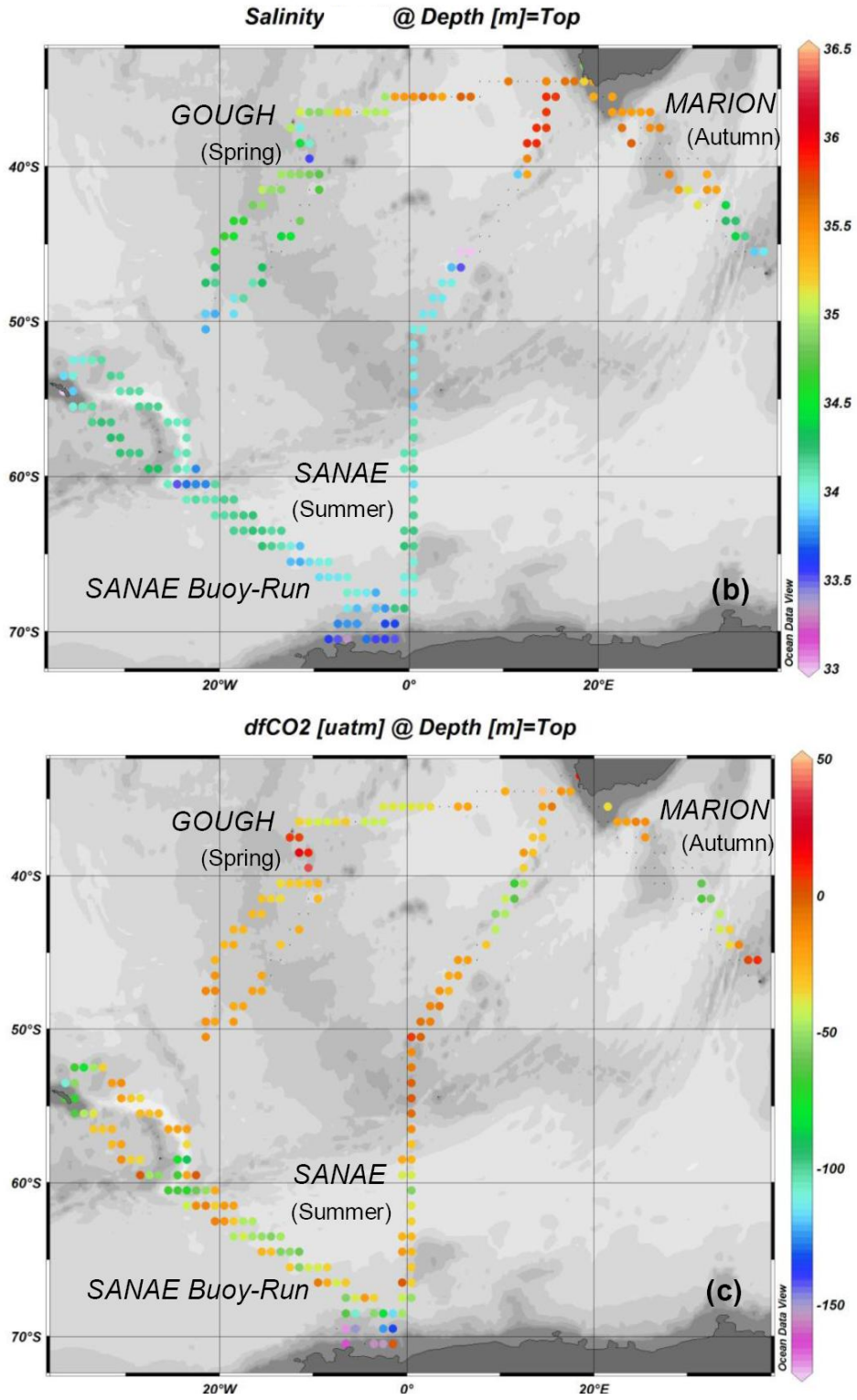

Figure 8: Plots showing physical properties from the three separate cruises during which the data were collected. Plot (a) shows the temperature (in °C), plot (b) is the salinity, and plot (c) is showing ΔfCO_2 (which was calculated as $fCO_{2ocean} - fCO_{2atmosphere}$) (in µatm).

The temperature data in Figure 8(a) show a steady decrease in temperature moving towards the Antarctic Shelf. It decreased from approximately 25°C in the Subtropical Zone at the African continent to below 0°C at the Antarctic continent. The spring temperatures on the Gough cruise were lower in the Subtropical Zone than the temperatures from summer (SANAE cruise) and autumn (Marion cruise). The temperatures on all three cruises between 40°S and 50°S (the Sub Antarctic Zone and the northern Polar Frontal Zone) ranged from 5°C to 15°C. The temperature on the SANAE cruise and the SANAE buoy run had temperatures from about 2°C to 5°C from 50°S to 60°S. From 60°S to the Antarctic Continent the temperature decreased to below 0°C, this is the eastern region of the Weddell Gyre. The salinity in Figure 8(b) also shows a poleward decrease moving towards the Antarctic continent. It is highest in the Subtropical Zone on the SANAE cruise. South of 45°S on the SANAE cruise the salinity ranged from 33.00 to 34.50, with the lowest salinity values being at the Shelf, and on the Gough Island cruise it ranged from 33.50 to 35.00 between 36°S and 50°S. The salinity values on the Marion cruise ranged from about 35.3 to about 35.5 between Cape Town and 43°S. The salinity values then decreased to between 34.00 and 34.50 south of 43°S to Marion Island. In the ΔfCO_2 plot (Figure 8c), the negative values are purple to orange in the colour bar and the positive values are the red points. The ΔfCO_2 was only positive twice, in an area near Gough Island (just above 40°S), and another area near Marion Island (around 45°S). This could be a result of the island effect. In those areas surrounding Marion and Gough Islands the fCO_2 values in the ocean were higher than the fCO_2 values in the atmosphere, when ΔfCO_2 is negative it means that the fCO_2 values are higher in the atmosphere than in the ocean. The ΔfCO_2 decreased south of 40°S on the SANAE cruise, and the Marion cruise to approximately -50µatm, but decreased again to approximately 0µatm around 45°S. The range of ΔfCO_2 at the Antarctic continent was approximately -125µatm to -175µatm. The ΔfCO_2 is approximately -100µatm at about 27°W and 55°S (South Georgia Island), and also at about 22°W and 60°S (South Sandwich Islands).

The data were averaged into zones, using the fronts as the boundaries, in order to get regional averages. The data were also separated into seasons, with each cruise representing a season; the Gough cruise occurred in austral spring, the SANAE cruise happened in austral summer, and the Marion cruise occurred in austral autumn. Figure 9 shows only three zones, from the subtropical front to the Polar Frontal Zone (North), because those are the only regions that all three seasons can be represented. Figure 10 shows the only the summer season or SANAE cruise data, as it is the only cruise that went further south than the Polar Frontal Zone (North).

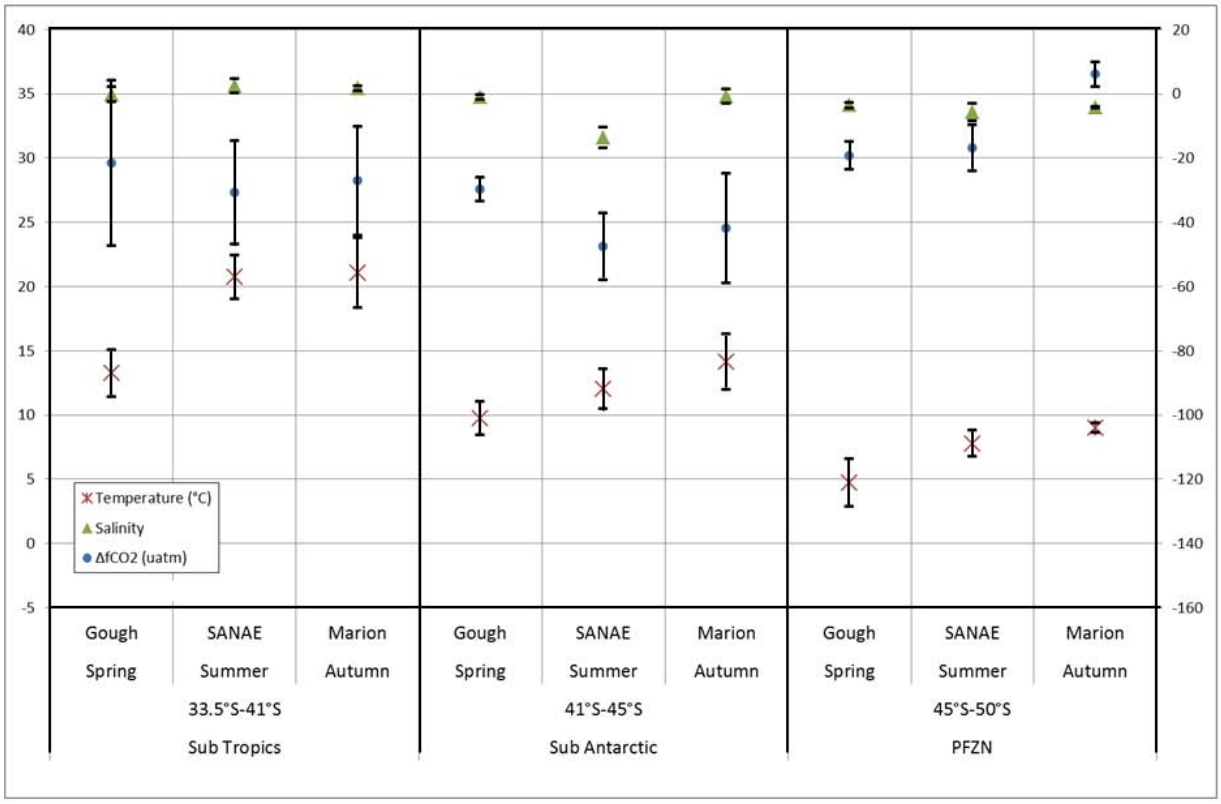

Figure 9: Graph showing the average seasonal variation of the physical properties in the Sub Tropics, Sub Antarctic Zone and Polar Frontal Zone (North). Temperature and salinity are on the primary axis, and ΔfCO_2 (which was calculated as $fCO_{2ocean} - fCO_{2atmosphere}$) is on the secondary axis. The standard deviation is shown by the error bars.

The average temperature was lowest during the spring (Gough cruise) and highest during the autumn (Marion cruise) in all three regions, the greatest range occurred in the Subtropical region, of ~10°C. The other regions have a range of about 5°C. The salinity averages were high in all of the regions, except for the summer (SANAE) average in the Sub-Antarctic region. The highest salinity averages occurred in the Sub Tropics. The salinities were lowest in the Polar Frontal Zone (North) (PFZN), and were constant throughout the seasons within this region. In the Subtropics ΔfCO_2 was highest in summer, and seasonally it ranged from -20µatm to approximately -30µatm. In the Sub Antarctic Zone ΔfCO_2 was highest again during the summer, but had a greater range than the Subtropical seasonal variability of approximately -30µatm to about -50µatm. The spring ΔfCO_2 value was the lowest in the PFZN, and increased in summer and again in autumn, it ranged between -20µatm and just under +10µatm. It was only positive once, during the Marion cruise in autumn in the PFNZ. This study excluded the data from the vicinity of the islands.

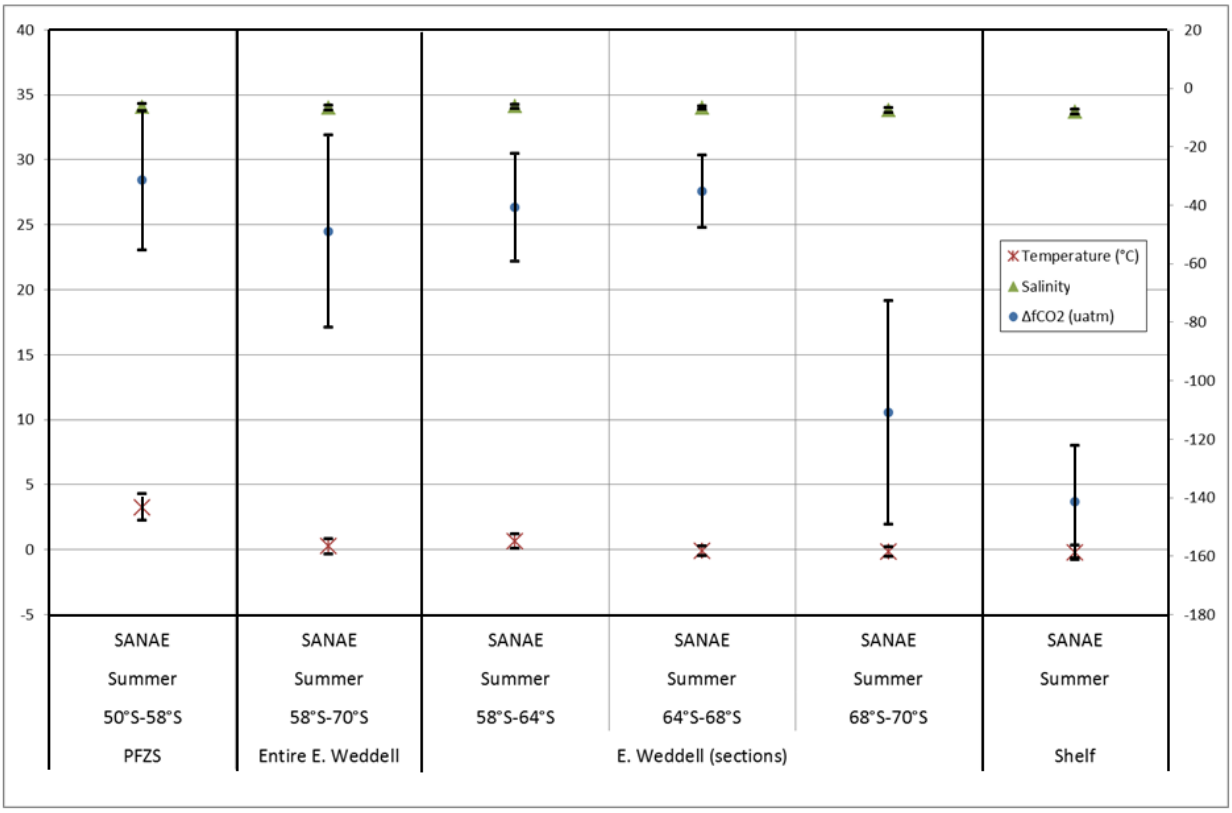

Figure 10: Graph showing the averages of temperature, salinity and ΔfCO_2 for each region from the Polar Frontal Zone (South) to the Shelf for the summer season. Temperature and salinity are on the primary axis, and ΔfCO_2 (which was calculated as $fCO_{2ocean} - fCO_{2atmosphere}$) is on the secondary axis. The standard deviation is shown by the error bars.

Figure 10 shows the temperature, salinity and ΔfCO_2 regional averages for the regions south of 50°S for the three seasons or cruises. The temperature was highest at Polar Frontal Zone (South) (PFZS), at about 4°C, decreased towards 0°C in the East Weddell, and was below 0°C at the shelf. The salinity values were constant, around 34, from the PFZS to the Antarctic Shelf. ΔfCO_2 ranged from ~-30µatm at PFZS, and -140µatm at the Shelf. The ΔfCO_2 increased rapidly from 68°S.

3.2.2 Wind Speed

The wind data were extracted from the SeaWinds dataset on QuikSCAT (http://www.ncdc.noaa.gov/oa/rsad/blendedseawinds.html) for the relevant periods, and were re-gridded to one degree blocks before being averaged again into the frontal regions. Two wind speed products are used, the first being the daily wind speed and the second is the average of the week preceding the daily wind using a weighted average. The reason for using two wind speed products is because if just daily wind speed was used it would not be known if the wind before the day had been strong or weak, which would have had an impact on the sea surface mixed layer. Therefore a weekly average with a weighting (found in Appendix 1), is also used to get an idea of whether the daily wind speed was an isolated incident or not. The wind speed was produced with an accuracy of $2 m.s^{-1}$ (Perry 2000).

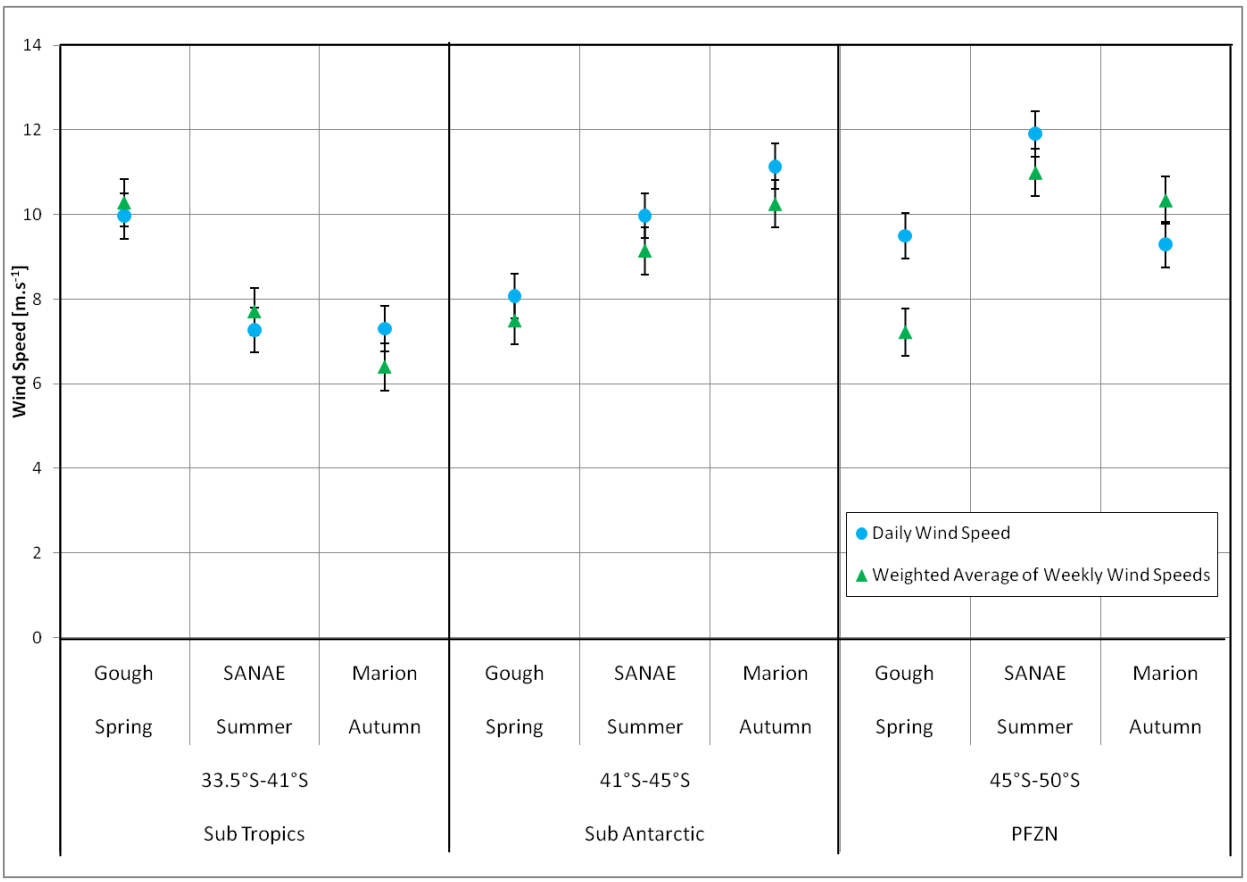

Figure 11: Graph showing the average seasonal variation of the daily wind speed and weighted average of the wind speed for the week preceding the day of daily wind for Sub Tropic Region, Sub Antarctic Zone and Polar Frontal Zone (North).

Figure 11 shows the daily wind speed and the weekly average wind speed for all three cruises or seasons, over three regions from the Subtropics to the Polar Frontal Zone (North). Figure 12 only has the wind speeds for the SANAE cruise during the summer season, because it was the only cruise that went further south than 50°S. In the Subtropical region, the wind speeds were highest in spring around 10m.s^{-1}, and then decreased in summer and again by a small margin in autumn. The daily wind speed and the weighted wind speed product were close in value for spring and summer, meaning that the wind was at a relatively constant speed throughout the week before the daily wind speed. It was slightly higher than the weighted wind speed in the autumn, meaning that the six days before the daily wind speed were calmer than that of the daily wind speed, but not significantly as they both lie within their standard errors. In

the Sub Antarctic region, the wind speeds were lowest in the spring, increased in summer, and increased again in autumn. The daily wind speed and the weighted wind speed for all three seasons differed by ~1m.s^{-1}, with the weighted wind speed being the smaller value. This means that the winds in the week before the daily wind speed were weaker than that of the daily wind speed, but both values for all three seasons did not differ by more than the standard errors of the values, meaning the difference was not substantial. In the PFZN, the highest value occurred in summer, it was also the highest value for all three regions. The lowest wind speed occurred in spring. The summer daily wind averages were only ~1m.s^{-1} higher than the weighted wind, but in the autumn, the weighted wind average was ~1m.s^{-1} higher than the daily wind speed product. This means that for autumn the wind speeds for the days in the week before the daily wind speed were slightly stronger than the daily wind speed. For both summer and autumn the differences were not substantial. For spring the daily wind speed was ~2m.s^{-1} greater than the weighted wind, and the difference was considerable because it is greater than the standard error. All wind speeds were higher than 6m.s^{-1}, which is considered a moderate wind speed. They did not go above 12m.s^{-1}, which can be considered as high wind speed. Moderate to high wind speed is expected in the Southern Ocean.

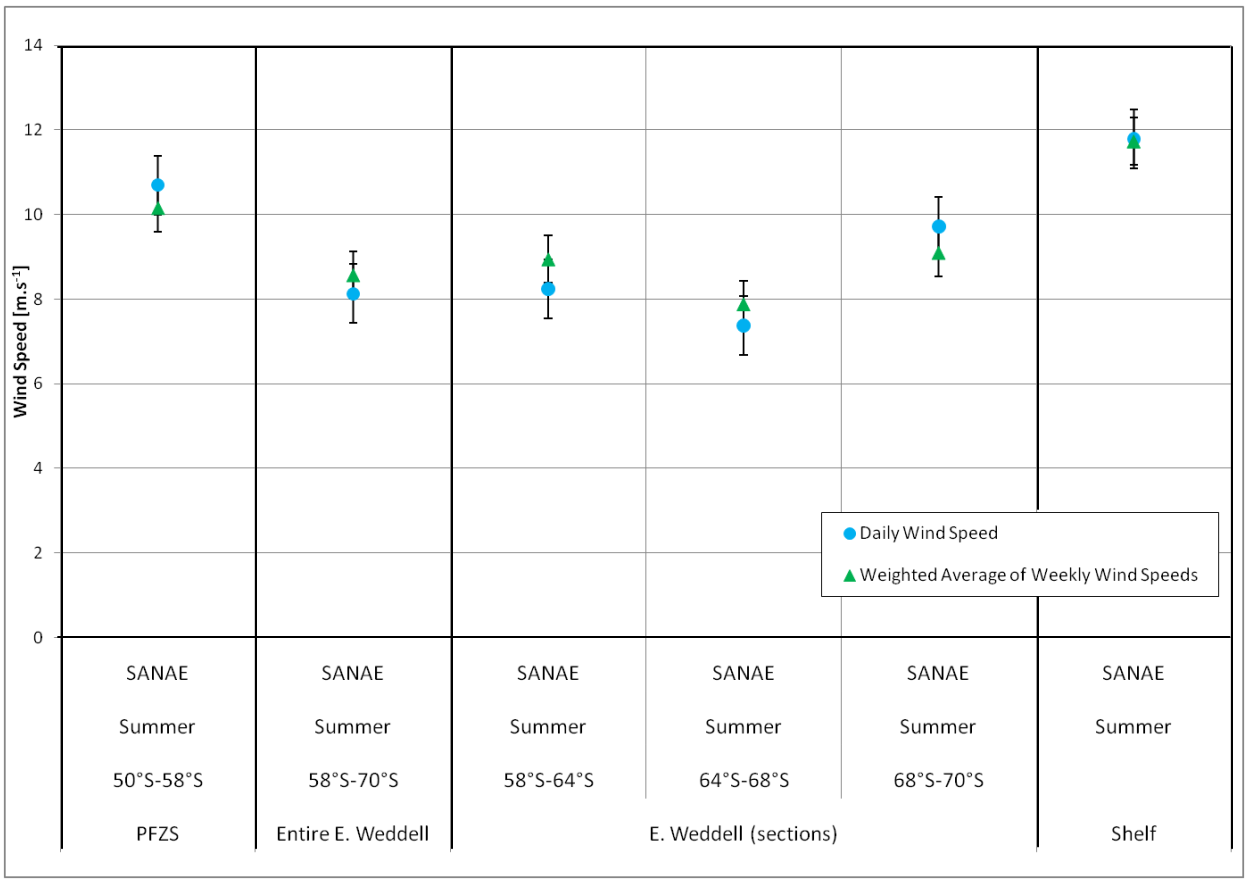

Figure 12: Graph showing the averages for each region from the Polar Frontal Zone (South) to the Shelf of daily wind speed and weighted average of the wind speed for the week preceding the day of daily wind for the summer season.

Figure 12 shows the two wind speed products from 50°S southwards to the Antarctic Shelf. The wind speeds ranged from ~7m.s^{-1} to 12m.s^{-1} south of 50°S. The highest wind speed occurred at the shelf at ~12m.s^{-1}, and the lowest wind speed occurred between 64-68°S. The daily wind speed and weighted wind speed at the shelf were almost the same, only ~0.1m.s^{-1} difference. This means that the winds were consistently high throughout the week before the day of the daily wind speed. The daily wind speed was higher than the weighted wind speed in the PFZS and between 68-70°S by about 1m.s^{-1} for both regions. Therefore the daily wind speed was slightly stronger than the winds in the week before it, but the wind speed was constant, although the difference is not significant. The weighted wind speed product was higher than the daily wind speed product between 58-64°S and 64-68°S, and also at the

average for the entire East Weddell region. Therefore the wind speed during the week was constantly higher than the daily wind speed but the difference only ranged between ~0.5m.s^{-1} and 1m.s^{-1}, and the difference was not significant as the values lie within the standard errors.

3.3 Gas Transfer Velocity

The gas transfer velocity in the study was calculated using five different models which represent different relationships between wind speed and gas transfer velocity.

3.3.1 Change in Gas Transfer Velocity Models with Wind Speed and the Uncertainty in the Wind Speed Product

Figure 13 was created by calculating the gas transfer velocities using the different relationships being examined in this study for three different wind regimes (low [3m.s^{-1}], medium [8m.s^{-1}] and high [14m.s^{-1}]). All gas transfer velocities were normalised to a Schmidt Number of 660. Firstly Figure 13 shows the response of each gas transfer velocity model to a change in the wind speed regime. Secondly it shows how much the value of *k* for each model in a wind regime is affected by the uncertainty of the wind product of 2m.s^{-1}, or the sensitivity of each model to the uncertainty in the wind speed product. This explains how much greater, or less, *k* would be at a wind speed 2m.s^{-1} stronger or weaker than the low, medium and high wind speed regimes.

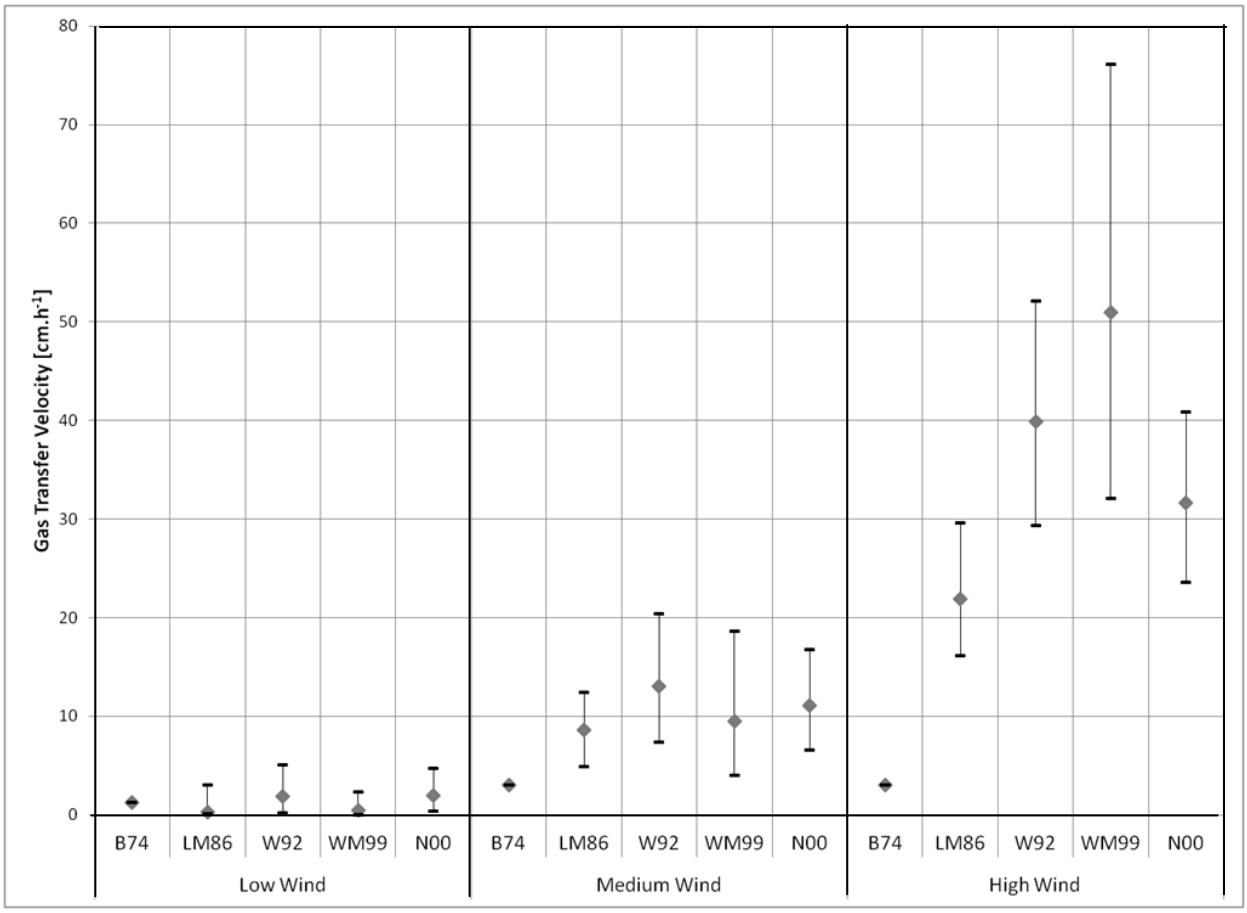

Figure 13: Graph showing the sensitivity of the gas transfer velocities (*k*) of each model to uncertainties in the wind product in low wind (3m.s^{-1}), medium strength wind (8m.s^{-1}) and high wind (14m.s^{-1}). The uncertainty of the wind speed from Seawinds on QuikSCAT is 2m.s^{-1} (Perry, 2000). All gas transfer velocities are normalised to a Schmidt number of 660. The error bars represent gas transfer velocities at wind speeds of =2m.s^{-1} (upper bar) or -2m.s^{-1} (lower bar) relative to the low, medium and high wind speeds. B74 is the Broecker and Peng 'Stagnant Film Model; LM86 is the Liss and Merlivat Relationship; W92 is the quadratic Wanninkhof Relationship; WM99 is the Wanninkhof and McGillis cubic relationship and N00 is the Nightingale et al. quadratic parameterisation.

In the low wind regime all five models have gas transfer velocities that are below 5cm.h^{-1}, with W92 and N00 having the highest *k*. In the medium wind regime the models have a greater variation in the values of *k*. B74 has only increased by a small amount, about 2cm.h^{-1}. LM86 has a greater increase, of about 8cm.h^{-1}. WM99 and N00 increase by just under 10cm.h^{-1} with N00 still having a higher value for *k* than WM99. W92 has the

largest increase of about 10cm.h^{-1}, and remains having the highest value for *k*. In the high wind regime the value of *k* for B74 hasn't changed, LM86 has increased, but by a smaller margin than the other three models, by about 15cm.h^{-1}, N00 has the third lowest increase of about 20cm.h^{-1}. W92 has the second greatest increase as the wind speed changes from a medium wind regime to a high wind speed regime, with just over a 25cm.h^{-1} increase in *k*, and WM99 has the greatest increase in *k* of 40cm.h^{-1}. The range of the gas transfer velocity values in the high wind speeds is just under 50cm.h^{-1}, with the lowest value being B74 (~4cm.h^{-1}) and the highest value being WM99 (~51cm.h^{-1}).

In the low wind range, the sensitivity of W92 and N00 *k* values increasing with an increase in wind speed of 2m.s^{-1} being the greatest of all the models. B74 appears unresponsive, with no change occurring in *k* at a low wind speed. In the medium wind range the range of the gas transfer velocities has increased to about 10cm.h^{-1}, with the lowest gas transfer velocity being B74 at ~4cm.h^{-1}, and the highest being W92 (~14cm.h^{-1}). The sensitivity of gas transfer velocity to a change in wind speed has increased for all the relationships except for B74, which again doesn't have a change with an increase or decrease in wind speed, this shows that B74 is only dependent on wind speed when moving from a low wind regime to a high wind regime. The greatest sensitivity occurs with WM99, with an increase in wind speed by 2m.s^{-1} leads to an increase in *k* of almost 10cm.h^{-1}, and a decrease in wind speed leads to a decrease of ~6cm.h^{-1}. There is a cubic relationship between the *k* defined by WM99, meaning a change in *k* with an increase in wind speed will be greater than the change in *k* with a decrease in wind speed. W92 is also relatively sensitive to the inaccuracy in wind speed of 2m.s^{-}1 with an increase in *k* of ~7cm.h^{-1}, and a decrease of ~5cm.h^{-1} with an increase or decrease in wind speed respectively. N00 sensitivity has a range of approximately 10cm.h^{-1}, and LM86 has a range of about 7cm.h^{-1}.

The smallest change occurs again with B74, with there being no change in gas transfer velocity with an increase or decrease with the uncertainty in wind speed. The greatest sensitivity occurs again with WM99, with an approximately 20cm.h^{-1} decrease in *k* with a 2m.s^{-1} decrease in wind speed, and ~25cm.h^{-1} increase in *k* with a 2m.s^{-1} increase is wind speed. W92 has the second greatest sensitivity to an increase or decrease in wind speed of 2m.s^{-1}. N00 has the third greatest sensitivity to an increase or decrease of wind speed. LM86 is the second lowest gas transfer velocity value (~22cm.h^{-1}), but is still about 20cm.h^{-1} greater than B74. LM86 has the second lowest sensitivity to a change in wind speed, but the change has increased from a medium wind speed to a high wind speed. All gas transfer velocity models, except B74, experience an increase in sensitivity as the wind regimes change from a low wind speed regime to a high wind speed regime, with the greatest changes occurring in the high wind speed regime.

3.3.2 The Gas Transfer Velocities Models plotted versus the Wind Speeds used in this study

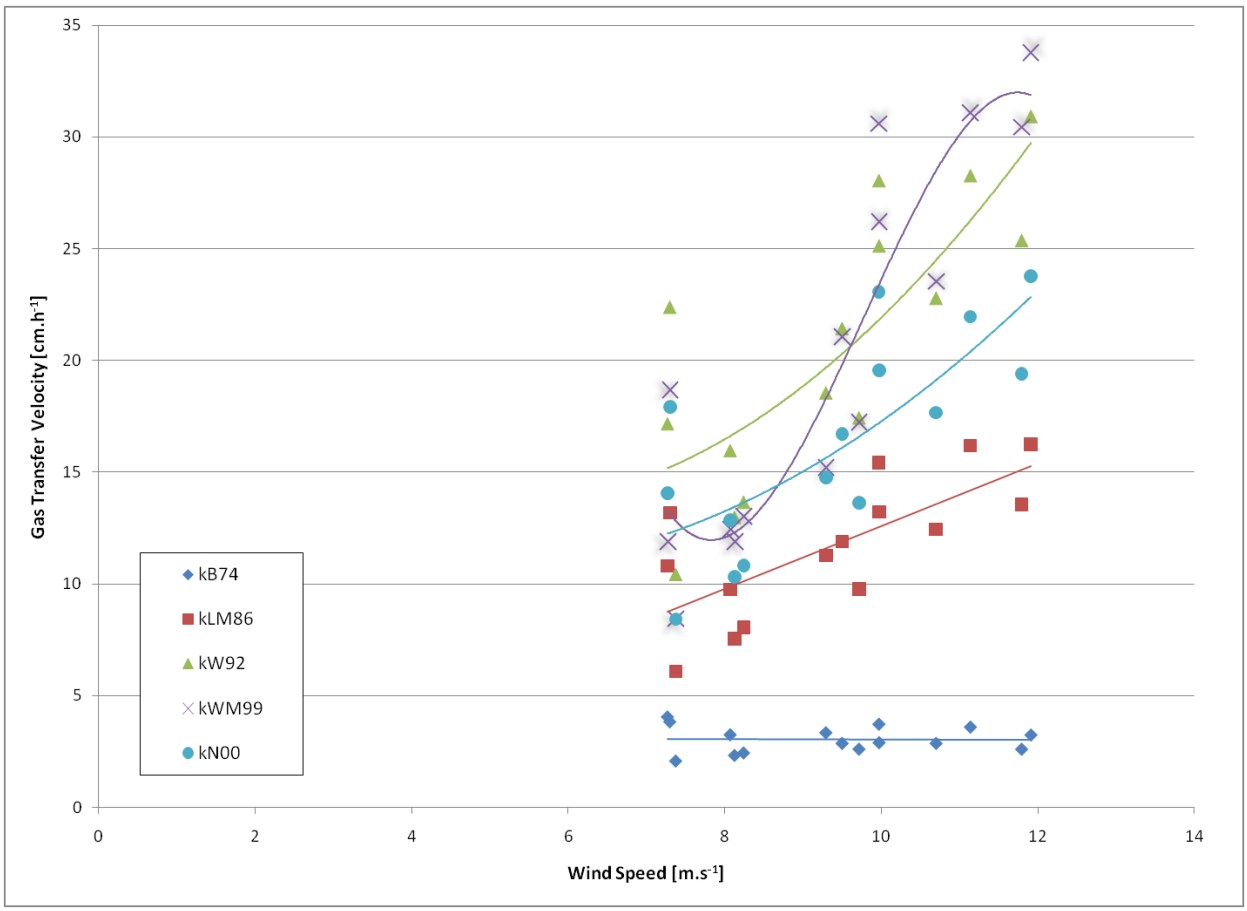

Figure 14: Plot of the wind speed from this study versus the gas transfer velocities. The wind speed used in this plot is the daily wind speed. The gas transfer velocities have been calculated using the different parameterisations. B74 is the Broecker and Peng 'Stagnant Film Model; LM86 is the Liss and Merlivat Relationship; W92 is the quadratic Wanninkhof Relationship; WM99 is the Wanninkhof and McGillis cubic relationship and N00 is the Nightingale et al. quadratic parameterisation.

Figure 14 shows the gas transfer velocities defined by using the data from this study, where the wind speed used is the daily wind speed product. It must be noted that because this data covers a large regional area, there will also be an impact of the temperature variations on the Schmidt number, which also has an impact on gas transfer velocity. This impact however, is not as significant as the change in wind

speed, and this figure is to show the impact of increasing wind speed on the gas transfer velocity. The Figure 14 agrees with Figure 13 in that the changes that occur in the gas transfer velocities become greater with an increase in wind speed. The range of *k* between the models is small, below 9m.s^{-1}. The different increases of *k* with wind speed for each model is evident in Figure 14 (besides for the unresponsive B74), as well as the different rates of change in *k* as the wind speed increases. The increase in sensitivity for all models, except for B74, occurs around 10m.s^{-1}, and the range of gas transfer velocity at 12m.s^{-1} is almost 35cm.h^{-1}. The most sensitive at high wind speeds is WM99, W92 is the second highest, then N00, and then LM86. It is clear in this plot that B74 does not change as expected as wind speed changes, because it is not dependent on wind. At lower wind speeds W92 has the highest gas transfer velocity values, which is in agreement with Figure 13, and then at higher wind speeds WM99 has the highest gas transfer velocity values.

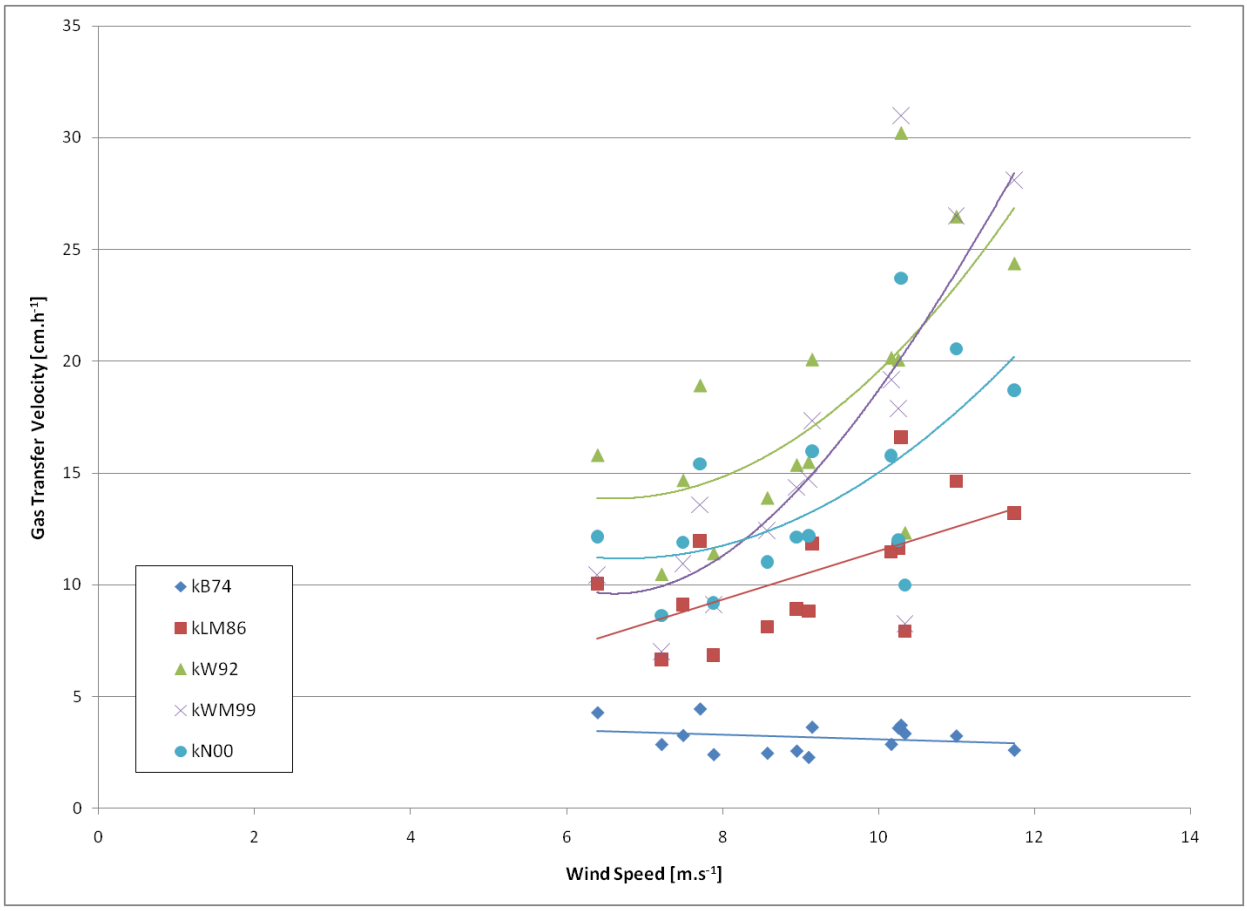

Figure 15: Plot of the wind speed from this study versus the gas transfer velocities. Wind speed used in this plot is weighted average wind speed. The gas transfer velocities have been calculated using the different parameterisations. B74 is the Broecker and Peng 'Stagnant Film Model; LM86 is the Liss and Merlivat Relationship; W92 is the quadratic Wanninkhof Relationship; WM99 is the Wanninkhof and McGillis cubic relationship and N00 is the Nightingale et al. quadratic parameterisation.

Figure 15 shows similar results to Figure 14, but the wind speed product is the weighted wind speed instead of the daily wind speed. B74 is the least responsive to a change in wind speed. It produces the lowest gas transfer velocities of all the models with some of the higher wind speeds producing lower values of *k* than some of the lower wind speeds. This emphasises the point that B74 is not affected by wind. W92 has the highest gas transfer velocity at lower wind speed values, and WM99 has the highest gas transfer velocity at high wind speeds. The range of all the gas transfer velocities at low wind speed is just over 10cm.h^{-1}, and at high wind speeds they have a range of about 30cm.h^{-1}. The linear relationship of LM86, the quadratic relationships of W92 and

N00, and the cubic relationship of WM99 are all evident when looking at the trendlines in Figure 14 and Figure 15, and the fact that there is no relationship between wind and gas transfer velocity is also visible for B74.

3.4 Air-Sea CO_2 Fluxes

The air-sea fluxes were calculated as a product of the solubility, gas transfer velocity and the change in ΔfCO_2. If the flux is positive, ΔfCO_2 in the atmosphere is greater than the ΔfCO_2 in the ocean (the ocean as a CO_2 source), and if the flux is negative, ΔfCO_2 in the atmosphere was less than ΔfCO_2 in the ocean (the ocean as a CO_2 sink).

3.4.1 Geographical Differences of Air-Sea CO_2 Fluxes

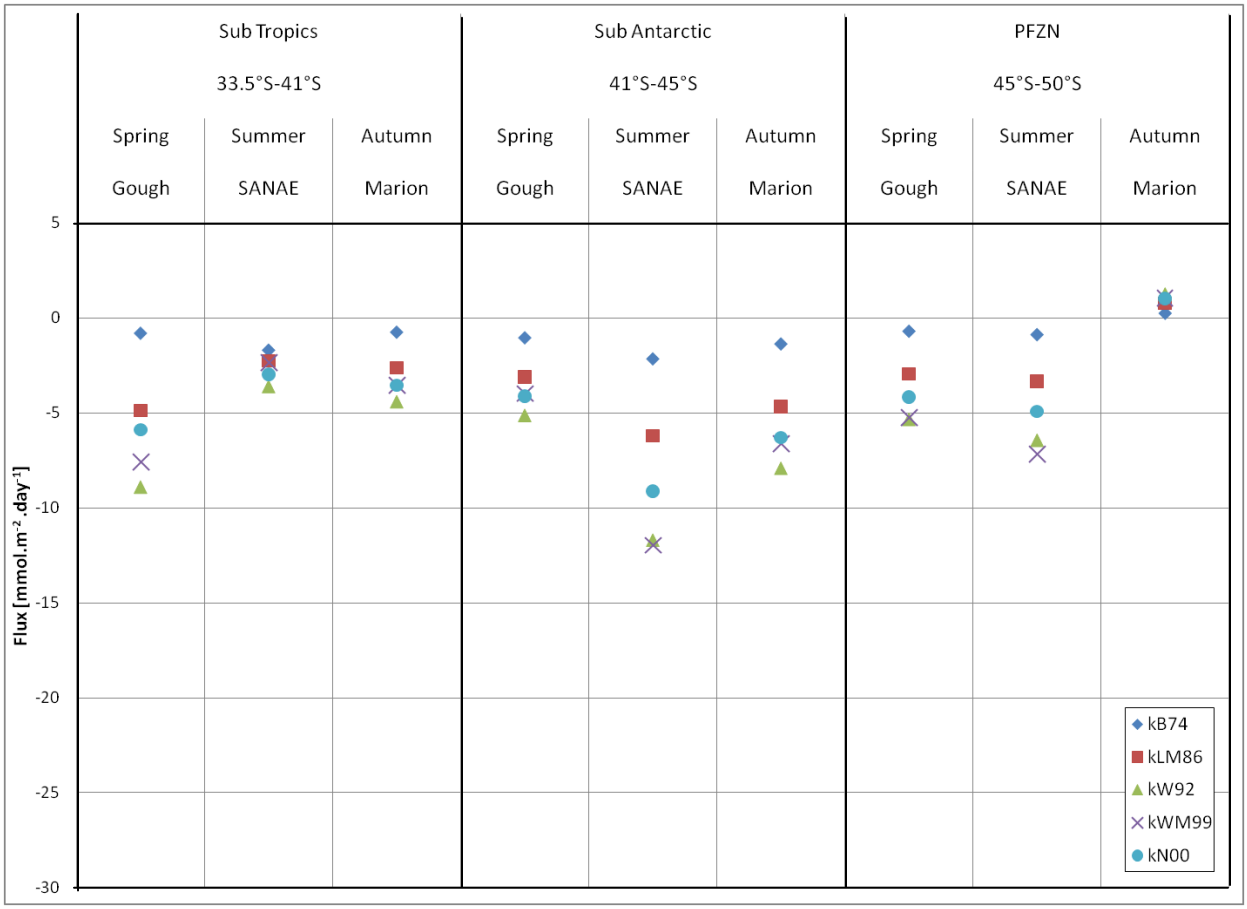

Figure 16: Graph showing the average air-sea CO_2 flux for each model across each region from the Sub Tropics to the Polar Frontal Zone (North), separated into seasons (cruises). The gas transfer velocities were calculated using a daily wind speed. Errors are shown in Table 3: Table showing the regional averages of the fluxes determined using *k* from the different relationships, included are the standard deviations from the mean for each region. It also includes the standard deviations. The different gas transfer velocities were calculated using the daily wind speed. The flux is in mmol.m^{-2}.day^{-1}. B74 is the Broecker and Peng 'Stagnant Film Model; LM86 is the Liss and Merlivat Relationship; W92 is the quadratic Wanninkhof Relationship; WM99 is the Wanninkhof and McGillis cubic relationship and N00 is the Nightingale et al. quadratic parameterisation. Positive values indicate sea-to-air fluxes, and negative values indicate air-to-sea fluxes. using standard deviations. B74 is the Broecker and Peng 'Stagnant Film Model; LM86 is the Liss and Merlivat Relationship; W92 is the quadratic Wanninkhof Relationship; WM99 is the Wanninkhof and McGillis cubic relationship and N00 is the Nightingale et al. quadratic parameterisation. Positive values indicate sea-to-air fluxes, and negative values indicate air-to-sea fluxes.

Figure 16 shows the average air-sea CO_2 fluxes in the regions from the Subtropics to north of the Polar Frontal Zone. The fluxes are for all three seasons or cruises, and were calculated using the five different gas transfer velocity models with the daily wind speed as the wind product. In the Subtropical region, the greatest flux occurred during spring (between ~-1mmol.m^{-2}.day^{-1} and -9mmol.m^{-2}.day^{-1}). This is also when the wind speed was high (10m.s^{-1}), which is why the different models have produced a wide range of fluxes for this season. Summer had the smallest flux (between ~-2mmol.m^{-2}.day^{-1} and ~3.5mmol.m^{-2}.day^{-1}, and it also had the smallest range of fluxes produced by the different models. In the Sub Antarctic region the greatest flux occurred in summer, ranging from -2mmol.m^{-2}.day^{-1} and -12mmol.m^{-2}.day^{-1} and the smallest flux occurred in spring. In PFZN the summer and spring fluxes were very similar, except that LM86, N00, W92 and WM99 were slightly greater in summer than in spring, ranging from -1mmol.m^{-2}.day^{-1} to -5mmol.m^{-2}.day^{-1} for spring and -7mmol.m^{-2}.day^{-1} for summer. Autumn had the smallest flux, and also the smallest range of fluxes created using the different models. It was the only positive flux.

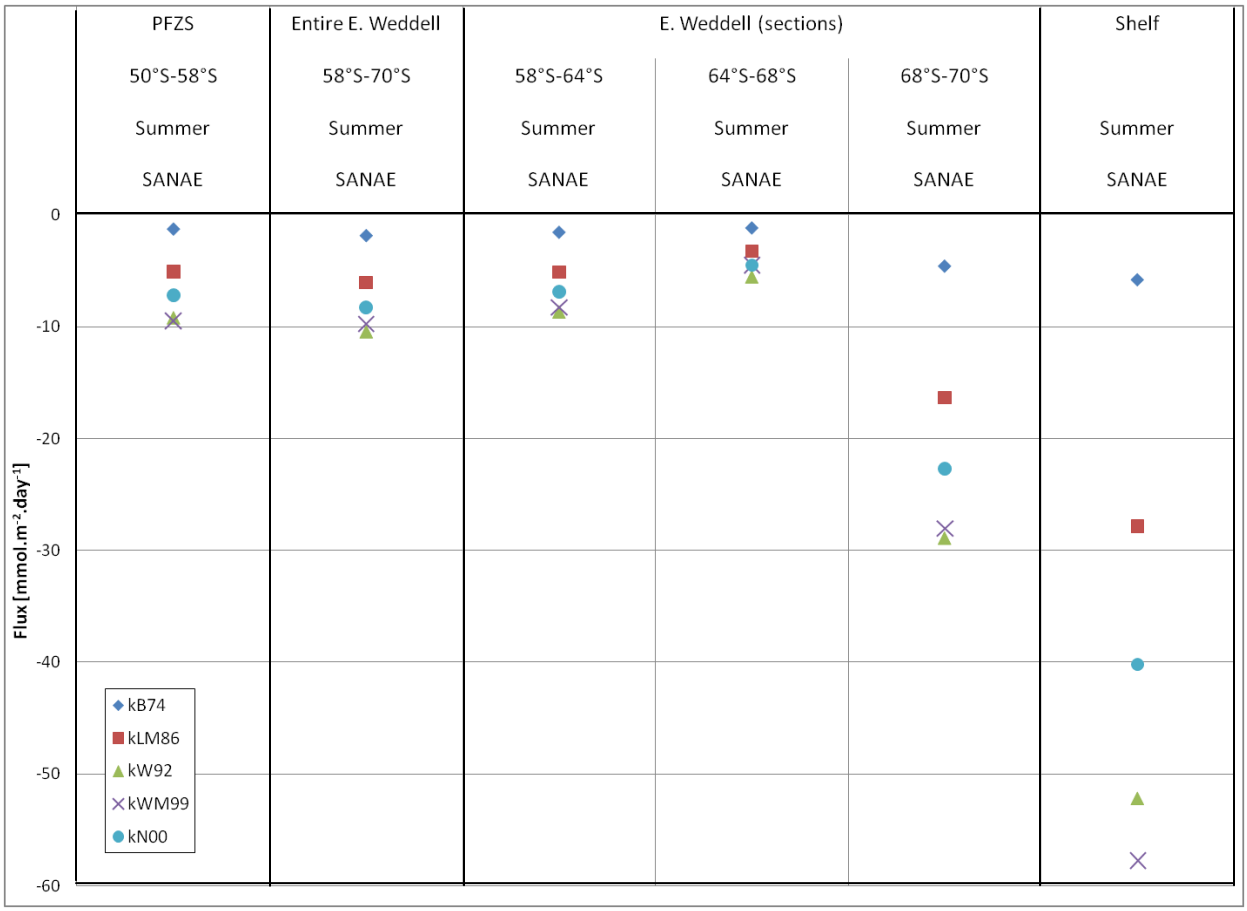

Figure 17: Graph showing the average air-sea CO_2 flux for each model for the summer season, for the regions from the Polar Frontal Zone (South) to the Antarctic Shelf. The gas transfer velocities were calculated using a daily wind speed. Errors are shown in Table 3: Table showing the regional averages of the fluxes determined using *k* from the different relationships, included are the standard deviations from the mean for each region. It also includes the standard deviations. The different gas transfer velocities were calculated using the daily wind speed. The flux is in mmol.m^{-2}.day^{-1}. B74 is the Broecker and Peng 'Stagnant Film Model; LM86 is the Liss and Merlivat Relationship; W92 is the quadratic Wanninkhof Relationship; WM99 is the Wanninkhof and McGillis cubic relationship and N00 is the Nightingale et al. quadratic parameterisation. Positive values indicate sea-to-air fluxes, and negative values indicate air-to-sea fluxes. using standard deviations. B74 is the Broecker and Peng 'Stagnant Film Model; LM86 is the Liss and Merlivat Relationship; W92 is the quadratic Wanninkhof Relationship; WM99 is the Wanninkhof and McGillis cubic relationship and N00 is the Nightingale et al. quadratic parameterisation. Note the scale change from Figure 16. Positive values indicate sea-to-air fluxes, and negative values indicate air-to-sea fluxes.

Figure 17 shows the average fluxes calculated using the different models and the daily wind speed for only the summer season, or the SANAE cruise. The regions shown are from the Polar Frontal Zone (South) to the Antarctic Shelf. The fluxes calculated using

the different parameterisations range from about 1mmol.m^{-2}.day^{-1} to ~10mmol.m^{-2}.day^{-1} at PFZS, 58-64°S and 64-68°S, with the smallest range occurring between 64-68°S. The range increased at 68-70°S from between -5mmol.m^{-2}.day^{-1} and -30mmol.m^{-2}.day^{-1} to between -5mmol.m^{-2}.day^{-1} and ~-60mmol.m^{-2}.day^{-1} at the Antarctic Shelf.

Table 3: Table showing the regional averages of the fluxes determined using *k* from the different relationships, included are the standard deviations from the mean for each region. It also includes the standard deviations. The different gas transfer velocities were calculated using the daily wind speed. The flux is in mmol.m^{-2}.day^{-1}. B74 is the Broecker and Peng 'Stagnant Film Model; LM86 is the Liss and Merlivat Relationship; W92 is the quadratic Wanninkhof Relationship; WM99 is the Wanninkhof and McGillis cubic relationship and N00 is the Nightingale et al. quadratic parameterisation. Positive values indicate sea-to-air fluxes, and negative values indicate air-to-sea fluxes.

				Flux B74	Flux LM86	Flux W92	Flux WM99	Flux N00
Sub Tropical Zone	33.5°S-41°S	Spring	*Gough*	-0.82±0.95	-4.87±2.99	-8.89±5.61	-7.58±7.26	-5.89±5.14
		Summer	*SANAE*	-1.71±0.55	-2.26±0.63	-3.60±1.03	-2.36±0.71	-2.98±0.88
		Autumn	*Marion*	-0.77±0.60	-2.62±1.86	-4.40±3.00	-3.54±2.59	-3.54±2.37
Sub Antarctic Zone	41°S-45°S	Spring	*Gough*	-1.06 ±0.23	-3.12±0.91	-5.11±1.48	-3.98±1.56	-4.12±1.11
		Summer	*SANAE*	-2.16±0.78	-6.21±3.44	-11.69 ±6.58	-11.97±8.35	-9.13±4.86
		Autumn	*Marion*	-1.38±0.67	-4.68±3.15	-7.90±5.53	-6.61±5.54	-6.31±4.26
Northern Polar Frontal Zone (PFZN)	45°S-50°S	Spring	*Gough*	-0.71±0.20	-2.95±1.09	-5.33±2.19	-5.25±2.73	-4.16±1.63
		Summer	*SANAE*	-0.89±0.39	-3.33±1.64	-6.42±3.39	-7.17±4.26	-4.93±2.57
		Autumn	*Marion*	0.23±0.14	0.78±0.50	1.28±0.83	1.05±0.70	1.02±0.66
Southern Polar Frontal Zone (PFZS)	50°S-58°S	Summer	*SANAE*	-1.25±0.92	-5.05±3.21	-9.20±5.95	-9.42±6.85	-7.16±4.57

Entire Eastern Weddell Zone	58°S-70°S	Summer	*SANAE*	-1.83±1.45	-6.04±6.61	-10.45 ±12.35	-9.70±15.10	-8.29±9.40
Eastern Weddell Zone (sections)	58°S-64°S	Summer	*SANAE*	-1.54±0.82	-5.10±5.42	-8.68± 10.28	-8.24±14.39	-6.88±7.68
	64°S-68°S	Summer	*SANAE*	-1.15±0.55	-3.23±2.08	-5.54±3.90	-4.44±4.70	-4.49±2.94
	68°S-70°S	Summer	*SANAE*	-4.57±1.57	-16.34 ±8.18	-28.91 ±16.22	-28.04 ±21.08	-22.69 ±12.15
Antarctic Shelf	70°S	Summer	*SANAE*	-5.79±0.78	-27.84 ±9.42	-52.21 ±18.75	-57.79 ±29.70	-40.21 ±13.67

Table 3 shows the same data used for Figure 17 but the data are in numerical form rather than in the form of a graph, and it includes the standard deviation of the mean for each model and zone. The table shows the fluxes calculated using daily wind speed rather than the weekly average wind speed. The actual values are easier to use to compare than a graphical representation because in some cases the values do not vary greatly, and although it is easy to see that in a graph, the actual difference is not known. This can be seen in tabular form. The CO_2 air-sea flux values that are calculated using the Broecker and Peng 'Stagnant Film Model' (B74) were between approximately 0.2 and -6mmol.m^{-2}.day^{-1}, they were mostly less than -2mmol.m^{-2}.day^{-1}, but increased closer to the shelf, at 68-70°S and again at the Shelf. The flux values calculated using the Liss and Merlivat relationship (LM86) ranged from approximately +1 to -28mmol.m^{-2}.day^{-1}. The flux values determined using the Wanninkhof relationship (W92) ranged from approximately +1 to -52mmol.m^{-2}.day^{-1}. The CO_2 air-sea flux values calculated using the cubic relationship of Wanninkhof and McGillis (WM99) ranged between +1 and -58mmol.m^{-2}.day^{-1}. The range of the Nightingale et al. relationship (N00) lies between +1 and -40mmol.m^{-2}.day^{-1}. The strongest flux for the all four of the last models

(LM86; W92; WM99; and N00) occurred at the continent, they were negative, and the weakest flux for these models occurred in the northern Polar Frontal Zone in autumn, they were all positive. All the models except B74 are in agreement with the direction of the flux, and are also in agreement with an increase and decrease of the CO_2 air-sea flux in comparison with the same regions and seasons, but they differ in the magnitude of the increase or decrease.

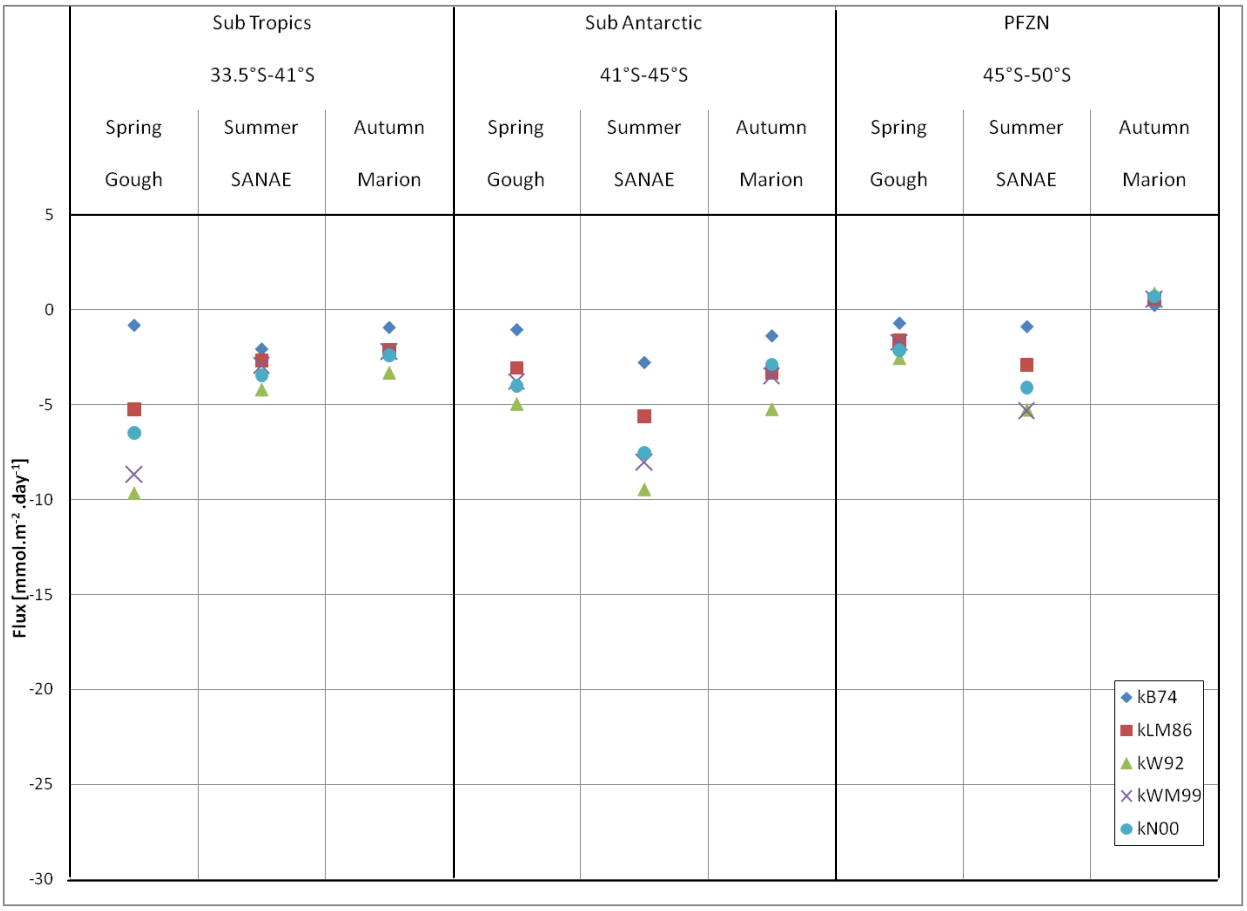

Figure 18: Graph showing the average air-sea CO_2 flux for each model across each region, separated into seasons (cruises). The gas transfer velocities were calculated using a weighted weekly average of the wind speed. Errors are shown in Table 4: Table showing the regional averages of the fluxes determined using *k* from the different relationships, included are the standard deviations from the mean for each region. It also includes the standard deviations. The different gas transfer velocities were calculated using the weighted weekly average of the wind speed. The flux is in mmol.m^{-2}.day^{-1}. B74 is the Broecker and Peng 'Stagnant Film Model; LM86 is the Liss and Merlivat Relationship; W92 is the quadratic Wanninkhof Relationship; WM99 is the Wanninkhof and McGillis cubic relationship and N00 is the Nightingale et al. quadratic parameterisation. Positive values indicate sea-to-air fluxes, and negative values indicate air-to-sea fluxes.

using standard deviation. B74 is the Broecker and Peng 'Stagnant Film Model; LM86 is the Liss and Merlivat Relationship; W92 is the quadratic Wanninkhof Relationship; WM99 is the Wanninkhof and McGillis cubic relationship and N00 is the Nightingale et al. quadratic parameterisation. Positive values indicate sea-to-air fluxes, and negative values indicate air-to-sea fluxes.

Figure 18 shows the average fluxes for the same regions and seasons as Figure 16, but the fluxes were calculated using weekly average wind speed, with the daily wind speeds each having a weighting according to importance (the day of the wind speed being of greatest importance and the day furthest before the day having the least importance). In the Subtropical region the greatest flux occurred in spring. Spring also had the greatest range in the different parameterisations used to calculate the flux (-1mmol.m^{-2}.day^{-1} to -~-9.5mmol.m^{-2}.day^{-1}). Summer had the next highest flux, ranging from about -2mmol.m^{-2}.day^{-1} to -4mmol.m^{-2}.day^{-1}, and then autumn, with a flux ranging from -1mmol.m^{-2}.day^{-1} to ~-3mmol.m^{-2}.day^{-1}. The only parameterisation that does not follow the same pattern as the others is B74. Its largest flux occurred in summer, then autumn, and then spring. In the Sub Antarctic region the greatest flux occurred in summer, this was also when the largest range occurred between the different parameterisations (~-3mmol.m^{-2}.day^{-1} to ~-9.5mmol.m^{-2}.day^{-1}). Spring had the smallest flux, but spring and autumn have similar ranges of the fluxes calculated using the different parameterisations of ~5mmol.m^{-2}.day^{-1}. In PFZN the greatest flux was in the summer, and the greatest range also occurred in summer (-1mmol.m^{-2}.day^{-1} to ~-5mmol.m^{-2}.day^{-1}). The smallest flux occurred in autumn, it was also the only positive flux that occurred from the subtropics to the PFZN, and it ranged from just above 0mmol.m^{-2}.day^{-1} to just below 1mmol.m^{-2}.day^{-1}.

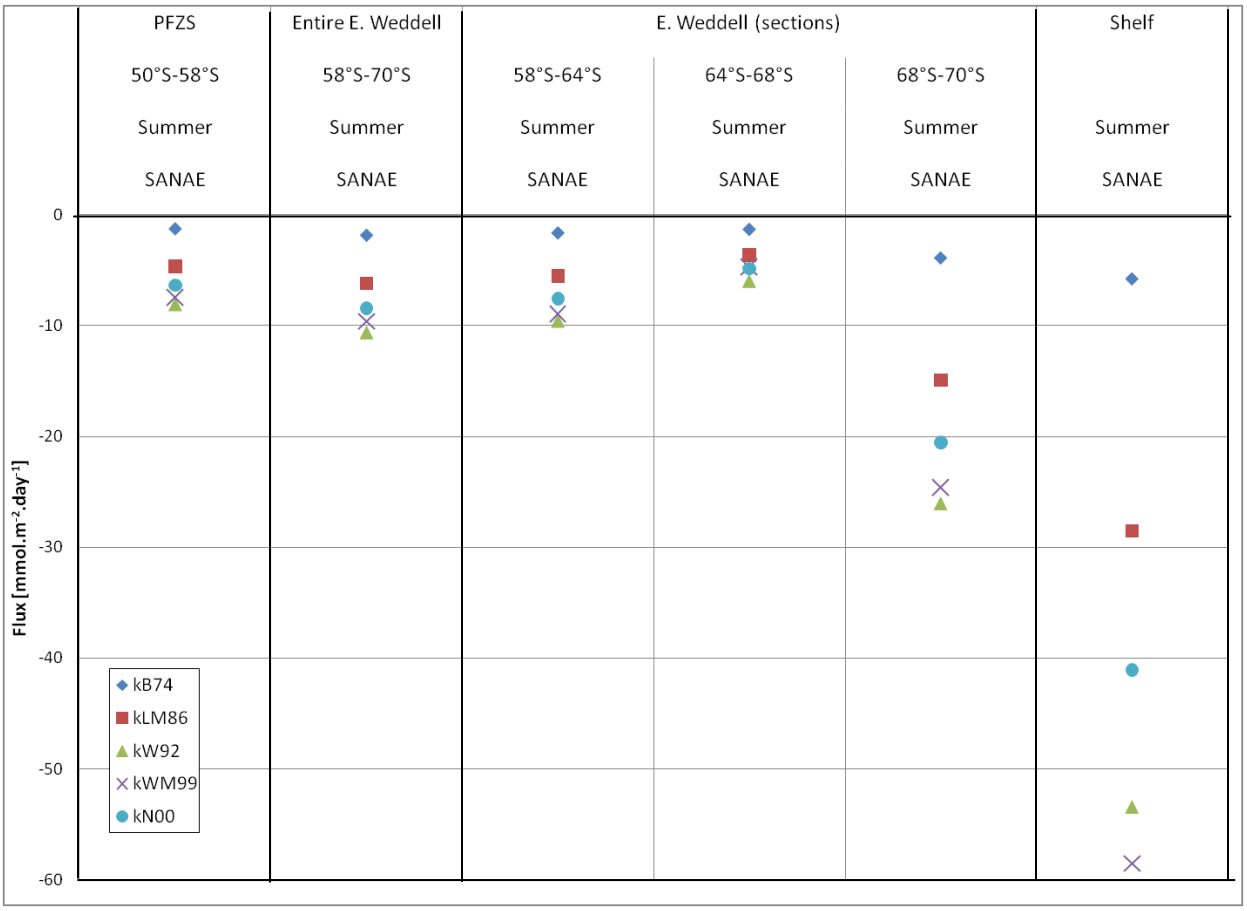

Figure 19: Graph showing the average air-sea CO_2 flux for each model for the summer season, for the regions from the Polar Frontal Zone (South) to the Antarctic Shelf. The gas transfer velocities were calculated using a weighted weekly average of the wind speed. Errors are shown in table Table 4: Table showing the regional averages of the fluxes determined using *k* from the different relationships, included are the standard deviations from the mean for each region. It also includes the standard deviations. The different gas transfer velocities were calculated using the weighted weekly average of the wind speed. The flux is in mmol.m^{-2}.day^{-1}. B74 is the Broecker and Peng 'Stagnant Film Model; LM86 is the Liss and Merlivat Relationship; W92 is the quadratic Wanninkhof Relationship; WM99 is the Wanninkhof and McGillis cubic relationship and N00 is the Nightingale et al. quadratic parameterisation. Positive values indicate sea-to-air fluxes, and negative values indicate air-to-sea fluxes. using standard deviation. B74 is the Broecker and Peng 'Stagnant Film Model; LM86 is the Liss and Merlivat Relationship; W92 is the quadratic Wanninkhof Relationship; WM99 is the Wanninkhof and McGillis cubic relationship and N00 is the Nightingale et al. quadratic parameterisation. Positive values indicate sea-to-air fluxes, and negative values indicate air-to-sea fluxes. Note the scale change from Figure 18.

Figure 19 shows the same regions as Figure 17, and it therefore also only has values for the summer season from the SANAE cruise. The smallest flux occurred between

64-68°S in the Eastern Weddell, with a range of about 5mmol.m^{-2}.day^{-1} between ~-1mmol.m^{-2}.day^{-1} and ~6mmol.m^{-2}.day^{-1}. The PFZS also had a small flux, but the range was slightly larger than between 64-68°S (about 8mmol.m^{-2}.day^{-1}). Between 58-64°S the flux was less than -10mmol.m^{-2}.day^{-1}, but it still had a range of about 8mmol.m^{-2}.day^{-1}. The flux increased at 68-70°S to between~-4mmol.m^{-2}.day^{-1} and ~-25mmol.m^{-2}.day^{-1}. This caused the average flux of the entire East Weddell section to increase. The flux increased again at the Antarctic Shelf, and the range was between about -6mmol.m^{-2}.day^{-1} and just below -60mmol.m^{-2}.day^{-1}.

Table 4: Table showing the regional averages of the fluxes determined using *k* from the different relationships, included are the standard deviations from the mean for each region. It also includes the standard deviations. The different gas transfer velocities were calculated using the weighted weekly average of the wind speed. The flux is in mmol.m^{-2}.day^{-1}. B74 is the Broecker and Peng 'Stagnant Film Model; LM86 is the Liss and Merlivat Relationship; W92 is the quadratic Wanninkhof Relationship; WM99 is the Wanninkhof and McGillis cubic relationship and N00 is the Nightingale et al. quadratic parameterisation. Positive values indicate sea-to-air fluxes, and negative values indicate air-to-sea fluxes.

				Flux B74	Flux LM86	Flux W92	Flux WM99	Flux N00
Sub Tropical Zone	33.5°S-41°S	Spring	*Gough*	-0.82±0.95	-5.25±3.25	-9.68±6.06	-8.67±7.45	-6.49±5.35
		Summer	*SANAE*	-2.08±1.01	-2.69±1.07	-4.23±1.64	-2.92±0.97	-3.46±1.38
		Autumn	*Marion*	-0.94±0.62	-2.14±1.24	-3.33±1.91	-2.18±1.20	-2.41±1.32
Sub Antarctic Zone	41°S-45°S	Spring	*Gough*	-1.05±0.21	-3.08±1.06	-4.98±1.88	-3.77±1.93	-4.02±1.43
		Summer	*SANAE*	-2.79±0.67	-5.63±1.53	-9.48±2.93	-8.03±3.68	-7.55±2.16
		Autumn	*Marion*	-1.38±0.67	-3.33±1.76	-5.25±2.70	-3.47±2.03	-2.88±1.23
Northern Polar Frontal Zone (PFZN)	45°S-50°S	Spring	*Gough*	-0.71±0.17	-1.64±0.45	-2.57±0.68	-1.71±0.56	-2.12±0.53
		Summer	*SANAE*	-0.89±0.39	-2.92±1.28	-5.29±2.38	-5.32±2.52	-4.11±1.83
		Autumn	*Marion*	0.23±0.14	0.55±0.36	0.85±0.56	0.57±0.38	0.69±0.46

Southern Polar Frontal Zone (PFZS)	50°S-58°S	Summer	*SANAE*	-1.25±0.92	-4.67±2.90	-8.08±4.90	-7.45±4.58	-6.35±3.87
Entire Eastern Weddell Zone	58°S-70°S	Summer	*SANAE*	-1.84±1.24	-6.17±5.82	-10.63± 10.93	-9.60±12.96	-8.43±8.34
Eastern Weddell Zone (sections)	58°S-64°S	Summer	*SANAE*	-1.62±0.78	-5.52±4.22	-9.57±8.39	-8.90±10.58	-7.56±6.33
	64°S-68°S	Summer	*SANAE*	-1.31±0.50	-3.61±1.64	-5.97±3.01	-4.67±3.40	-4.84±2.29
	68°S-70°S	Summer	*SANAE*	-3.89±1.72	-14.90 ±8.74	-26.04 ±16.89	-24.57 ±22.34	-20.55 ±12.61
Antarctic Shelf	70°S	Summer	*SANAE*	-5.79±0.78	-28.52 ±3.60	-53.42 ±8.73	-58.54 ±15.63	-41.09 ±6.26

Table 4: Table showing the regional averages of the fluxes determined using *k* from the different relationships, included are the standard deviations from the mean for each region. It also includes the standard deviations. The different gas transfer velocities were calculated using the weighted weekly average of the wind speed. The flux is in $mmol.m^{-2}.day^{-1}$. B74 is the Broecker and Peng 'Stagnant Film Model; LM86 is the Liss and Merlivat Relationship; W92 is the quadratic Wanninkhof Relationship; WM99 is the Wanninkhof and McGillis cubic relationship and N00 is the Nightingale et al. quadratic parameterisation. Positive values indicate sea-to-air fluxes, and negative values indicate air-to-sea fluxes. shows the data in Figure 19: Graph showing the average air-sea CO_2 flux for each model for the summer season, for the regions from the Polar Frontal Zone (South) to the Antarctic Shelf. The gas transfer velocities were calculated using a weighted weekly average of the wind speed. Errors are shown in table Table 4:

Table showing the regional averages of the fluxes determined using *k* from the different relationships, included are the standard deviations from the mean for each region. It also includes the standard deviations. The different gas transfer velocities were calculated using the weighted weekly average of the wind speed. The flux is in mmol.m^{-2}.day^{-1}. B74 is the Broecker and Peng 'Stagnant Film Model; LM86 is the Liss and Merlivat Relationship; W92 is the quadratic Wanninkhof Relationship; WM99 is the Wanninkhof and McGillis cubic relationship and N00 is the Nightingale et al. quadratic parameterisation. Positive values indicate sea-to-air fluxes, and negative values indicate air-to-sea fluxes. using standard deviation. B74 is the Broecker and Peng 'Stagnant Film Model; LM86 is the Liss and Merlivat Relationship; W92 is the quadratic Wanninkhof Relationship; WM99 is the Wanninkhof and McGillis cubic relationship and N00 is the Nightingale et al. quadratic parameterisation. Positive values indicate sea-to-air fluxes, and negative values indicate air-to-sea fluxes. Note the scale change from Figure 18. in numerical format. The data includes the error in standard deviation of the mean for each model in each of the frontal zones. The fluxes were calculated using the weighted weekly average of the wind speed. The strongest negative flux occurs at the Antarctic Shelf, calculated using WM99 model. In PFZN the flux in autumn is positive for all models, although it is less than 1mmol.m^2.day^{-1}. It is the only time that the flux is positive, and is also where the weakest flux occurs. The largest error occurs in the region between 68°S and 70°S, using WM99. In this region the standard deviation for both W92 and WM99 are high.

3.4.2. Response of the difference Air-Sea CO_2 Fluxes to the uncertainty in Wind Speed of 2m.s^{-1}

Figure 20 was created by calculating the air-sea CO_2 flux using *k* from the five different models being examined in this study for three different wind regimes (low [3m.s^{-1}], medium [8m.s^{-1}] and high [14m.s^{-1}]). All gas transfer velocities were normalised to a

Schmidt Number of 660, and were created with the same ΔfCO_2, temperature, salinity and pressure, the only this to vary is the wind speed.

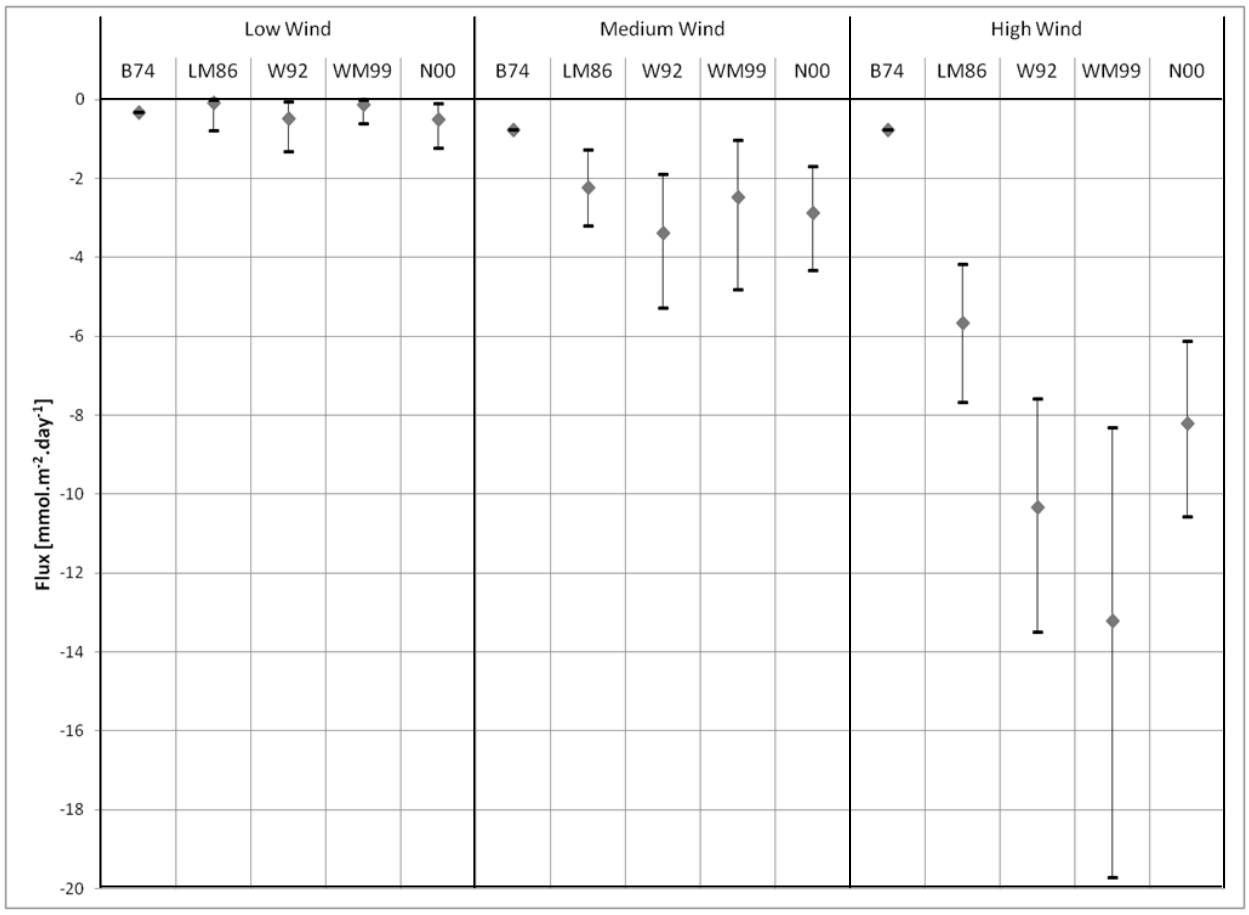

Figure 20: Graph showing the sensitivity of the fluxes calculated with the gas transfer velocities of each model to uncertainties in the wind product in low wind (3m.s^{-1}), medium strength wind (8m.s^{-1}) and high wind (14m.s^{-1}). The uncertainty of the wind speed from Seawinds on QuikSCAT is 2m.s^{-1} (Perry, 2000). All gas transfer velocities are normalised to a Schmidt number of 660. The error bars represent gas transfer velocities at wind speeds of =2m.s-1 (upper bar) or -2m.s-1 (lower bar) relative to the low, medium and high wind speeds. The fluxes were calculated using ΔfCO_2=-20µatm, temperature=5°C, salinity=33.5, and pressure=0.5bar. B74 is the Broecker and Peng 'Stagnant Film Model; LM86 is the Liss and Merlivat Relationship; W92 is the quadratic Wanninkhof Relationship; WM99 is the Wanninkhof and McGillis cubic relationship and N00 is the Nightingale et al. quadratic parameterisation. Negative values indicate air-to-sea fluxes.

In the low wind speed range, all of the flux values are low (less than -1mmol.m^{-2}.day^{-1}). The largest fluxes are from W92 and N00, and the largest changes in magnitude of the flux with an increase or decrease in wind speed by 2m.s^{-1} also occur with W92 and N00. The smallest flux occurs using the WM99 model, with a value only just greater than 0mmol.m^{-2}.day^{-1}. There is no sensitivity to a change in wind speed occurring in B74. In the medium wind speed range all the fluxes increase, although the increase in B74 is much smaller than the other models (only ~0.5mmol.m^{-2}.day^{-1}). The largest flux is W92 (~-3.5mmol.m^{-2}.day^{-1}), but the greatest sensitivity occurs in WM99, with a decrease of about 1.5mmol.m^{-2}.day^{-1} with a decrease in wind of 2m.s^{-1}, and an increase in flux of about 2.5mmol.m^{-2}.day^{-1} with an increase in wind speed of 2m.s^{-1}.

W92 still has a large sensitivity to a change in wind speed, with the range of the sensitivity being ~4.5mmol.m^{-2}.day^{-1}. N00 has the second highest flux (~-5mmol.m^{-2}.day^{-1}), and has a sensitivity range of ~2.5mmol.m^{-2}.day^{-1}. LM86 is the second smallest flux, and has a sensitivity range of about 2mmol.m^{-2}.day^{-1}. In the high wind speed range, all the fluxes has a large increase in magnitude and sensitivity, except for B74 which does not change from the medium wind speed range. The highest flux is WM99 (~-13mmol.m^{-2}.day^{-1}), and WM99 also has the greatest sensitivity to an increase or decrease in wind speed, ~6.5mmol.m^{-2}.day^{-1} with an increase in wind speed of 2m.s^{-1}, and ~5mmol.m^{-2}.day^{-1} with a decrease in wind speed of 2m.s^{-1}. The least responsive model, aside from B74, is LM86 (~-5.5mmol.m^{-2}.day^{-1}), which also has the smallest response to a change in wind speed of 2m.s-1, with the range in responsiveness being just under 4mmol.m^{-2}.day^{-1}. N00 has a magnitude of ~8mmol.m^{-2}.day^{-1}, and the range in sensitivity to a change in wind speed of 2m.s^{-1} is ~4.5mmol.m^{-2}.day^{-1}. The second greatest flux is W92, and it also has the second largest sensitivity to the change in wind speed, ~3mmol.m^{-2}.day^{-1} decrease with a decrease in wind speed of 2m.s^{-1}, and ~3mmol.m^{-2}.day^{-1} increase with an increase in wind speed of 2m.s^{-1}.

3.4.3 Response of the Air-Sea CO_2 flux to the uncertainty in Temperature and ΔfCO_2

Refer to Appendix 2 for the tables showing the information on the uncertainties. Table 7: Table showing change in the Flux because of uncertainty in the temperature of 0.05°C, which affects solubility. A change in temperature also affects the Schmidt number, and in turn, the gas transfer velocity. All columns except for Temperature and Solubility remain to 4 decimal points to show the small changes that occur. is calculated using a ΔfCO_2 of -2µatm. An increase or decrease of 0.05°C in temperature only affects solubility a small amount, it also affects the Schmidt number, which has an impact on *k*, and the resulting change in the flux at low temperatures is approximately 0.08%. At high temperature, the change in the flux is smaller, at approximately 0.03% change in the flux. The impact of the uncertainty is greater when the temperature is lower, because a lower temperature means a higher solubility, which would then have a greater impact on the flux.

Table 8: Table showing change in the Flux because of uncertainty in ΔfCO_2 of 1µatm. Temperature used to calculate Solubility is 5°C, Salinity is 33.50 is calculated using a temperature of 5°C. An increase or decrease in ΔfCO_2 has less of an impact on the flux as ΔfCO_2 increases. The range of change as a percentage of the flux at a small ΔfCO_2 was 20%, and at large ΔfCO_2 it is 6.67%. The influence of ΔfCO_2 on the flux is greater than temperature and the uncertainty of the flux increases more with ΔfCO_2 than with temperature.

Chapter 4:

DISCUSSION

4.1 Introduction

This study set out to examine the differences in the gas transfer velocity models and their response to different wind speeds, and the uncertainty of the wind speed product as a result of their assumptions and limitations. The choice of using the 'classical' models was to show the increase in understanding of gas transfer velocity over time. More complex models exist that use a number of different parameters that take into account the different processes that occur at the ocean's surface that could increase gas transfer velocity (Glover et al., 2005; Woolf, 2005). The parameters used to determine *k* are wind speed and the Schmidt number, this is because wind speed is easily available on a global scale from satellite.

In this discussion the typical regional oceanography of the Southern Ocean will be examined in comparison to that found in this study. The differences of the five gas transfer velocity models used in determining the CO_2 flux will be explained, and a comparison will be made of the CO_2 flux calculated in this study using the Wanninkhof relationship with that determined in Takahashi et al., (2009).

4.2 Oceanography of the Southern Ocean

4.2.1 Fronts and Physical Properties

This study uses a simplified means of determining the fronts, and their frontal zones. This is for the comparison of the three cruise lines, as well as a comparison with the study of Takahashi et al., (2009).

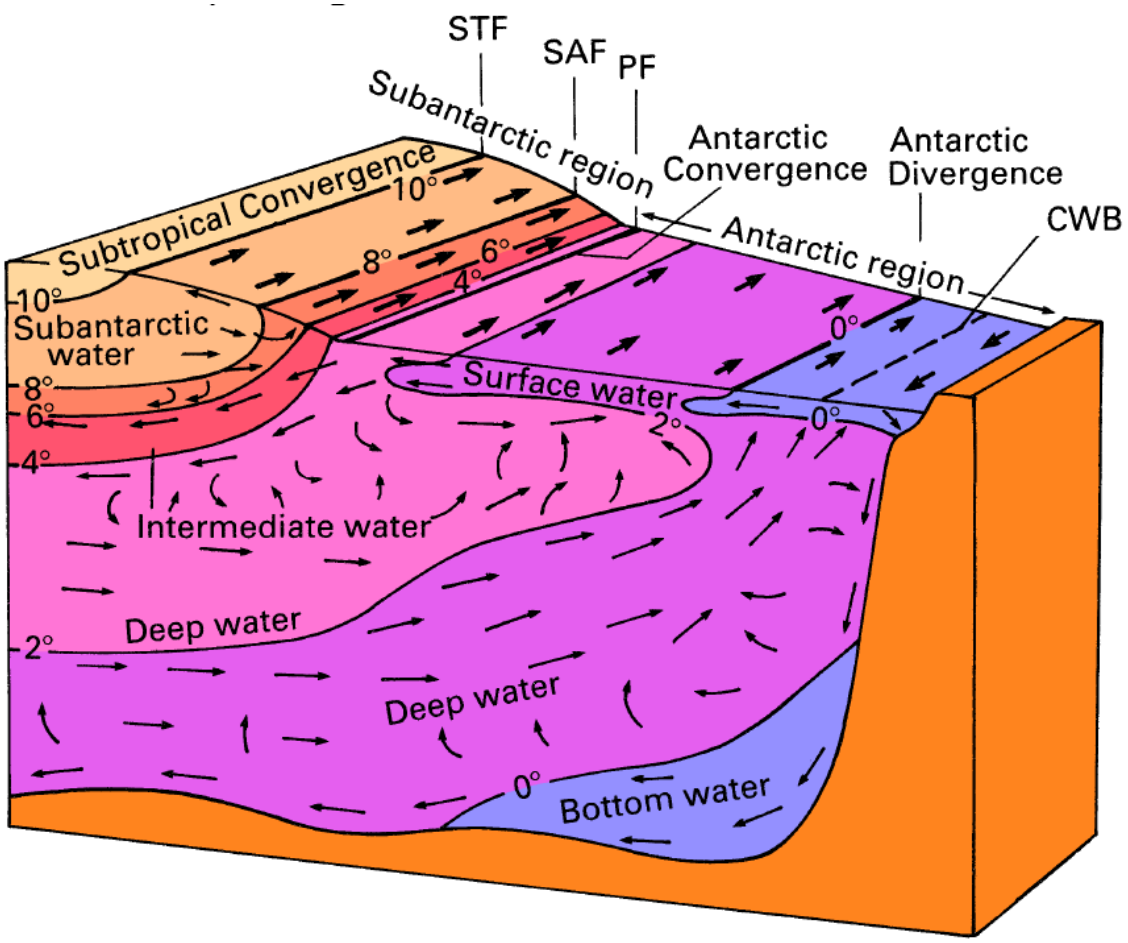

Figure 21:Block diagram showing the water circulation of the Southern Ocean from Sverdrup et al., (1942), with the addition of the frontal locations (STF: Subtropical Front, SAF: Sub Antarctic Front, PF: Polar Front, CWB: Continental Water Boundary) (Tomczak and Godfrey (2003)) South of the Polar Front the Deep Water is the North Atlantic Deep Water (NADW) and the Circumpolar Deep Water (CDW), the Intermediate Water is the Antarctic Intermediate Water (AAIW), the Bottom Water is the Antarctic Bottom Water (AABW) and the Surface Water is the Antarctic Surface Water (AASW).

The Subtropical Front is the boundary between the fresher Southern Ocean and the more saline and warmer tropical waters (Orsi et al., 1995). The salinity data presented in Figure 8b show a decrease from 33.5°S to the Antarctic Shelf and has its biggest change occurring at the Sub Tropical Front at approximately 41°S. The salinity is higher in the Subtropical Zone than in the other regions. This is because the Subtropical Zone is an area of high evaporation leading to saline surface waters (35.00) (Talley et al., 2011). The Subtropical Front is usually marked with a temperature decrease as well as

a salinity decrease, moving from the Subtropical Surface Water (STSW) to the Sub Antarctic Surface Water (SASW). The results from this study show a constant decrease in temperature from the African continent to the Antarctic Shelf. The variation in the temperature data of the Gough Island cruise from the SANAE and Marion Island cruises in the Sub-Tropical Zone could result from the Agulhas Current on the east coast and the Benguela Current on the west coast of Southern Africa. The Marion Island and SANAE cruises would be affected by the warm Agulhas current on the east of Southern Africa, and although the beginning of the Gough Island cruise is not fully in the region of the cold Benguela current on the west coast of Southern Africa, and the beginning of the cruise would be out of reach of the Agulhas current or perhaps even the warm eddies that detach from the Agulhas current and move west. The temperature results could vary because the three cruises took place in during different seasons, therefore seasonal changes would occur. The results from this study show that the Subtropical Zone has high salinity and temperature (35.00 and 14-22°C respectively), and surface water fCO_2 increases with salinity and temperature, it would follow that the region should have high surface water fCO_2. Therefore we would assume that the Subtropical Region would be a source of CO_2 to the atmosphere, Mikaloff Fletcher et al., 2007 also state that the Subtropical region is a source of CO_2. This study recorded a ΔfCO_2 range of -30µatm in summer to -20µatm in spring, which would result in the ocean being a sink of CO_2. The results are in disagreement with the previous statement. This could be due to an error in the autonomous system in oceanic pCO_2, or perhaps our estimate of 384.5µatm overestimates the atmospheric pCO_2.

In the view of Metzl et al., (1999) and McNeil et al., (2007), the Sub Antarctic Zone, located between the Subtropical Front and the Sub Antarctic Front, is considered to be one of the strongest oceanic sinks for atmospheric CO_2. This is because of the high winds and low sea surface pCO_2 relative to the atmospheric pCO_2. The winds from this study are considered high in this region (approximately $8m.s^{-1}$ to $11m.s^{-1}$). The ΔfCO_2 for this recorded in this study for this region is negative (~-30µatm in spring to ~50µatm in summer), so the surface water fCO_2 is less than the fCO_2 in the atmosphere. The

Sub Antarctic Front is recognised by the sinking of the low salinity Antarctic Intermediate Waters (AAIW), which yields penetration of anthropogenic pCO_2 below the mixed layer (Metzl et al., 1999). The temperature range of the SASW in summer spans 4-14°C and salinity ranges from 33.90-34.90, but can reach as low as 33.00 due to the melting of sea ice in summer (Tomczak and Godfrey, (2003)). This study's results show a temperature range of 10-14°C and salinity range of approximately 32.00-35.00. The reasons for the low salinity values are not known, but they could be a result of rainfall in the region.

The Northern Polar Frontal Zone separates the Sub Antarctic Front and the Polar Front. At the Polar Front there is a large temperature gradient along the salinity minimum of the Antarctic Surface Waters (AASW). The results from this study show that the temperature ranges from about 10°C in autumn in the northern region of the Polar Frontal Zone to about 5°C in spring. The salinity remains constant at 34.00. The fCO_2 shown in these results is negative for the Polar Frontal Zone (approximately -20µatm), except in autumn in the northern region of the Polar Frontal Zone (~+8µatm). The positive ΔfCO_2 value, meaning that surface water fCO_2 is greater than the atmospheric fCO_2, could be a result of the location. This is in the proximity of Marion Island, and could be due to minor scale upwelling, or biological remineralisation. Bakker et al., (2007) recorded that there is oceanic productivity occurring downstream of islands in the Antarctic Circumpolar Current (ACC) in summer is high.

The Southern Polar Frontal Zone is located between the Polar Front and the Eastern Weddell Gyre. Because of the different terms used in describing the regions in the Southern Ocean, there is not a lot that can be found on this area. Therefore is could be an appropriate region for further investigation. The temperature result in this study for this region is approximately 3°C, and salinity is 34.00. ΔfCO_2 is ~-30µatm, therefore there would be a flux of CO_2 into the ocean.

The Eastern Weddell region is recognised by the upwelling of the high salinity Circumpolar Deep Water (CDW) that has moved south from the Equator. Tomczak and Godfrey (2003) suggest that his upwelling is unique as the water being upwelled is from great depths in the Atlantic. This region can also be referred to as the Antarctic Divergence. The deep upwelling occurs because the Antarctic Intermediate Water moves equatorward, as does the Antarctic Bottom Water (AABW). Because of reasons of mass conservation, this water must be replaced by the poleward movement of water at the deep water depth and lifted to the surface to replace the water that sank in order to form the AAIW and AABW. Deep waters are usually high in CO_2 because of the of remineralisation process of the decaying organisms that release CO_2 as they sink (Mikaloff-Fletcher et al., 2007; Arrigo et al., 2008; Fabry et al., 2008; Doney et al., 2009). The upwelling of CDW in the Eastern Weddell region is evident in Figure 10 showing the salinity results for the region, as the deep water is more saline than the surrounding waters; the increase in salinity is up to 0.50. Because of this upwelling of CO_2 rich waters in the Eastern Weddell region, one would expect it to be a source of CO_2 to the atmosphere. The results show that the ΔfCO_2 for this region ranges from approximately -35µatm between 64-68°S and -110µatm between 68-70°S, with the entire Eastern Weddell Gyre having an average ΔfCO_2 of ~50µatm. This means that the results are in disagreement with the expectation of the Eastern Weddell Region being a CO_2 source. Hoppema et al., (1999) did a study in the Weddell Gyre and found that biological drawdown had the greater impact when they compared the conflicting effects of upwelling and biological drawdown on the CO_2 concentration on the surface ocean. Perhaps this is also true in this study.

The region just north of the Antarctic Shelf is an important area of ventilation in carbon dioxide (Arrigo et al., 2008) because is characterised by the sinking of Antarctic Bottom Water (AABW), which is extremely cold and has elevated salinity due to the formation of sea ice. In the view of Orsi et al. (1995), the shelf waters are near freezing temperatures. The cold temperature (just below 0°C) and the high salinity (about 34.00) of this water make it very dense, so it sinks and the moves north. If this study had taken

place in winter, the water at the Shelf should be highly saline because of the formation of sea ice, but the salinity at the continent recorded in these results was recorded in summer, and has low values in Figure 8b. This is maybe because of ice melt, or the presence of ice bergs. There also could have been a period of rainfall or snowfall. The ΔfCO_2 values at the shelf were high and negative (-140µatm), due to the low oceanic fCO_2. As the temperature of the water decreases, the concentration of fCO_2 will decrease because CO_2 gas solubility increases with temperature. This could explain the low CO_2 concentration in the surface water at the Antarctic Shelf. It could also be due to biological production near the Antarctic Shelf, carbon dioxide is used up the in the process of photosynthesis (Hoppema, 2002), although it cannot account for the entire deficit. There could have been an overestimating in the ocean pCO_2, as the vessel was stationary at the ice for a considerable amount of time.

Metzl et al., (1999), Wanninkhof et al., (2004), Ho et al, (2006) and Le Quéré et al (2007) propose that the Southern Ocean as a whole is considered to be a sink of CO_2 from the atmosphere into the ocean. Sabine et al., 2004 stated that the Southern Ocean has been the only 'true' sink of CO_2 over the last 200 years. The sink could be due to the biological and solubility pumps. In the Southern Ocean, the Southern Annular Mode (SAM) is the dominant mode of atmospheric variability (Barbero et al., 2011). A positive trend in SAM intensifies the westerlies and is also results in a poleward shift of the westerlies, this then increases the CO_2 ventilation from nutrient rich-deep waters (Lovenduski et al., 2007). Research has suggested that the ability of the Southern Ocean to take up anthropogenic CO_2 may have decreased since the 1980s as a result of the Southern Annular Mode (Le Quéré et al., 2007; Lovenduski et al., 2008).

4.2.2 Wind Speed

The Southern Ocean is characterised by moderate to high wind speeds (Wanninkhof et al., 2004; Ho et al., 2006). Wanninkhof et al, (2004) suggest that the high winds and long fetches cause an environment with sustained significant wave heights and large swells. This is shown in the results, as the wind speeds range from 6m.s^{-1} to 12m.s^{-1} for each region and season. This confirms that the data were not recorded in a year of anomalous low wind speed. Ho et al., (2006) performed a $^{3}He/SF_6$ dual tracer release experiment in the Southern Ocean southeast of New Zealand in order to measure air-sea gas exchange at high wind speeds. They found that the wind speeds ranged from 7.4m.s^{-1} to 16m.s^{-1} for the ship based measurements as well as the QuikSCAT measurements. There were only two occasions where the observed wind speed measurements differed to the QuikSCAT wind speeds by more than 3m.s^{-1}, and it was suggested that the spatial variability for the QuikSCAT measurements was greater than that of the ship based measurements. It was then decided that they would continue to use the QuikSCAT measurements in order to guarantee consistency with previous and future experiments in the derivation of the relationship between wind speed and gas transfer velocity.

Winds are variable at a synoptic scale, therefore we need to understand the sensitivity of calculated CO_2 flux to differences in instantaneous winds vs. Integrated winds. Daily wind speed was used in this study, as well as the average of the wind speeds for the week previous to the daily wind, where each day has a weighting according to the order of the day in the week (Figure 11 and Figure 12). The wind dataset was weighted so that recent winds would have a high weighting because they would have a greater impact on the observed oceanic conditions than the less recent winds. This did lead to a difference in the gas transfer velocity when calculated with one of the two wind speed products, but the difference in the flux eventually determined using *k* was minimal. If the daily wind speed is higher than the weekly average of the weighted wind speed, the

wind on that day would have been stronger than the wind of the week before the day, and if it was weaker, than the wind of the week before the day would have been stronger than the wind on the day. If there is little or no difference between the two wind speed products, then wind speed would have been constantly weak or strong throughout the week. The difference in *k* because of the different wind speed products would have occurred in regions where the two wind speeds differed greatly. There was only one instance when the daily wind and weekly averaged winds were different. This was in spring in the Polar Frontal Zone (North), and the difference in the two wind products was about $2m.s^{-1}$, larger than the standard errors of the wind. The daily wind speed was approximately $9.5m.s^{-1}$ and the weighted wind speed was $7m.s^{-1}$. This suggests that the wind during the course of the week previous to the observed wind was weaker than the wind that occurred on the day.

The study from Takahashi et al. (2009) had lower wind speeds than this study in the area south of 62°S, but the results from this study show that the wind speeds south of 62°S were moderate to high, ranging from $8m.s^{-1}$ to $12m.s^{-1}$, with the highest wind speed in this region occurring at the Antarctic continent. This could have an effect in the comparison between the CO_2 flux calculated in this study and that calculated in Takahashi et al., (2009).

4.3 Comparison of the Fluxes calculated using the Different Gas Transfer Velocity Models

Gas Transfer Velocity, the rate at which gases move across the air-sea interface, is a function of wind speed, temperature, salinity and the Schmidt Number. This study focuses on five different parameterisations in determining the gas transfer velocity used in calculated the gas flux for CO_2. They are the Stagnant Film Model used in Broecker and Peng (1974) [B74], the linear relationship between wind speed and gas transfer

velocity that is separated into three wind regimes (low, medium and high) as suggested by Liss and Merlivat (1986) [LM86], the quadratic relationship from Wanninkhof (1992) [W92], the cubic relationship by Wanninkhof and McGillis (1999), and from Nightingale et al., (2000), a quadratic relationship [N00]. The parameterisations were created using different methods to study gas transfer velocity and relationship between wind speed and directly observed gas transfer velocities.

1. The Stagnant Film Model (Broecker and Peng, 1974)

$$\mathrm{k} = \frac{\mathrm{D}}{\mathrm{z}} \qquad (2)$$

D = molecular diffusivity [$cm^2.s^{-1}$]

z = thickness of film [μ]

z is affected by the agitation for CO_2 in seawater: high agitation = 129μ

low agitation = 311μ

2. Liss and Merlivat (1986)
   a) For a zonal component of surface wind speeds ($u \leq 3.6 m.s^{-1}$) (Smooth Surface or Boundary Layer Regime)

$$k_{600} = (0.17\mathrm{u})Sc^{-2/3} \qquad (3.1)$$

   b) For a zonal component of surface wind speeds ($3.6 m.s^{-1} < u \leq 13 m.s^{-1}$) (Rough Surface or Surface Renewal Regime)

$$\mathrm{k}_{600} = (2.85\mathrm{u} - 9.65)\mathrm{Sc}^{-1/2} \qquad (3.2)$$

   c) For a zonal component of surface wind speeds ($u > 13 m.s^{-1}$) (Breaking Wave Regime)

$$\mathrm{k}_{600} = (5.9\mathrm{u} - 49.3)\mathrm{Sc}^{-1/2} \qquad (3.3)$$

3. Wanninkhof (1992)

$$k_{660} = 0.31u^2Sc^{-1/2} \quad (4)$$

4. Wanninkhof and McGillis (1999)

$$k_{660} = 0.0283u^3Sc^{-1/2} \quad (5)$$

5. Nightingale et al. (2000)

$$k_{600} = (0.222u^2 + 0.333u)Sc^{-1/2} \quad (6)$$

4.3.1 Change in Gas Transfer Velocity Models with Wind Speed and the Uncertainty in the Wind Speed Product

The results showed that there is only one time when B74 experiences a change in its magnitude, moving from a low wind regime to a medium wind regime. There is no change in B74 due to the uncertainty in the wind speed product in any of the three wind regimes. This is because B74 is not dependent on wind speed, and therefore there is no relationship. The models with the greatest response to the uncertainty in the wind speed product in the low wind regime are W92 and N00. This could be due to the quadratic relationship in these models between wind speed and gas transfer velocities. W92 has the greatest change in magnitude when changing wind regimes from a low to and medium wind speed. But WM99 has the greatest sensitivity that it would change due to the uncertainty in the wind product of 2m.s^{-1} in the medium wind speed regime due to the cubic relationship between wind speed and *k*. All models, besides for B74 have an increase in *k* of at least 10cm.h^{-1} when changing from a low wind regime to a medium wind regime. WM99 has the greatest change in the value of *k* when moving from a medium wind regime to a high wind regime. It also experiences the largest change due to the uncertainty in the wind product. All of the values for *k* defined by the

different models experience an increase in *k* of about 15cm.h^{-1}, except for the unresponsive B74.

There is only a single increase in gas transfer velocity of B74 at a wind speed of 6m.s^{-1}, which is because of the change in thickness of the stagnant film separating the well mixed bodies of air and water, and gas transfer velocity is controlled by the molecular diffusivity of CO_2 in seawater divided by the thickness of the sea surface microlayer (SSML).

The thickness is dominated by the agitation of the sea surface, and as the wind speed increases the agitation of the sea state increases thereby decreasing the thickness of the film. In Broecker and Peng (1974) only two film thicknesses are given: 129μ for high agitation and 311μ for low agitation for CO_2 in seawater. There was no clear relationship between wind speed and gas transfer velocity calculated using the Stagnant Film Model, and *k* was unresponsive to a change in wind speeds, meaning there is no wind parameterisation.

LM86 is controlled by three linear regimes: smooth surface regime (weak winds: less than 3.6m.s^{-1}), rough surface regime (moderate winds: between 3.6m.s^{-1} and 13m.s^{-1}) and breaking wave regime (strong winds: above 13m.s^{-1}). This is evident in the results, as the rate of increase in *k* intensifies moving from the weak winds to moderate winds, and again to high winds. It is often considered to be the lower bound of gas transfer-wind speed relationships (Feely et al., 2001), which is in agreement with the results of this study, except that this study includes the Stagnant Film Model (B74), which has yielded even lower values than LM86. The linear relationship between wind speed and gas transfer velocity defined by Liss and Merlivat can be seen in the results. The differences are particularly large at high wind speeds (14m.s^{-1}). This could be because

other processes would affect gas transfer velocity at high wind speeds, such as bubble entrainment

The result of increasing or decreasing the wind speed by the uncertainty in the wind speed product of 2m.s^{-1} seems significant at the low wind speed regime, with the change in wind speeds totalling 5cm.h^{-1}. The change in *k*W92 with the uncertainty in the wind speed increases from the low wind regime to the medium wind regime, and again at the high wind regime. The increase in *k* is much greater from the medium to the high regime than from the low to the medium regime. This is due to the quadratic relationship that Wanninkhof assumed of wind speed and gas transfer velocity at steady wind speeds. It would follow then that the *k* would be more sensitive to an error at high wind speeds than at low wind speeds. Wanninkhof's quadratic model for steady winds should have been replaced in this study by Wanninkhof's quadratic model for long-term winds:

$$k_{660} = 0.39u^2Sc^{-1/2} \qquad (7)$$

All four of the gas transfer velocity relationships that are a function of the Schmidt Number show an increase in *k* from the low wind regime to the medium regime, and then again at the high wind regime, with the increases in *k* larger from the medium wind regime to the high wind regime than from the low wind regime to the medium wind regime.

N00 increases in *k* are smaller in the medium and high wind speeds than W92 and WM99. Woolf (2005) also agrees that the gas transfer velocity of WM99 is the greatest at high wind speeds, the gas transfer velocity determined from W92, followed by *k* from N00, and LM86 is the lowest of these four parameterisations. Wanninkhof (1992) states that LM86 may exhibit a weaker dependence on wind speed than W92 because it was developed using data from fetch limited environments. W92 has the largest increases

in the change of gas transfer velocity in the medium wind speed regime and WM99 has the largest increases in the change of *k* in the higher wind speed regimes, which is in agreement with the statement from Feely et al., (2001) that WM99 shows a weaker dependence on wind for wind speeds lower than $10m.s^{-1}$ and a significantly stronger dependence at higher wind speeds because of the cubic relationship gas transfer velocity has with wind speed. This would be because of the cubic relationship that wind speed and gas transfer velocity have in WM99. W99 is also based on steady winds, which is impractical for the Southern Ocean, because it is characterised by high speed winds (Ho et al., 2006).

Ho et al., (2006) state that LM86, W92, WM99 and N00 all diverge widely at high wind speeds (greater than $10m.s^{-1}$), and this leads to significant uncertainties in estimates of CO_2 uptake by regions dominated by high wind speed, such as the Southern Ocean. LM86 and N00 are small scale experiments and produce average global gas transfer velocities smaller than those determined by W92 (Sweeney et al., 2007). N00 has potential faults, as it was based on the $^3He/SF_6$ data that were collected in the coastal ocean, which may experience different wind speed and gas transfer velocity relationship because of factors such as a smaller fetch and higher occurrence of surfactants (Ho et al., 2006). W92 is one of the most favoured parameterisations (Feely et al., 2001; Wanninkhof et al., 2009), because it yields consistent results when applied to global ocean biogeochemical circulation models that use the same bomb ^{14}C that was used in the determination of the Wanninkhof parameterisation as a constraint.

According to Wanninkhof et al., (2004) and Ho et al., (2006) the $^3He/SF_6$ dual tracer method used in N00 is considered the most effective approach to integrated measurement of gas transfer velocity in the field. It shows a strong relationship between wind speed and gas transfer velocity. But the experiments only cover wind speeds ranging only up to $11.3m.s^{-1}$, therefore seriously limiting the substantiation of the

existing wind speed/gas transfer velocity parameterisations, especially at high wind speeds.

The quadratic relationship for wind speed and gas transfer velocity as stated by Wanninkhof (1992) and Nightingale et al., (2000) can be seen using a trendline for the data shown in this study when the gas transfer velocity was plotted against the wind speed using Figure 14 and Figure 15 in the results, as is the cubic relationship from Wanninkhof and McGillis (1999). It is also visible in the increases in *k* caused by a change of wind speed into higher wind regimes.

Both LM86 and W92 were developed for instantaneous winds (Nightingale et al., 2000). LM86 is based on gas transfer velocity measurements over 1-2 days on a small lake, therefore, because of the short time interval of measurements LM86 will result in low gas transfer velocities if long-term averaged winds over the ocean are used (Wanninkhof, 1992).

4.3.2 Change in the Air-Sea CO_2 Fluxes with Wind Speed and the Uncertainty in the Wind Speed Product

The CO_2 fluxes were calculated with the same values for ΔfCO_2 and solubility, but the values for *k* were determined using the five different gas transfer velocity parameterisations.

B74 showed no change except once between the low wind regime and the medium wind regime. There was no change in any regime due to the uncertainty in the wind speed product of $2 m.s^{-1}$. In the low wind regime, W92 and N00 had the highest flux

values and they showed the greatest response to a change in wind speed of $2m.s^{-1}$. WM99 has the smallest response to a change in wind speed of $2m.s^{-1}$ in the low wind regime. W92 had the largest change between the low wind regime and the medium wind regime, but WM99 had the greatest response to the uncertainty in the wind product. All fluxes increased (besides for B74) by at least $2mmol.m^{-2}.day^{-1}$ from the low wind regime to the medium wind regime. In the high wind speed regime WM99 showed the biggest change going from a medium wind speed regime to a high wind speed regime, and it also had the largest response to a change in wind speed of $2m.s^{-1}$ in the medium and high wind regimes. The cubic relationship between gas transfer velocity and wind speed of WM99 is clear in the small response at low wind speeds and the considerable response at high wind speeds to a change in the uncertainty in the wind speed product of $2m.s^{-1}$

Although it has been shown in the results that the CO_2 air-sea flux is sensitive to an increase in wind speed, the sensitivity is variable. This is due to the sensitivity of the gas transfer velocity to wind speed, and the high dependence of air-sea fluxes on gas transfer velocity. Ho et al., (2006) point out that the difference in net global CO_2 fluxes calculated using the different parameterisations are mainly due to wind speed differences in the range of $4\text{-}17m.s^{-1}$, this matches the results of this study in the sensitivity of the flux to an increase in wind speed, with the greatest changes happening from $5m.s^{-1}$ to stronger wind speeds ($16m.s^{-1}$).

This study is in agreement with the view of Takahashi et al., (2009) that the flux difference is primarily attributed to the choice of gas transfer velocity parameterisations and wind speeds. The reliability of air-sea CO_2 flux therefore depends on the accuracy of the ΔpCO_2 and that of the relationship between gas transfer velocity and wind speed used in the flux calculation but the uncertainty from the parameterisation is much greater than the uncertainty of ΔpCO_2.

According to Doney et al., (2009) efforts are in process to increase the coverage of pCO_2 through more frequent measurements and data assimilation techniques, utilising remote sensing of parameters such as sea surface temperature and wind speed. A higher precision of fluxes will lead to better boundary conditions for models and improved forecasts of atmospheric CO_2 concentrations.

4.4 Comparison of the Flux from this study with the Flux from Takahashi et al., (2009)

We will use Wanninkhof's 1992 quadratic relationship between gas transfer velocity and wind speed, for steady winds, Equation 4, to calculate the air-sea CO_2 flux in this comparison between the results from this study, and those determined by Takahashi et al., (2009).

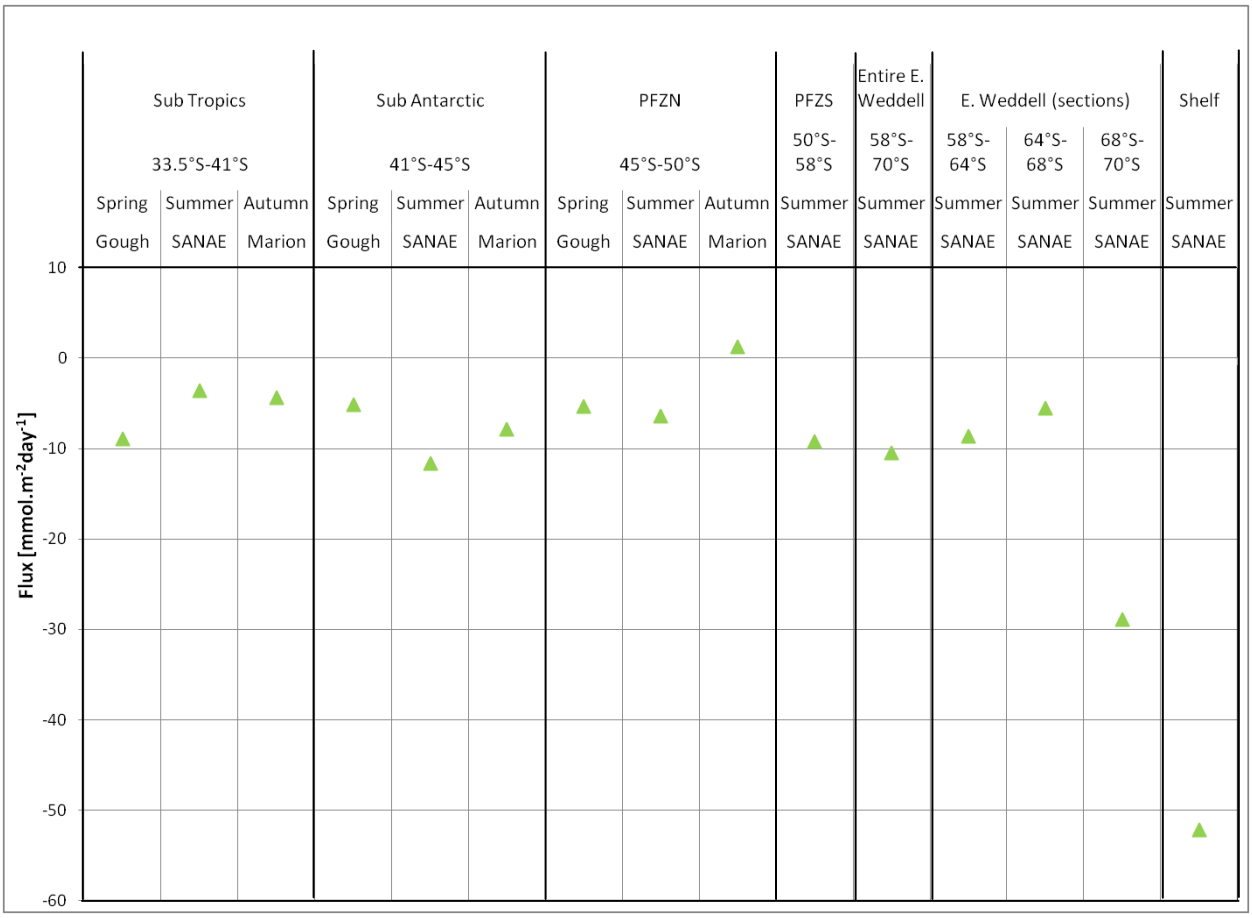

Figure 22: Graph showing the average air-sea CO_2 flux calculated using the gas transfer velocity model from Wanninkhof (1992) and the ΔfCO_2 recorded in this study. The gas transfer velocity was determined using daily wind speed. Note that positive values indicate sea-to-air fluxes, and negative values indicate air-to-sea values.

Our results show that the mean seasonal fluxes in the Subtropical region (33.5-41°S) were negative, ranging from approximately -4mmol.m^{-2}day^{-1} in summer to -9mmol.m^{-2}.day^{-1} in spring, with autumn yielding a CO_2 flux of -5mmol.m^{-2}.day^{-1}. In the Sub Antarctic region (41-45°S) the ocean was a sink for CO_2 for all three seasons, with the air-sea CO_2 fluxes ranging from -5mmol.m^{-2}.day^{-1} in spring to -12mmol.m^{-2}.day^{-1} in summer In this region a CO_2 flux of -8mmol.m^{-2}.day^{-1} was experienced in autumn. In the Northern Polar Frontal Zone (PFZN) (45-50°S) the ocean is a sink of CO_2 in summer and spring (approximately -6mmol.m^{-2}.day^{-1} for both seasons), but was a source of CO_2 in autumn with a flux of +2mmol.m^{-2}.day^{-1}. In the Southern Polar Frontal

Zone (PFZS) (50-58°S) south towards the Antarctic Shelf (70°S) there is only a seasonal mean flux for summer, and the air-sea CO_2 flux for all the following regions was into the ocean. All the values are approximate. In the Southern Polar Frontal Zone there was a flux of -9mmol.m^{-2}.day^{-1}. Between 58-64°S in the Eastern Weddell region the CO_2 flux was -8mmol.m^{-2}.day^{-1}. In the region of 64-68°S the CO_2 flux was -5mmol.m^{-2}.day^{-1}. The CO_2 flux increases significantly between 68-70°S to -29mmol.m^{-2}.day^{-1}, and it increases again at the Antarctic Shelf at 70°S to -53mmol.m^{-2}.day^{-1}.

(a)

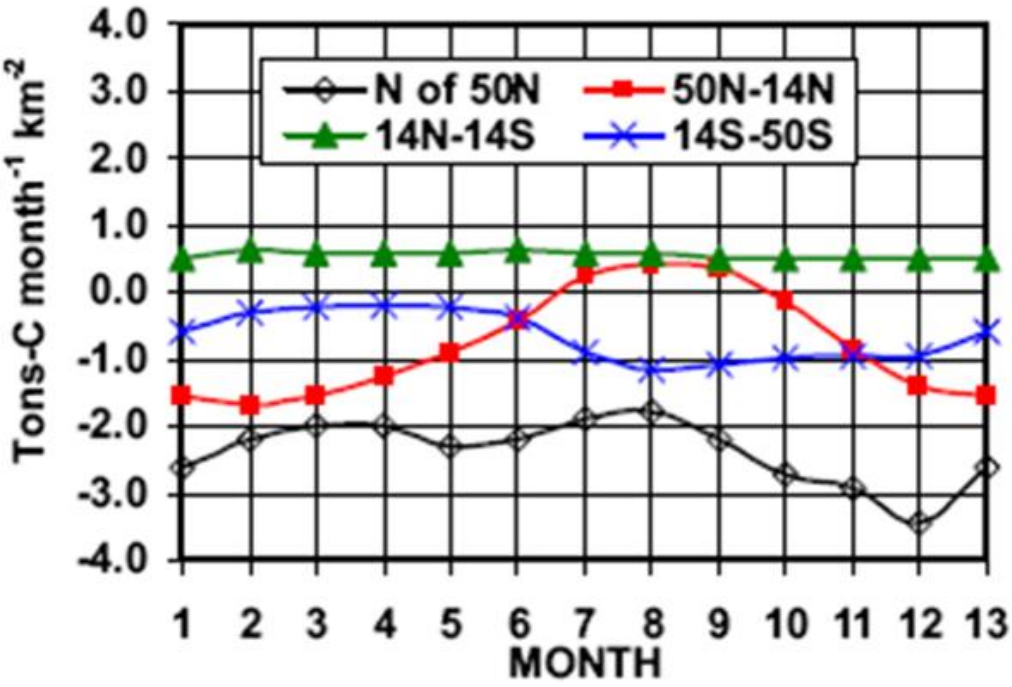

(b)

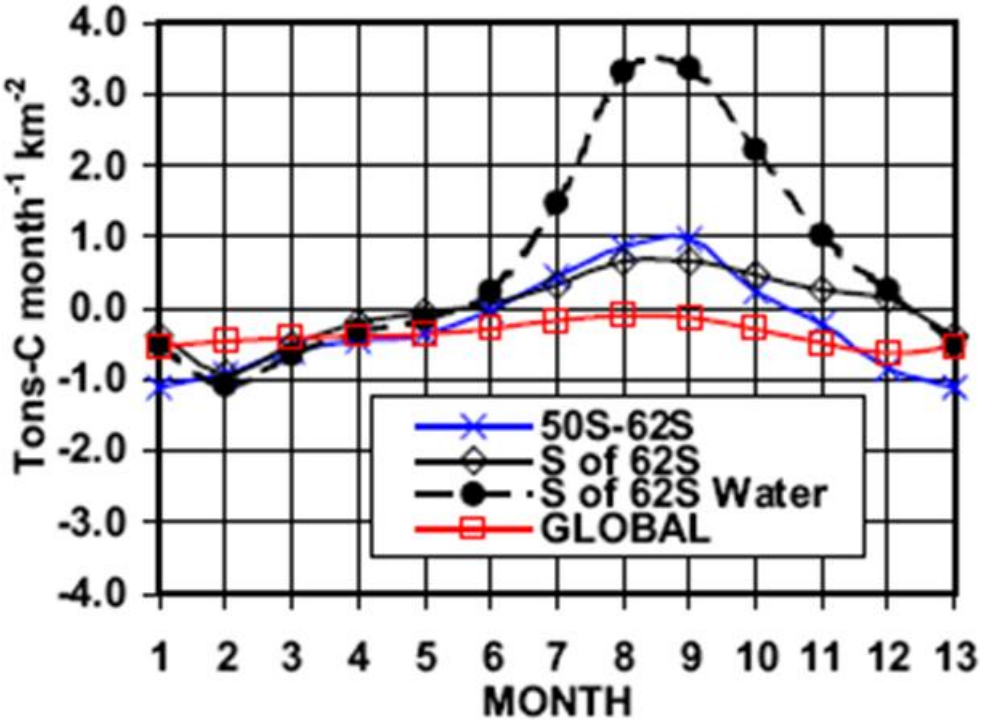

Figure 23: Plot (a) shows the monthly mean sea-air CO_2 flux of the Atlantic Ocean and plot (b) shows the monthly mean sea-air CO_2 flux of the Southern and Global Oceans. The fluxes are in the unit of Tons-C.km^{-2}.month^{-1} (Ton=10^{6}g). Months 1 and 13 are January and Month 12 is December. For the region 'South of 62°S' the black solid curve with open diamonds indicates the flux per km^2 of geographic area including ice cover; and the black dashed curve with solid circles indicates the flux per km^2 of water exposed to the air in leads and polynyas in the ice fields. Positive values indicate sea-to-air fluxes, and negative values indicate air-to-sea fluxes. Figure 23 is taken from Takahashi et al., (2009).

Figure 23(a) and (b) are taken from Takahashi et al., (2009) and show the sea-air CO_2 fluxes in Tons-C.month^{-1}.km^{-2}. Figure 23(a) is the Atlantic Ocean and Figure 23(b) shows the Southern and Global Oceans. The months are in numbers, from 1-13, with 1 and 13 being January. The information in Figure 23(a) that is relevant to this study is the blue line with an 'x' as its marker and months 1; 2; 4; 9; 10 and 13 (January; February; April; September; October and January). In Figure 23(b) the information relevant to this study is the black line with solid black circles and the blue line with an 'x' as its marker, the months used in plot Figure 23(b) are 1; 2 and 13 (January and February). In order to compare Takahashi's results with that from this study, we will approximate the values from the Figure 23 and include them in a graph with the flux calculated using *k* defined by Wanninkhof 1992. The units in Takahashi et al., (2009)

have been converted from Tons-C.month^{-1}.km^{-2} to mmol.m^{-2}.day^{-1}. The daily wind speed was used in calculating the gas transfer velocity for the CO_2 fluxes of this study because it has been shown that there is a very small difference in the resulting flux between daily wind speed and the weighted average wind speed for the week previous to the day of daily wind speed.

Table 5: The air-sea CO_2 flux values used in the comparison between the results from this study to the results from Takahashi et al., (2009). The values from Takahashi et al., (2009) were taken from Figure 23 and then converted from tons-C.km^{-2}month^{-1} into the same units used in this study (mmol.m^{-2}day^{-1}). The Wanninkhof (1992) relationship between wind speed and gas transfer velocity was used to determine the air-sea CO_2 flux in the comparison.

				From this Study	TAKAHASHI et al.,(2009)	
				mmol.m^{-2}.day^{-1}	*t-C.km^{-2}month^{-1}*	mmol.m^{-2}.day^{-1}
Sub Tropical Zone	33.5°S-41°S	Spring	Gough	-8.8888	*-1.05*	-2.8200
		Summer	SANAE	-3.5972	*-0.3*	-0.8057
		Autumn	Marion	-4.3966	*-0.2*	-0.5371
Sub Antarctic Zone	41°S-45°S	Spring	Gough	-5.1135	*-1.05*	-2.8200
		Summer	SANAE	-11.6891	*-0.3*	-0.8057
		Autumn	Marion	-7.9013	*-0.2*	-0.5371
Northern Polar Frontal Zone (PFZN)	45°S-50°S	Spring	Gough	-5.3269	*-1.05*	-2.8200
		Summer	SANAE	-6.4236	*-0.55*	-1.4771
		Autumn	Marion	1.2766	*-0.2*	-0.5371
Southern Polar Frontal Zone (PFZS)	50°S-58°S	Summer	SANAE	-9.2055	*-1*	-2.6857
Entire Eastern Weddell Zone	58°S-70°S	Summer	SANAE	-10.4519	*-0.9*	-2.4171
Eastern Weddell Zone (sections)	58°S-64°S	Summer	SANAE	-8.6800	*-1.1*	-2.9543
	64°S-68°S	Summer	SANAE	-5.5362	*-1.1*	-2.9543
	68°S-70°S	Summer	SANAE	-28.9142	*-0.5*	-1.3429
Antarctic Shelf	70	Summer	SANAE	-52.2096	*-0.5*	-1.3429

The values that were extrapolated from Figure 23 (a) and (b) for the comparison in Figure 24 are shown in Table 5. Table 5 has been included because values are not readily obtainable from Figure 24. A comparison is now described referring to Figure 24.

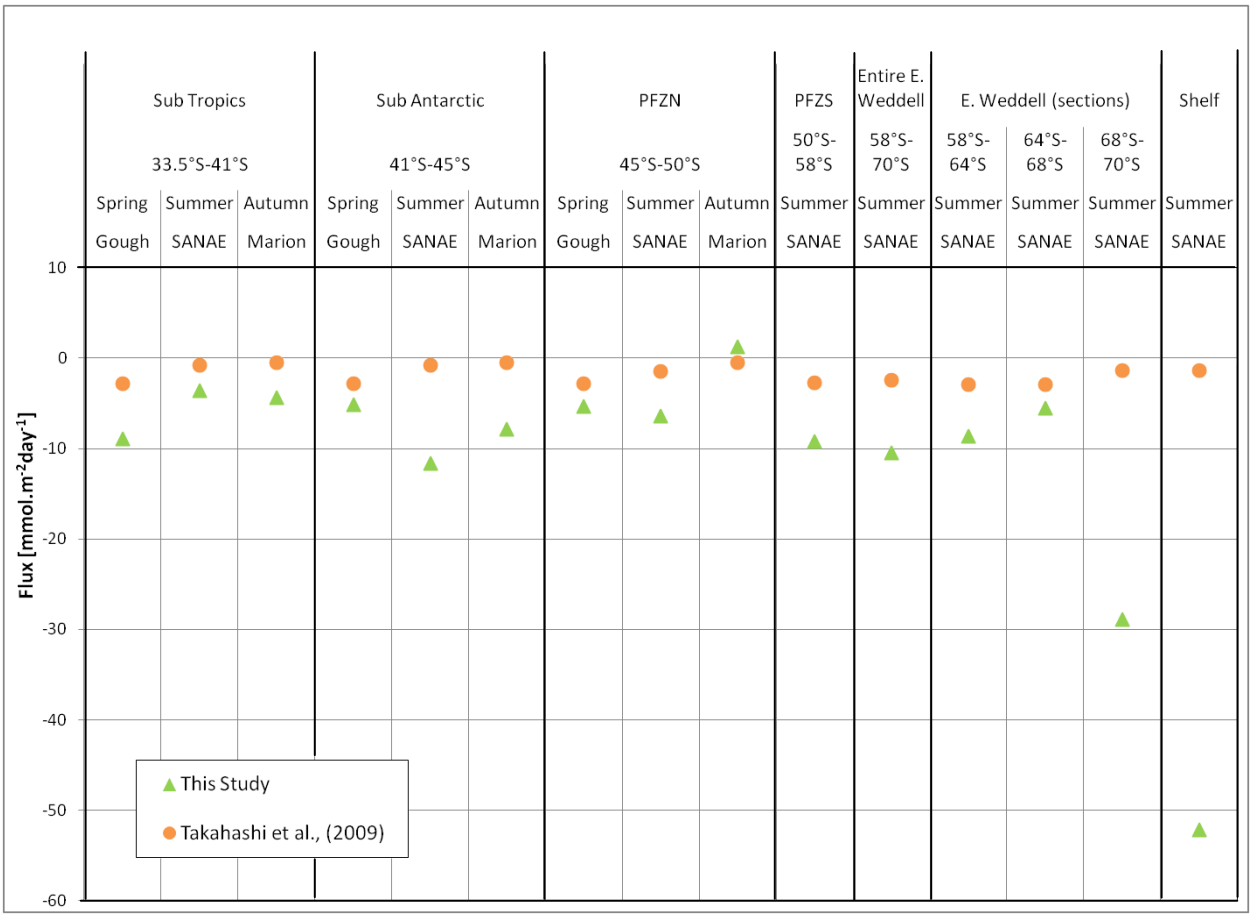

Figure 24: Graph showing the CO_2 flux data extrapolated from Takahashi et al., (2009) in Figure 23 with the air-sea CO_2 flux data from this study. The flux from this study was calculated using daily winds. The gas transfer velocity model used in determining the CO_2 flux is Wanninkhof (1992). Note that positive values indicate sea-to-air fluxes, and negative values indicate air-to-sea values.

Figure 24 shows the CO_2 fluxes that were calculated in this study with the Wanninkhof 1992 quadratic relationship between *k* and wind speed using the daily wind speed that was recorded as the green triangles, and the flux values were approximately extracted

from the study by Takahashi et al., (2009) shown in Figure 23(a) and (b). Because the values for Takahashi et al., (2009) were roughly approximated using Figure 23 it is only a first order comparison. The results from Takahashi et al. are on such a large scale that it will be easier to downsize those results rather than upsizing the small-scale results from this study, because the error will be smaller, but the error of doing so is still large. The extracting of the data from Takahashi et al. in the graph is also approximate as it is averaged monthly rather than seasonally. Potential errors in this approach include the following: the estimation of the flux values from a graph, the zonal averaging used by Takahashi is different to that used in this study, this study used instantaneous local data, and the positions of flux values from Takahashi et al. that have been placed into Figure 24: because of the different averaging spatially and temporally.

The air-sea CO_2 flux from Takahashi et al., (2009) is less than the CO_2 flux results calculated in this study in all the regions, and the CO_2 flux from Takahashi et al., (2009) is negative (air-to-sea flux) from the Subtropical Zone to the Antarctic Shelf for all seasons. The spring CO_2 flux from Takahashi et al., (2009) is the greatest in the Subtropical Zone, the Sub Antarctic Region and the Northern Polar Frontal Zone (PFZN) (at about -3mmol.m^{-2}.day^{-1}) and autumn yields the lowest CO_2 flux for those three regions (just below 0mmol.m^{-2}.day^{-1}). From the Polar Frontal Zone (South) (PFZS) the flux is about 2.5mmol.m^{-2}.day^{-1} and it decreases steadily towards the Antarctic Continent to approximately -1mmol.m^{-2}.day^{-1}. The results from this study range from about +2mmol.m^{-2}.day^{-1} during autumn in the PFZN to -52mmol.m^{-2}.day^{-1} at the Antarctic Shelf in summer.

Table 6: Table showing the mean difference between the air-sea CO_2 fluxes calculated in this study, with the Wanninkhof (1992) relationship between wind speed and gas transfer velocity, using the daily wind speed, and the CO_2 fluxes extrapolated from Figure 23(a) and (b) from Takahashi et al., (2009) and shown in Table 5 and Figure 24

				Mean Difference in Air-Sea CO_2 Flux values
				$mmol.m^{-2}.day^{-1}$
Sub Tropical Zone	33.5°S-41°S	Spring	Gough	6.07
		Summer	SANAE	2.79
		Autumn	Marion	3.86
Sub Antarctic Zone	41°S-45°S	Spring	Gough	2.29
		Summer	SANAE	10.88
		Autumn	Marion	7.36
Northern Polar Frontal Zone (PFZN)	45°S-50°S	Spring	Gough	2.51
		Summer	SANAE	4.95
		Autumn	Marion	-1.81
Southern Polar Frontal Zone (PFZS)	50°S-58°S	Summer	SANAE	6.52
Entire Eastern Weddell Zone	58°S-70°S	Summer	SANAE	8.03
Eastern Weddell Zone (sections)	58°S-64°S	Summer	SANAE	5.73
	64°S-68°S	Summer	SANAE	2.58
	68°S-70°S	Summer	SANAE	27.57
Antarctic Shelf	70 S	Summer	SANAE	50.87

In the Subtropical Zone (33.5-41°S) the difference between the CO_2 flux values calculated in this study and those approximated from Takahashi et al., (2009) ranges from $6.07mmol.m^{-2}.day^{-1}$ in spring to $2.79mmol.m^{-2}.day^{-1}$ in summer. In the Sub Antarctic region (41-45°S) the biggest difference is in summer ($10.88mmol.m^{-2}.day^{-1}$) and the smallest difference occurs in spring ($2.29mmol.m^{-2}.day^{-1}$). The Northern Polar Frontal Zone (PFZN) (45-50°S) has the smallest overall differences between Takahashi et al., (2009) and this study, with the largest difference occurring in summer

(4.95mmol.m^{-2}.day^{-1}). The smallest difference occurs in autumn in the PFZN (-1.81mmol.m^{-2}.day^{-1}), it is also the only time that the CO_2 flux from Takahashi et al., (2009) is greater than the CO_2 flux calculated in this study. From the Southern Polar Frontal Zone (PFZS) (50-58°S) to the Antarctic Shelf (70°S) the difference in the CO_2 fluxes ranges from 2.58mmol.m^{-2}.day^{-1} (between 64-68°S) and 50.87mmol.m^{-2}.day^{-1} (at the Antarctic Shelf).

Because there was only one instance when the CO_2 flux determined by Takahashi et al., (2009) is greater than the CO_2 flux determined in this study (in spring in the Northern Polar Frontal Zone), it could mean the results from this study may be overestimating the ocean uptake of carbon dioxide in the Southern Ocean. We need to look at other estimations of the Southern Ocean CO_2 sink in order to know whether this study greatly overestimates the CO_2 flux. The earlier flux estimates range from 0.10 to 0.56 PgC.yr^{-1} (Takahashi et al., 2002; McNeil et al., 2007; Mikaloff-Fletcher et al., 2007), but Takahashi et al., (2009) estimates a smaller sink of 0.05 PgC.yr^{-1}. This decrease in the sink is a result of improved spatial and temporal resolution, as well as improvements in the understanding of air-sea gas transfer over time.

This is such a rough comparison, and it is impossible to properly compare the data in the way that the Takahashi et al., (2009) fluxes were extrapolated and then scaled down so extremely. The important part of this comparison is that the fluxes from Takahashi et al., (2009) are negative, the same as the results from this study, except for PFZN in autumn. Barbero et al., (2011) state that direct comparisons of the global oceanic carbon uptake are difficult to compare directly, because various authors define the Southern Ocean very differently.

Chapter 5:

SYNTHESIS

It is important to be able to measure the air-sea CO_2 fluxes in the Southern Ocean, because the Southern Ocean plays such an important role in the world's oceans and it is here that most of the deep waters are ventilated by exchanging carbon dioxide with the atmosphere. It is a vastly under-sampled area which creates large gaps in the knowledge of the trends and magnitude of the fluxes. It is important to be able to accurately estimate the air-sea flux of CO_2 in order to improve our understanding of global CO_2. Takahashi et al., (2009) created a worldwide pCO_2 dataset compiling 3 million pCO_2 values for the seawater, in order to estimate the inter annual variability in the pCO_2 of the surface water

The data for this study was collected on three separate cruises in the South Atlantic Ocean by the SA Agulhas as part of the SANAP programme, to Gough Island, Antarctica and Marion Island. This was in order to get data for the austral spring, summer and autumn seasons, and to be able to compare them. The data was collected using an autonomous underway pCO_2 measuring system, and the wind product was extracted from the SeaWinds data set. The data was averaged into simplified frontal zones, for a regional comparison.

There are five gas transfer velocity parameterisations that were used in this study. They each define gas transfer velocity and wind as having a different relationship, and each used a different method of studying gas transfer velocity. Broecker and Peng (1974) use the Stagnant Film Model (B74), which states that a thin layer of film separates two uniform bodies of water and air, and the thickness of the film is dependent on the sea state. High agitation leads to a thin film, and low agitation of the sea leads to a thicker film. The gas transfer velocity is dependent on the film thickness and the molecular diffusivity of the gas. Liss and Merlivat (1986) (LM86) developed a linear relationship that is controlled by three wind regimes, smooth surface regime, rough surface regime, and breaking wave regime. Wanninkhof (1992) (W92), which was developed for steady winds, has a quadratic relationship between wind speed and

gas transfer velocity. A cubic relationship was stated by Wanninkhof and McGillis (1999) (WM99), and is used for steady, short term winds. The final parameterisation is that of Nightingale et al., (2000) (N00), which is also a quadratic relationship.

It was found that the Stagnant Film Model (B74) only changes when the thickness of the film decreased, which was when the wind changed from a low wind speed to a high wind speed. LM86 had a weak relationship, but it was affected by changes in the wind speed regime. The gas exchange model of Nightingale et al., (2000) appeared to be strongly dependant on wind at low wind speeds, but was less responsive to a change at high wind speeds. The model from Wanninkhof and McGillis had a weak relationship with wind in a low wind regime, but as soon as the wind speed was in the mid-to-high wind regime, it was significantly sensitive and had a high response to a small change in wind speed, due to its cubic relationship. The Wanninkhof (1992) model seemed to be the most stable, showing a moderate change in *k* at low wind speeds, medium and high wind speeds.

The error for estimating air-sea CO_2 fluxes is high, mainly due to the different parameterisations used in calculating gas transfer velocity, and methods for in situ data collection need to be improved. Wind is not the only factor that affects gas transfer velocity, but because wind speeds are easily available globally through satellite data, it is the best way in the present day in calculating *k.* Many of the models used in this study would have been impractical for use in the Southern Ocean because of the high wind speeds, and the resulting impact on the ocean surface because of high winds. The error in the Southern Ocean is also high due to the lack of sampling done in this region, and perhaps the high wind speeds that are experienced over the Southern Ocean.

The comparison of the results from this study with those from Takahashi et al., (2009) was not valuable. Changing the scale of Takahashi et al., (2009) in order to compare with these results was too much of a rough estimate to be able to properly compare the data as values, so only the direction of the flux could be compared. The results of this study agreed with Takahashi et al., (2009) that the Southern Ocean is a sink of CO_2

More studies are needed that are on a smaller time scale and space scale, in order to get a more accurate estimate of the CO_2 fluxes, and decrease the error in the air-sea CO_2 flux. Studies could also use the more complex gas transfer velocity models that don't just use wind speed as a parameter, and use the parameters like bubble entrainment and chemical enhancement, leading to a more accurate value of gas transfer velocity, which will in turn, lead to a more accurate air-sea CO_2 flux, especially in the Southern Ocean.

APPENDIX 1

Weighting of the winds for weighting average

Day of wind	= 100%
1 day before	= 50%
2 days before	= 25%
3 days before	= 12.5%
4 days before	= 6.25%
5 days before	=3.125%
6 days before	=1.625%

APPENDIX 2

Table 7: Table showing change in the Flux because of uncertainty in the temperature of 0.05°C, which affects solubility. A change in temperature also affects the Schmidt number, and in turn, the gas transfer velocity. All columns except for Temperature and Solubility remain to 4 decimal points to show the small changes that occur.

Temperature *(°C)*	**Solubility *(mol.kg^{-1} atm^{-1})***	kW92 (at u=8m.s^{-1}) *(cm.h^{-1})*	ΔfCO_2 *(atm)*	Flux *(mmol.m^{-2}.day^{-1})*	Range of Uncertainty	Range as Percentage of Flux	Mean	Standard Deviation
-0.05	**65.25**	11.1775	$-2x10^5$	-3.5007	0.0031	0.0876	-3.4991	0.0015
0	**65.12**	11.1945		-3.4991				
0.05	**64.99**	11.2114		-3.4976				
9.95	**45.51**	15.0976		-3.2979	0.0013	0.0401	-3.2972	0.0007
10	**45.43**	15.1196		-3.2972				
10.05	**45.36**	15.1416		-3.2966				
19.95	**33.58**	19.7266		-3.1800	0.0011	0.0344	-3.1794	0.0005
20	**33.54**	19.7506		-3.1794				
20.05	**33.49**	19.7746		-3.1789				

Table 8: Table showing change in the Flux because of uncertainty in ΔfCO_2 of 1µatm. Temperature used to calculate Solubility is 5°C, Salinity is 33.50

Solubility *(mol.kg^{-1} atm^{-1})*	kW92 (at u=8m.s^{-1}) *(cm.h^{-1}))*	**ΔfCO_2 *(atm)***	Flux *(mmol.m^{-2}.day^{-1})*	Range of Uncertainty	Range as Percentage of Flux	Mean	Standard Deviation
53.99	13.03	**-0.9x10^5**	-1.52	0.34	20	-1.69	0.17
		-1.0x10^5	-1.69				
		-1.1x10^5	-1.86				
		-1.9x10^5	-3.21	0.34	10	-3.38	0.17
		-2.0x10^5	-3.38				
		-2.1x10^5	-3.54				
		-2.9x10^5	-4.90	0.34	6.67	-5.06	0.17
		-3.0x10^5	-5.06				
		-3.1x10^5	-5.23				

Table 9: Table showing change in the Flux because of the uncertainty in the wind product of 2m.s^{-1}. Temperature used to calculate Solubility is 5°C, Salinity is 33.50.

Solubility *(mol.kg^{-1} atm^{-1})*	Wind *(m.s^{-1})*	**kW92 *(cm.h^{-1})***	ΔfCO_2 *(atm)*	Flux *(mmol.m^{-2}.day^{-1})*	Range of Uncertainty	Range as Percentage of Flux	Mean	Standard Deviation
53.99	1	**0.21**	-2x10^5	-0.05	1.27	266.67	-0.62	0.64
	3	**1.83**		-0.47				
	5	**5.09**		-1.32				
	6	**1.33**		-1.90	3.38	100	-3.52	1.69
	8	**13.03**		-3.38				
	10	**20.36**		-5.28				
	12	**29.32**		-7.60	5.91	57.14	-10.49	2.96
	14	**39.90**		-10.34				
	16	**52.12**		-13.51				

REFERENCES

- Anderson, R.F., and W.O. Smith Jr., (2001) 'The US Southern Ocean Joint Global Ocean Flux Study: Volume Two', *Deep Sea Research II*, vol. 48, pp.3883-3889.
- Arrigo, K.R., G. van Dijken, and M. Long, (2008), 'Coastal Southern Ocean: A Strong anthropogenic CO_2 sink', *Geophysical Research Letters*, vol. 35, L21602, doi:10.1029/2008GL036524, 6pp.
- Asher, W., and R. Wanninkhof, (1998), 'Transient tracers and air-sea gas transfer', *Journal of Geophysical Research*, vol. 103, no. C8, pp. 15939-15958
- Bakker, D.C.E, M.C. Nielsdóttir, P.J. Morris, H.J. Venables, and A.J. Waston, (2007), 'The Island Mass Effect and Biological Carbon Uptake for the Subatnarctic Crozet Archipelago', *Deep Sea Research II*, vol. 54, pp. 2174-2190.
- Barbero, L.,J. Boutin, L. Merlivat, N. Martin, T. Takahashi, S.C. Sutherland, and R. Wanninkhof, (2011), 'Importance of Water Mass Formation Regions for the Air-Sea CO_2 flux estimate in the Southern Ocean', *Global Biogeochemical Cycles*, vol. 25, GB1005, doi:10.1029/2010GB003818, 16pp.
- Boudreau, B.P., (1997), *Diagenetic Models and Their Implementation: Modelling Transport and Reactions in Aquatic Sediments,* Springer, pp.93-109.
- Bourassa, M.A., D.M. Legler, J.J. O'Brien, and S.R. Smith, (2003), 'SeaWinds Validation With Research Vessels', *Journal of Geophysical Research*, vol. 108, no. C2. Pp. 3019-3034.
- Broecker, H.C., J. Petermann, and W. Siems, (1978), 'The Influence of wind of CO_2-exchange in a wind-wave tunnel, including the effects of monolayers', *Journal of Marine Research*, vol. 36, pp. 595-610.
- Broecker, W.S., and T.H. Peng, (1971), 'The vertical distribution of radon in the BOMEX area', *Earth and Planetary Science Letter*, pp.99-108.
- Broecker, W.S., and T.H. Peng, (1974), 'Gas Exchange rates between air and sea', *Tellus*, vol. 26, pp. 21-35.
- Broecker, W.S., and T.H. Peng, (1982), 'The Atmospheric Imprint: Cycles of Gas within the Sea', *Tracers in the Sea*, Eldigio Press Lamont Doherty Geological Observatory, pp. 110-1631

- Businger, J.A., (1997), 'Measurement of the Transfer of Gases across the Air-Sea Interface', *Journal of Applied Meteorology and Climatology*, vol. 36, no. 8, pp113-115.
- Canadell, J.G., C. Le Quéré, M.R. Raupach, C.B. Field, E.T. Buitenhuis, P. Ciais, T.J. Conway, N.P. Gillett, R.A. Houghton, and G. Marland, (2007), 'Contributions to accelerating atmospheric CO_2 growth form economic activity, carbon intensity, and efficiency of natural sinks', *PNAS*, vol. 104, no. 47, 5pp.
- D'Asaro, E., and C. McNeil, (2008), 'Air-sea gas exchange at extreme wind speeds measured by autonomous oceanographic floats', *Journal of Marine Systems*, vol. 74, pp. 722-736.
- DeGrandpre, M.D., W.R. McGillis, N.M. Frew, and E.J. Bock, (1995) 'Laboratory Measurements of Seawater CO_2 Gas Fluxes', in B. Jähne and E. Monahan (eds.), *Air-Water Gas Transfer*, AEON Verlag, pp. 375-383.
- Doney, S.C., B. Tilbrook, S. Roy, N. Metzl, C. Le Quéré, M. Hood, R.A. Feely, and D. Bakker, (2009), 'Surface-Ocean CO_2 Variability and Vulnerability', *Deep Sea Research II*, vol. 56, pp. 504-511.
- Fabry, V.J., B.A. Seibel, R.A. Feely, and J.C. Orr, (2008), 'Impacts of ocean acidification on Marine Fauna and Ecosystem Process', *ICES Journal of Marine Sciences*, vol. 65, pp. 414-432.
- Fangohr, S., and D.K. Woolf, (2007), 'Applications of new parameterisations of gas transfer velocity and their impact on regional and global marine CO_2 budgets', *Journal of Marine Science*, vol. 66, pp. 195-203.
- Feely, R.A., C.L. Sabine, T. Takahashi, and R. Wanninkhof, (2001), 'Uptake and Storage of the Carbon Dioxide in the Ocean: The Global CO_2 Survey', *Oceanography*, vol. 14, no. 4, pp. 18-32.
- Feely, R.A., C.L. Sabine, K. Lee, W. Berelson, J. Kleypas, V.J. Fabry, and F.J. Millero, (2004), 'Impact of Anthropogenic CO_2 on the $CaCO_3$ system in the Oceans', *Science*, vol. 305, no. 5682, pp. 362-366.
- Glover, D.M., N.M. Frew, S.J. McCue, and E.J. Bock, (2002), "A multiyear time series of global gas transfer velocity from the TOPEX dual frequency, normalised radar backscatter algorithm", in M.A. Donelan, W.M. Drennan, E.S. Saltzman, R.

Wanninkhof (eds.), *Gas Transfer at Water Surfaces*, *Geophysical Monograph Series,* vol. 127. AGU Washington DC, pp. 325-331.

- Griessbaum, F., B.I. Moat, Y. Narita, M.J. Yelland, O. Klemm, and M. Uematsu, (2009), 'Uncertainties in wind speed dependent CO_2 transfer velocities due to airflow distortion at anemometer sites on ships', *Atmospheric Chemistry and Physics Discussions*, vol. 9, pp.18839-18865.
- Gruber, N., M. Gloor, S.E. Mikaloff Fletcher, S.C. Doney, S. Dutkiewicz, M.J. Follows, M. Gerber, A.R. Jacobson, F. Joos, K. Lindsay, D. Menemenlis, A. Mouchet, S.A. Müller, J.L. Sarmiento, and T. Takahashi, (2009), 'Oceanic Sources, Sinks, and Transport of Atmospheric CO_2', *Global Biogeochemical Cycles*, vol. 23, GB1005.
- Ho, D.T., C.S. Law, M.J. Smith, P. Schlosser, M. Harvey, and P. Hill, (2006) 'Measurements of air-sea gas exchange at high winds speeds in the Southern Ocean: Implications for global parameterisations', *Geophysical Research Letters*, vol. 33, L16611.
- Hoppema, M., E. Fahrbach, M.H.C. Stoll, and H.J.W. de Baar, (1999), 'Annual uptake of the atmospheric CO_2 by the Weddell Sea derived from a surface layer balance, including estimations of entrainment and new production', *Journal of Marine Systems*, vol. 19, pp. 219-233.
- Hoppema, M., H.J.W. de Baar, R.G.J. Bellerby, E. Fahrbach, K. Bakker, (2002), 'Annual export production in the interior Weddell Gyre estimated from a chemical mass balance of nutrients', *Deep Sea Research II*, vol. 49, pp. 1675-1689.
- Jähne, B., W. Huber, A. Dutzi, T. Wais, and J. Ilmberger, (1984), 'Wind/Wave-Tunnel Experiment on the Schmidt Number – and Wave Field Dependence of Air/Water Gas Exchange', in W. Brutsaert and G.H. Jirka (eds.), *Gas Transfer at Water Surfaces,* D. Reidel Publishing Company, pp.303-309.
- Jähne, B., G. Heinz, and W. Dietrich, (1987), 'Measurement of the Diffusion Coefficients of Sparingly Soluble Gases in Water', *Journal of Geophysical Research*, vol. 92, no. C10, pp. 10767-10776.
- Jähne, B., and H. Hauβecker, (1998), 'Air-Water Gas Exchange', *Annual Review of Fluid Mechanics*, vol. 30, pp. 443-468.

- Jähne, B., R. Nielsen, C. Popp, U. Schimpf, and C Garbe, (2005), 'Air-Sea Gas Transfer; Schmidt Number Dependency and Intermittency', *Gas Transfer at Water Surfaces*, at the 37th International Liège Colloquium on Ocean Dynamics.
- Kuss, J., and B. Schneider, (2004), 'Chemical Enhancement of the CO_2 gas exchange at a smooth seawater surface', *Marine Chemistry*, vol. 91, pp. 165-174.
- Le Quéré, C., M.R. Raupach, J.G. Canadell, G. Marland, L. Bopp, P. Ciais, T.J. Conway, S.C. Doney, R.A. Feely, P. Foster, P. Friedlingstein, K. Gurney, R.A. Houghton, J.I. House, C. Huntingford, P.E. Levy, M.R. Lomas, J. Majkut, N. Metzl, J.P. Ometto, G.P. Peters, I.C. Prentice, J.T. Randerson, S.W. Running, J.L. Sarmiento, U. Schuster, S. Sitch, T. Takahashi, N. Viovy, G.R. van der Werf, and F.I. Woodward, (2009), 'Trends in the Sources and Sinks of Carbon Dioxide', *Nature Geosciences*, vol. 2, pp. 1-6.
- Le Quéré, C., C. Rödenbeck, E.T. Buitenhuis, T.J. Conway, R. Langenfelds, A. Gomez, N. Metzl, N. Gillett, and M. Heinmann, (2007), 'Saturation of the Southern Ocean CO_2 Sink Due to Recent Climate Change', *Science*, vol. 316, pp. 1735-1738.
- Levin, I., and V. Hesshaimer, (2000), 'Radiocarbon – A unique tracer of Global Carbon Cycle Dynamics', *Radiocarbon*, vol. 42, no.1, pp. 69-80.
- Liss, P.S., and P.G. Slater, (1974), 'Flux of Gases across the Air-Sea Interface', *Nature*, vol. 247, no. , pp. 181-185.
- Liss, P.S., and L. Merlivat, (1986), 'Air-Sea Gas Exchange Rates: Introduction and Synthesis', in P. Mérnard (ed.), *The Role of Air-Sea Exchange in Geochemical Cycling*, Reidel, Dordrecht, pp. 113-127.
- Liss, P.S., M. Heimann, and W. Roether, (1988), 'Tracers of Air-Sea Gas Exchange', *Philosophical Transactions of the Royal Society of London. Series A, Mathematical and Physical Sciences*, vol. 325, no. 1583, pp. 93-103.
- Liss, P.S., A.L. Chuck, S.M. Turner, and A.J. Watson, (2004), 'Air-sea gas exchange in Antarctic Waters', *Antarctic Science*, vol. 16, no. 4, pp. 517-529.
- Lovenduski, N.S., N. Gruber, S.C. Doney, and I.D. Lima, (2007), 'Enhanced CO_2 outgassing in the Southern Ocean from a positive phase of the Southern Annular

Mode', *Global Biogeochemical cycles*, vol. 21, GB2026, doi:10.1029/2006GB002900. 14pp.

- Lovenduski, N.S., N. Gruber, and S.C. Doney, (2008), 'Toward a mechanistic understanding of the decadal trends in the Southern Ocean carbon sink', *Global Biogeochemical Cycles*, vol. 22, GB3016, doi:10.1029/2007GB003139, 9pp.
- Matthews, B.J.H., (2000), 'The Rate of Air-Sea CO_2 Exchange: Chemical Enhancement and Catalysis by Marine Micoalgoe', PhD Thesis, University of East Anglia. Retrieved on 10 September 2010, from www.chooseclimate.org/
- McNeil, B.I., N. Metzl, R.M. Key, R.J. Matear, and A. Corbiere, (2007), 'An Empirical Estimate of the Southern Ocean air-sea CO_2 Flux', *Global Biogeochemical Cycles,* vol. 21, GB3011.
- Metzl, N., B. Tilbrook, and A. Poisson, (1999), 'The Annual fCO_2 cycle and the Air-Sea CO_2 flux in the sub-Antarctic Ocean', *Tellus*, vol. 51, no. 4, pp. 849-861.
- Metzl, N., C. Brunet, A. Jaboaud-Jan, A. Poisson, B. Schauer, (2006), 'Summer and Winter Air-Sea CO_2 Fluxes in the Southern Ocean', *Deep Sea Research I*, vol. 53, pp.1548-1563.
- Mikaloff Fletcher, S.E., N. Gruber, A.R. Jacobson, M. Gloor, S.C. Doney, S. Dutkiewicz, M. Gerber, M. Follows, F. Joos, K. Londsay, D. Menemenlis, A. Mouchet, S.A. Müller, and J.L. Sarmiento, (2007), 'Inverse estimates of the oceanic sources and sinks of natural CO_2 and the implied oceanic carbon transport', *Global Biogeochemical Cycles*, vol.21, GB1010, doi:10.1029/2006GB002751.
- Monteiro, P.M.S., U. Schuster, M. Hood, A. Lenton, N. Metzl, A. Olsen, K. Rogers, C. Sabine, T. Takahashi., B. Tilbrook, J. Yoder, R. Wanninkhof, A.J. Watson.(2010), "A global sea surface carbon observing system: assessment of changing sea surface CO_2 and air-sea CO_2 fluxes". In: Hall, J., Harrison D.E. and Stammer, D. Eds. Proceedings of the 'OceanObs'09: Sustained Ocean Observations and Information for Society' Conference, Venice, Italy, 21-25 September 2009, ESA Publication WPP-306; doi:10.5270/OceanObs09.cwp.64
- Nightingale, P.D., G. Malin, C.S. Law, A.J. Watson, P.S. Liss, M.I. Liddicoat, J. Boutin, and R.C. Upstill-Goddard, (2000), 'In situ evaluation of air-sea gas

exchange parameterizations using novel conservative and volatile tracers', *Global Biogeochemical Cycles*, vol. 14, no. 1, pp.373-387.

- Nightingale, P.D., and P.S. Liss, (2004), 'Gases in Seawater', in H. Elderfield and H.D. Holland (vol. eds.), K.K. Turekian (exec ed.) *Treatise on Geochemistry Volume 6: The Oceans and Marine Geochemistry*, Elsevier Pergamon, pp. 49-81
- Olsen, A., R. Wanninkhof, J.A. Triñanes, and T. Johannessen, (2005), 'The effect of wind speed products and wind speed-gas exchange relationships on the interannual variability of the air-sea CO_2 gas transfer velocity', *Tellus*, vol. 58B, no. 2, pp.95-106.
- Orsi, A.H., T. Whitworth III, and W.D. Nowlin Jr., (1995), 'On the Meridional Extent and Fronts of the Antarctic Circumpolar Current', *Deep Sea Research I*, vol. 42, no. 5, pp. 641-673.
- Perry, K.L., (2000), 'Seawinds on QuikSCAT Level 3 Daily, Gridded Ocean Wind Vectors (JPL Seawinds Project)', *Guide Document,* Retrieved on 25 October 2010, from http://podaac.jpl.nasa.gov:2031/DATASET_DOCS/qscat_l3.html/
- Post, W.M., T.H Peng, W.R. Emanuel, A.W. King, V.H. Dale, and D.L. DeAngelis, (1990), 'The Global Carbon Cycle', *American Scientist*, vol. 78, pp.310-327.
- Raupach, M.R., and J.G. Canadell, (2008), 'Observing a Vulnerable Carbon Cycle', in A.J. Dolman, R. Valentini, A. Freibauer (eds.), *The Continental-Scale Greenhouse Gas Balance of Europe*, Springer, New York, pp. 5-32.
- Sabine, C.L., R.A. Feely, N. Gruber, R.M. Key, K. Lee, J.L. Bullister, R. Wanninkhof, C.S. Wong, D.W.R. Wallace, B. Tilbrook, F.J. Millero, T.H. Peng, A. Koyzr, T. Ono, and A.F. Rios, (2004), 'The Oceanic Sink for Anthropogenic CO_2', *Science*, vol. 305, no. 5682, pp. 367-371.
- Sabine, C.L., and R.A. Feely, (2007), 'Chapter 3: The Oceanic Sink for Carbon Dioxide', in D. Reay, N. Hewitt, J. Grace, and K. Smith (eds.), *Greenhouse Gas Sinks*, pp.31-49.
- Sarmiento, J.L., N. Gruber, (2006), 'Chapter 3: Air-Sea Interface', *Ocean Biogeochemical Dynamics*, Princeton University Press, pp.73-99.
- Schimel,D., I.G. Enting, M. Heinmann, T.M.L. Wigley, D. Raynaud, D. Alves, and U. Sinegenthaler, (1994), 'CO_2 and the Carbon Cycle (Extracted from the

Intergovernmental Panel on Climate Change (IPCC) Report, “Climate Change, 1994”’, in T.M.L. Wigley and D.S. Schimel (eds.), (2000) *The Carbon Cycle*, Cambridge University Press.

- Schudlich, R., and S. Emerson, (1996), “Gas supersaturation in the surface ocean: The roles of heat flux, gas exchange, and bubbles”, *Deep Sea Research II*, vol. 43, no. 2-3, pp.569-589.
- Sweeney, C., E. Gloor, A.R. Jacobson, R.M. Key, G. McKinley, J.L. Sarmiento, and R. Wanninkhof, (2007), ‘Constraining Global Air-Sea Exchange for CO_2 with recent bomb ^{14}C Measurements’, *Global Biogeochemical Cycles*, vol. 21, GB2015, doi:10.1029/2006GB002784
- Sweeney, C., T. Takahashi, and A. Gnanadesikan, (2002), ‘Spatial and Temporal Variability of Surface Water pCO_2 and Sampling Strategies’, Appendix D (pages 155 – 175) in *A Large Scale CO_2 Observing Plan: In Situ Oceans and Atmosphere (LSCOP)*, M. Bender, S. Doney, R.A. Feely, I. Fung, N. Gruber, D.E. Harrison, R. Keeling, J.K. Moore, J. Sarmiento, E. Sarachik, B. Stephens, T. Takahashi, P. Tans, and R. Wanninkhof, April 2002, National Technical Information Service, Springfield.
- Takahashi, T., S.C. Sutherland, C. Sweeney, A. Poisson, N. Metzl, B. Tilbrook, N. Bates, R. Wanninkhof, R.A. Feely, C. Sabine, J. Olafsson, and Y. Nojiri, (2002), ‘Global sea-air CO_2 flux based on climatological surface ocean pCO_2, and seasonal biological and temperature effects’, *Deep Sea Research II*, vol. 49, pp. 1601-1622,
- Takahashi, T., S.C. Sutherland, R. Wanninkhof, C. Sweeney, R.A. Feely, D.W. Chipman, B. Hales, G. Friederich, F. Chavez, C. Sabine, A. Watson, D.C.E. Bakker, U. Schuster, N. Metzl, H. Yoshikawa-Inoue, M. Ishii, T. Midorikawa, Y. Nojiri, A. Körtzinger, T. Steinhoff, M. Hoppema, J. Olafsson, T.S. Arnarson, B. Tilbrook, T. Johannessen, A. Olsen, R. Bellerby, C.S. Wong, B. Delille, N.R. Bates, and H.J.W. de Baar, (2009), ‘Climatological mean and decadal change in surface ocean ΔpCO_2, and net sea-air CO_2 flux over the global oceans’, *Deep Sea Research II*, vol. 56, pp. 554-577, doi:10.1016/j.dsr2.2008.12.009.

- Talley, L.D., G.L. Pickard, W.J. Emery, J.H. Swift, (2011), 'Chapter 14: Global Circulation and Water Properties', *Descriptive Physical Oceanography: An Introduction*, 6th Edition, Elsevier Ltd.
- Tomczak, M., and J.S. Godfrey, (2003), 'Chapter 6: Antarctic Oceanography', *Regional Oceanography: An Introduction*, Daya Publishing House, Delhi, retrieved on 19 July 2009, from http://www.es.flinders.edu.au/~mattom/regoc/pdffiles/colour/single/06P-Antarctic.pdf
- Wanninkhof, R. (1992), 'Relationship between wind speed and gas exchange over the ocean', *Journal of Geophysical Research*, vol. 97, no. C5, pp. 7373-7382.
- Wanninkhof, R., and W.R. McGillis, (1999), 'A cubic relationship between are-sea CO_2 exchange and wind speed', *Geophysical Research Letters*, vol. 26, no. 13, pp. 1889-1892.
- Wanninkhof, R., and R. Feely, (2004), *Observing the Global Oceanic Carbon Cycle,* Retrieved on 26 December, 2008, from http://www.pmel.noaa.gov/co2/OCO_Report/
- Wanninkhof, R., W.E. Asher, D.T. Ho, C. Sweeney, W.R. McGillis, (2009), 'Advances in Quantifying Air-Sea Gas Exchange and Environmental Forcing.' *Annual Review of Marine Science*, vol. 1, pp. 213-244.
- Woolf, D.K. (2005), 'Parameterisation of gas transfer velocities and sea-state-dependent wave breaking', *Tellus B*, vol. 57, no. 2, pp. 87-94/
- Zhang, H.-M., R.W. Reynolds, and J.J. Bates. 2006: 'Blended and Gridded High Resolution Global Sea Surface Wind Speed and Climatology from Multiple Satellites: 1987 – Present'. *American Meteorological Society 2006 Annual Meeting*, Paper #P2.23, Atlanta, GA, January 29 - February 2, 2006.